



LUND UNIVERSITY

Dynamics of Photogenerated Charge Carriers in III-V Bulk and Nanowire Semiconductors

Zou, Xianshao

2020

Document Version:
Other version

[Link to publication](#)

Citation for published version (APA):

Zou, X. (2020). *Dynamics of Photogenerated Charge Carriers in III-V Bulk and Nanowire Semiconductors* (1 ed.). [Doctoral Thesis (compilation), Chemical Physics]. Media-Tryck, Lund University, Sweden.

Total number of authors:
1

Creative Commons License:
CC BY-NC

General rights

Unless other specific re-use rights are stated the following general rights apply:

Copyright and moral rights for the publications made accessible in the public portal are retained by the authors and/or other copyright owners and it is a condition of accessing publications that users recognise and abide by the legal requirements associated with these rights.

- Users may download and print one copy of any publication from the public portal for the purpose of private study or research.
- You may not further distribute the material or use it for any profit-making activity or commercial gain
- You may freely distribute the URL identifying the publication in the public portal

Read more about Creative commons licenses: <https://creativecommons.org/licenses/>

Take down policy

If you believe that this document breaches copyright please contact us providing details, and we will remove access to the work immediately and investigate your claim.

LUND UNIVERSITY

PO Box 117
221 00 Lund
+46 46-222 00 00



Dynamics of Photogenerated Charge Carriers in III-V Bulk and Nanowire Semiconductors

XIANSHAO ZOU | DIVISION OF CHEMICAL PHYSICS | LUND UNIVERSITY



Dynamics of Photogenerated Charge Carriers in III-V Bulk and Nanowire Semiconductors

Dynamics of Photogenerated Charge Carriers in III-V Bulk and Nanowire Semiconductors

Xianshao Zou



LUND
UNIVERSITY


DOCTORAL DISSERTATION


by due permission of the Faculty Science, Lund University, Sweden.
To be defended at lecture hall C, Kemicentrum, Naturvetarvägen 14, 22363 Lund.
Friday, the 16th of October 2020 at 01:00 pm.

Faculty opponent
Prof. Dr. Tze-Chien Sum
Nanyang Technological University

Organization LUND UNIVERSITY Division of Chemical Physics Department of Chemistry P. O. Box 124 SE-221 00 Lund, Sweden		Document name Doctoral Dissertation	
		Date of issue 2020-10-16	
Author(s) Xianshao Zou		Sponsoring organization	
Title and subtitle Dynamics of Photogenerated Charge Carriers in III-V Bulk and Nanowire Semiconductors			
Abstract <p>As a solution to solving energy consumption and environment problems, photovoltaics has become one type of the promising devices to convert solar energy into electricity directly. In some special areas like in space, a kind of photovoltaics with lightweight and reliable properties is needed to supply power. Therefore, photovoltaics based on the group III-V semiconductor nanowires has been emerged and developed nowadays. However, a large surface-to-volume ratio in nanowires leads to high-density surface traps and therefore could degrade the performance of photovoltaics. In general, the properties of applications are dominated by the behaviours of charge carriers in semiconductors. Therefore, it is important to understand all processes which are related to charge carriers in semiconductors.</p> <p>In this thesis, a series of surface passivation methods are applied to lower the density of trap states and consequently improve the lifetime of photogenerated charge carriers in group III-V bulk and nanowire materials. We show that the GaNAs and AlGaAs passivation layers help to lower the trap density at the GaAs surface. Similarly, we have investigated the $Al_yIn_{(1-y)}P$ passivated $Ga_xIn_{(1-x)}P$ nanowires with a great potential for multi-junction photovoltaic applications. Concerning InP nanowires, we investigated why optimal HCl etching provides less surface defects. Although the density of surface defect in InP is lower than in GaAs, an insulating layer is still needed to isolate the active InP nanowires and the electrodes. In this respect, we demonstrated that an appropriate PO_x/Al_2O_3 capped layer works as a passivation and insulating layer.</p> <p>By means of several steady-state and time-resolved spectroscopies, such as time-resolved photoluminescence, transient absorption, and time-resolved terahertz spectroscopy, prospective passivation layers or conditions are screened for GaAs bulk, GaAs NW, InP NW, and GaInP NW materials. On the fundamental side, we find that charge trapping by several types of trap states dominates the primary steps of charge carrier dynamics and results in predominantly non-radiative recombination of photogenerated charges. Some trapping channels can be saturated via high charge generation rate under irradiation of the semiconductors by high intensity short optical pulses. Meanwhile, the atomic composition in ternary semiconductors, like Ga in $Ga_xIn_{1-x}P$ NWs plays a crucial role in the unexpected formation of deep traps. With the increase of Ga fraction, the fast electron trapping, hole trapping, and non-radiative recombination become more efficient.</p> <p>These spectrum studies in this thesis not only help us to select a potential passivation method for group III-V bulk and nanowires materials, but also reveal the carrier behaviour in these materials. Based on these understanding, several methods of characterization of the optoelectronic materials performance are derived.</p>			
Key words Time-resolved spectroscopy, group III-V semiconductor, nanowires, carrier recombination, trapping, passivation			
Classification system and/or index terms (if any)			
Supplementary bibliographical information		Language English	
ISSN and key title		ISBN 978-91-7422-750-5 (Print) 978-91-7422-751-2 (PDF)	
Recipient's notes		Number of pages: 122	Price
		Security classification	

I, the undersigned, being the copyright owner of the abstract of the above-mentioned dissertation, hereby grant to all reference sources permission to publish and disseminate the abstract of the above-mentioned dissertation.

Signature 



Date 2020-09-10

Dynamics of Photogenerated Charge Carriers in III-V Bulk and Nanowire Semiconductors

Xianshao Zou



LUND
UNIVERSITY

Coverphoto by Yajun Shi, Bo He, and Xianshao Zou.

Copyright pp i-xv and pp 1-96 (Xianshao Zou)

Paper 1 © American Chemical Society

Paper 2 © All authors (manuscript unpublished)

Paper 3 © Royal Society of Chemistry

Paper 4 © American Chemical Society

Paper 5 © All authors (manuscript unpublished)

Paper 6 © All authors (manuscript unpublished)

Faculty of Science

Department of Chemistry

Division of Chemical Physics

ISBN 978-91-7422-750-5 (Print)

ISBN 978-91-7422-751-2 (PDF)

Printed in Sweden by Media-Tryck, Lund University

Lund 2020



Media-Tryck is a Nordic Swan Ecolabel certified provider of printed material. Read more about our environmental work at www.mediatryck.lu.se

MADE IN SWEDEN 

*To my family,
and the people who care about me.*

勤、谨、和、缓。



勤吃苦耐劳；谨，
不苟且，不潦草，小
心求证；和，做学问
要和气，虚心，不却
火气；缓，就是不
急，不轻易下结论。

字给外孙贤助

壬辰年初夏甫



——出自朱熹《小学》

Diligently, Prudently, Harmoniously, and Patiently.

——From *《Primary Learning》* by Zhu Xi (1130 – 1200 A.D.)

Table of Contents

Abstract	i
Popular Science Summary	ii
Acknowledgement.....	v
List of Publications.....	ix
My Contribution to the Publications	x
Publications are not included in the thesis	xi
Abbreviations	xiii
Chapter 1 Introduction	1
1.1 Background	1
1.1.1 Current Situation of Energy Consumption	1
1.1.2 Problems in Global Energy Mix	2
1.1.3 Solutions to Optimize Energy Consumption Structure	3
1.2 Technological Development of Solar Cells.....	5
1.3 Principles of P-N Junction Solar Cells	7
1.4 Group III-V Semiconductor Materials	9
1.5 Group III-V NWs Semiconductor and Its Photovoltaic Applications....	10
1.6 Passivation in Group III-V Semiconductor	12
1.7 Photo-physical Processes in Group III-V NWs Semiconductor.....	15
1.8 Spectroscopy Study in Group III-V NWs Semiconductor	19
1.8.1 Exciton Recombination	19
1.8.2 Ultrafast Carrier Dynamics.....	19
1.8.3 Doping Correlated Carrier Recombination.....	20
1.8.4 Surface Passivation.....	21
Chapter 2 Experimental Methods.....	23
2.1 Steady-state Spectroscopy	24
2.1.1 Steady-state Absorption.....	24
2.1.2 Steady-state Photoluminescence and Absolute Quantum Yield.	26
2.1.3 Models for Analysing Carrier Recombination by PLQY	28
2.2 Time-resolved Spectroscopy	32
2.2.1 Transient Absorption (TA)	32
2.2.2 Time-resolved Terahertz Spectroscopy (TRTS).....	35
2.2.3 Time-resolved Photoluminescence (TRPL)	37

Chapter 3 Results & Discussion	39
3.1 Carrier Recombination Processes in GaAs Bulk Wafers Passivated by Wet Nitridation.....	39
3.2 Carrier Dynamics in Core-shell AlGaAs/GaAs NWs array	49
3.3 Growth Improvement in InP NWs by Hydrogen Chloride Etching	60
3.4 Carrier Recombination Processes in $Ga_xIn_{1-x}P$ NWs	66
3.5 Surface Passivation of $Ga_xIn_{(1-x)}P$ NWs by $Al_yIn_{(1-y)}P$	73
3.6 The Influence of Oxides Passivation on Photovoltaic InP NWs	79
Chapter 4 Conclusion.....	81
Outlook.....	83
References	85

Abstract

As a solution to solving energy consumption and environment problems, photovoltaics has become one type of the promising devices to convert solar energy into electricity directly. In some special areas like in space, a kind of photovoltaics with lightweight and reliable properties is needed to supply power. Therefore, photovoltaics based on the group III-V semiconductor nanowires has been emerged and developed nowadays. However, a large surface-to-volume ratio in nanowires leads to high-density surface traps and therefore could degrade the performance of photovoltaics. In general, the properties of applications are dominated by the behaviours of charge carriers in semiconductors. Therefore, it is important to understand all processes which are related to charge carriers in semiconductors.

In this thesis, a series of surface passivation methods are applied to lower the density of trap states and consequently improve the lifetime of photogenerated charge carriers in group III-V bulk and nanowire materials. We show that the GaNAs and AlGaAs passivation layers help to lower the trap density at the GaAs surface. Similarly, we have investigated the $\text{Al}_y\text{In}_{(1-y)}\text{P}$ passivated $\text{Ga}_x\text{In}_{(1-x)}\text{P}$ nanowires with a great potential for multi-junction photovoltaic applications. Concerning InP nanowires, we investigated why optimal HCl etching provides less surface defects. Although the density of surface defect in InP is lower than in GaAs, an insulating layer is still needed to isolate the active InP nanowires and the electrodes. In this respect, we demonstrated that an appropriate $\text{PO}_x/\text{Al}_2\text{O}_3$ capped layer works as a passivation and insulating layer.

By means of several steady-state and time-resolved spectroscopies, such as time-resolved photoluminescence, transient absorption, and time-resolved terahertz spectroscopy, prospective passivation layers or conditions are screened for GaAs bulk, GaAs NW, InP NW, and GaInP NW materials. On the fundamental side, we find that charge trapping by several types of trap states dominates the primary steps of charge carrier dynamics and results in predominantly non-radiative recombination of photogenerated charges. Some trapping channels can be saturated via high charge generation rate under irradiation of the semiconductors by high intensity short optical pulses. Meanwhile, the atomic composition in ternary semiconductors, like Ga in $\text{Ga}_x\text{In}_{1-x}\text{P}$ NWs plays a crucial role in the unexpected formation of deep traps. With the increase of Ga fraction, the fast electron trapping, hole trapping, and non-radiative recombination become more efficient.

These spectrum studies in this thesis not only help us to select a potential passivation method for group III-V bulk and nanowires materials, but also reveal the carrier behaviour in these materials. Based on these understanding, several methods of characterization of the optoelectronic materials performance are derived.

Popular Science Summary

Do you know where the most energy we are using comes from directly or indirectly? It is the sun. From IEA (the International Energy Agency) data in 2019, coal, oil, and gas dominate 77.5% energy consumption in the world in 2017. Originally, these energy sources all come from the sun but with more additional complicated chemical reactions. Although using coal, oil, gas and other types of fossil fuel could be currently the most convenient and the cheapest way for people to get energy, the efficiency for naturally regenerating these kinds of sources is fairly low due to the extremely long reaction period. So, these energy sources are defined as non-renewable energy sources. In addition to the non-renewable nature, the contaminants from burning fossil fuel continuously damage our environment, leading to global warming, species extinction, and respiratory diseases. Therefore, finding a novel way to solve the energy needs yet avoiding pollution problems is urgent. Most people may know that photovoltaics now is widely used as renewable energy generating devices that can convert light energy directly into electricity. Sweden has been chasing the replacement of traditional energy sources with renewable energies. From the data reported by the Swedish Energy Agency (Energimyndigheten), it is not surprising that in 2019, the total installed capacity of the solar cells in Sweden amounted to 698 MW (increased by ~70% between 2018 and 2019) and this number is constantly increasing.

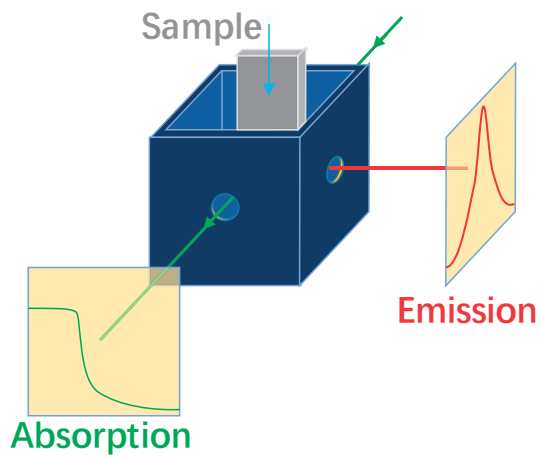
With regards to photovoltaics, only some specific materials have been shown to be efficient. For differentiating materials by electrical properties, we can roughly classify materials into three categories, of which, conductors (like metal) and insulators (like plastic, rubber, and ceramic) are the most common types in our minds. However, as the third type of material, semiconductors (like silicon), which has a conductive capacity between a conductor and an insulator, are very rare in nature but still can be artificially synthesized. This kind of semi-insulating materials has been widely used in the manufacture of electronic chips for various integrated circuits, different types of light-emitting diodes, and of course for solar cells.

Although the best efficiency of photovoltaics has reached 39.2% under 1 sun and 47.1% under 143 suns, it is still a challenge to manufacture high-efficiency, low-cost, and anti-photocorrosive photovoltaics to wide energy conversion applications. In pursuit of excellent photovoltaics, materials science, interface and surface engineering, and manufacturing technologies have been broadly studied. Based on existing materials and device fabrication methods, interface and surface properties of optoelectronic materials appear as key factors to determine the optoelectronic performance of photovoltaics. It is very similar to that the rusty layer at the surface of the iron products deteriorates the mechanical properties. Therefore, to improve the performance of semiconductor materials and further to obtain high efficiency and long durability of the corresponding solar cells, careful surface treatments

called “passivation” should be conducted to reduce the defects on the surface of the semiconductors, especially in nanoscale semiconductors, which have higher surface defect density than bulk semiconductor materials. To test the surface passivation effects, ordinarily, the most direct way is to test the performance of the photovoltaic devices through measuring the generated power of the devices. However, it is tedious, very time consuming and therefore is not the most efficient approach for researchers in materials and surface science. Although some techniques, such as electroluminescence, have been developed for characterizing the performance of the photovoltaic correlated materials, it is still a problem to realize the non-contact measurement. Therefore, in recent decades, optical methods arise at this opportune moment.

In our daily life, optical technology has been used to solve common problems. For example, the application of optical polarization techniques to achieve selective transmission of specific polarized light has led us to apply them to cameras, sunglasses, 3d movies, and virtual reality. Of course, the use of optics is much wider than this, including some advanced high-tech applications. For example, optics can be used for the purpose of recording information. Similar to that our eyes can sense light by its wavelength and intensity, and consequently transfer the signal to the information about the object we are looking at, in the investigation of semiconductor materials, we also can use novel spectroscopic techniques to detect the light which can interact with materials non-destructively and quickly. Light carries information what we can extract from the materials and then reflects the performance of them.

In this thesis, a variety of surface passivation methods were used to address the effects of surface defect states of semiconductor materials on the performance of optoelectronic devices. We used several spectroscopic techniques to study the properties of semiconductor materials before and after passivation effect in photoelectric conversion applications. For example, transient absorption, fluorescence, and terahertz techniques are employed to analyse the trapping and recombination processes of electrons and holes in semiconductors. However, these techniques we currently used still can be improved in terms of cost and measurement time. We expect that soon when researchers manufacture a range of semiconductor materials, what they need to do is just put samples into spectroscopy test equipment. After a fast light-matter interaction, the output light with matter information tells researchers the properties of the materials. If this technique comes true, it will greatly reduce the amount of work on the materials, increase research efficiency, and accelerate our use of high-efficiency, low-cost, stable, and environmentally friendly renewable energy conversion devices.



**Insert sample; Light comes in;
Spectrum comes out.
Output: Good or bad material?**

Acknowledgement

It has been a great pleasure to work with so many outstanding researchers in such an unforgettable city over the past four years. I feel so lucky to have this opportunity to complete my doctoral studies here. If without the concern, help, and guidance from all of them, I have to say, it is impossible to finish my Ph.D. work successfully. Thank them all! I appreciate my motherland and Sweden for financial support, dear family, supervisors, colleagues, and friends for many understanding and assistance.

First of all, I would like to thank my family for selfless love, endless understanding, and strong support. Especially to my parents, they always gave me a lot of freedom and financial support to do what I am interested in. To my grandmothers, they always make me lots of delicious food and make me grow up healthy. To my grandfathers, they taught me a lot about nature, science, technology, and the living truth. I still keep a series of encyclopaedias as a gift from one of my grandfathers when I was a teenager. These books were the beginning of my interest in science and technology. To all of my family, I must say thank you and I love all of you forever!

Throughout this four-year study, I would like to deeply thank my main supervisor, Prof. Arkady Yartsav, for his guidance and support both in my studies and in my life. I still remember that he insisted to pick up me in Malmö Sturup Airport at around 11 p.m., and luckily, I first time saw such a strong and tall deer on the side of the road when he drove me to my dormitory at that night. We had great memories of playing soccer and basketball, having meetings in Sweden and China, and working and travelling together in Guangzhou and Xi'an. During his guidance, teaching, and discussion, I realize that he has a very professional and rigorous attitude toward research. In most of the experiments, he shows very rich experience, great skills, and superior talents. I feel fortunate to have had the opportunity to join in his research group and have learned much knowledge and skills from him. Besides, I must say sorry to him for pushing him too much when he was very busy most of the time.

Next, I appreciate my two co-supervisors, Prof. Wei Zhang and Prof. Ergang Wang for their help and discussions with me. To Wei, he spent a lot of time training me in the Time-resolved Photoluminescence lab. He always answers my questions with much patience. We discussed very often even he had left Lund. He shows very experienced experiment skills, good and deep thinking, and efficient working attitude. In addition to my co-supervisor, Wei is also one of my best friends. I still miss I dined, drank, watched movies, and travelled together with him and his whole family. To Ergang, many thanks to him for recommending me to Arkady. He knows which subjects and projects are suitable for me. We had much cooperation in polymer solar cells. I saw he has a very deep understanding of chemistry and physics

in conjugated polymer and its applications. I am looking forward to more collaboration with both of them.

It is a pleasure to acknowledge Prof. Tõnu Pullerits not only for his contribution to the establishment of good research environment in Chemical Physics and keeping the department running well, but also for talented modelling for trap filling processes in GaAs nanowires materials. His preciseness and efficiency impressed me a lot. I am also indebted to Prof. Ebbe Nordlander and Chuanshuai Li for chemical risk assessment and so many times dangerous wet experiments. Without their help, I cannot have any chances to study the surface influence of semiconductor performance. I worked with Dr. Nicklas Anttu at Altto University in one project. He shows professional skills in modeling and computing. Several discussions we had in this project impressed me a lot. These discussions were also helpful to spawn the manuscript. Dr. Daniel Finkelstein-Shapiro was an important help for designing and manufacturing a good optical chamber. Besides, his spot-on comments provide many novel ideas and improvement basis on his deep understanding. It is also a pleasure to thank Prof. Ivan Scheblykin for his helpful suggestion in several accurate measurements, for the laser safety walls in TRPL lab, and for showing me many experiences in the workshop. I still remember that the automobile tyre problem gave him a very bad and unforgettable experience when he went for a meeting in Linköping. I must present my apology to him. To Prof. Donatas Zigmantas, I am thankful to him for exactly find the problem in our QY modelling, for his beam profiler suggestion, for instrument handling in the workshop, and for the course and study plan arrangement and organizing.

In two polymer projects, I am very grateful for Prof. Geng Dong and Guanzhao Wen's molecular structure simulation by using Density Functional Theory (DFT). In the nanowire piezoelectric project, I would like to thank Weihua Lin for the TA measurement and Jie Meng for EDS, SEM, and TEM measurement. In Group III-V semiconductor project, I truly enjoyed the collaboration with Prof. Magnus Borgström, Dr. Xulu Zeng, Lukas Hrachowina, Austin Irish, Dr. Aditya Prakash Saxena, David Alcer, Dr. Yang Chen, Dr. Yuwei Zhang, and Dr. Enrique Barrigón in Physics at LU; Dr. Erik Svensson, Dr. David Lindgren, and Dr. Yuxuan Sun from SolVotais AB. For several other project cooperation with Dr. Xiaofeng Xu and Dr. Qunping Fan at CTH; Prof. Dongfeng Dang at XJTU; Prof. Feng Gao and Jianwei Yu at LiU; Prof. Xingfu Wang, Jiangqi Dong, and Kang Zhang at SCNU; Prof. Xugang Guo and Dr. Huiliang Sun at SUSTech; Prof. Kaibo Zheng, Qian Zhao, Jie Meng, Mingli Liang at DTU; Prof. Jiamin Cao at HUST; Dr. Wenyan Su at Soochow University; Qiao Wang at GISIT, GDAS, I feel very grateful that I can work and discuss together with them. Thanks a lot!

In our research group, Dr. Xiaojun Su, Yuchen Liu, Dr. Fei Ma, Dr. Zehan Yao, Yen Hoang Hai Tran, and Dr. Pierre-Adrien Mante provided great support in my

research and my life. The nice cooperation and interesting discussion speed up my projects. We exchanged knowledge, experimental experiences, and ideas many times. Thank them so much. In many experiments, so many colleagues helped me a lot. Particularly, I must thank Dr. Pavel Chábera, Dr. Jens Uhlig, and Jun Li for the safety assessment and experiment arrangement for the laser lab and wet lab. I believe every colleague in Chemphys has kindly provided their help. However, I am sorry for that I cannot say thank you to them one by one, but still, I am grateful for their help. Thank Dr. Dan Hessman in Division of Solid State Physics for helping me solve some problems in the physics of semiconductor. His course on semiconductors was very useful in helping me understand the properties of semiconductor materials.

Every now and then, my former supervisors, Prof. Yong Zhang and Prof. Yanqing Tian concern me a lot. They helped me so much in experimental skills and in fabricating my scientific thinking and logic. They always continuously teach me how to do the research, show me some up-to-date interesting research papers, and tell me the research environment trends in China. Every time when I visited them, they always kindly ordered a hotel for me, and invited me to dinner together. Meanwhile, some samples are provided by them without any hesitation when I asked them. So, I appreciate them for endless support and many constructive suggestions.

I also would like to thank Dr. Meiyuan Guo, Dr. Torbjorn Pascher, Wenzhong Xia, Editor-in-Chief Cangzhu Xu, Dr. Jiawei Jiang, Dr. Bi Wang, Yuhan Ma, Dr. Xuedan He, Qiong Zhong, Zehua Li, Bo He, and Yajun Shi for business cooperation. I must to say it is very interesting and exciting to work with them. It was a very good experience to apply commercial funding together with Dr. Meiyuan Guo, Wenzhong Xia, Dr. Xuyan Lan, Dr. Shang Xiang, Dr. Hai Zhu, and Dr. Fan Wu. Thanks a lot for their support.

Thank many friends (Dr. Bing Yang, Dr. Chen Sun, Chuanshuai Li, Dr. Fan Wu, Dr. Fengying Zhang, Dr. Huifang Geng, Juanzi Shi, Jun Li, Dr. Junsheng Chen, Dr. Meiyuan Guo, Meng Dan, Dr. N. Sessa Bamini, Qi Shi, Rui An, Dr. RuiYun Chen, Weihua Lin, Dr. Xiaojun Su, Yang Liu, Yong Li, Yuchen Liu, Yunqian Zhong, Dr. Zehan Yao, Zhengjun Wang in Chemical Physics, LU; Dr. Chen Liu, Prof. Geng Dong, Haiyue Gong, Dr. Haoran Yu, Hong'e Zhou, Hong Jiang, Dr. Huiting Ma, Dr. Jian Li, Dr. Jingyuan Zhu, Dr. Lingdong Jiang, Lingping Zhang, Dr. Lu Yu, Mi Huang, Nan Hu, Dr. Rui Lu, Dr. Taiping Lu, Xiaoqin Hou, Xin Liu, Dr. Yi Lu, Yutang Li, Dr. Zhong Ren, and Dr. Xiao Cai in Science, LU; Dr. Changfei Zhou, Dr. Chao Wang, Cheng Qian, Dong An, Jie Zhang, Dr. Jing Zhang, Jixing Ding, Dr. Qianjin Li, Kena Li, Yuchen Yang, Yajun Huang, Jing Yang, Yan Li at LTH; Shaoxiao Chen, Dr. Sunxun Pan, Xiaoyan Xu, and Zhonghao Pan in BMC, LU; Dr. Wenjun Wen in Economics, LU; Dr. Shiwen Lei in Mathematics, LU; Dr. Shuangyi

Li in Literature, LU; Dr. Bei Yang, Dr. Jun Yuan, Dr. Qinzhen Bian, Dr. Rui Zhang, and Dr. Xuehong Zhou at LiU; Gongjin Lan at VU; Dr. Xiujuan Qiao at SLU; Yanxia Yu at KU Leuven; Yao Wang, Yuchen Cheng, Yuhan Ma, Yue Wu, and so on), we went fishing, camping, BBQ, party, hiking, self-drive traveling, playing basketball, playing badminton, playing ping pong, playing tennis, playing board game, and picking wild vegetables. They make my life colourful. Thanks a lot!

Ann-Christin Wikander, Caroline Lindblom, Maria Lövgren, Linnéa Hellman, and many other KILU people provided a lot of help to me over the past four years. Many thanks to them. Paula Leckius gave me so much help in text and figures layout in my thesis. I'm so grateful to her. I also would like to thank Prof. Wei Zhang, Dr. Meiyuan Guo, Dr. Qinzhen Bian, and Dr. Zehan Yao again for proofreading my thesis. Thank Prof. Tze-Chien Sum, Prof. Fengling Zhang, Prof. Saulius Marcinkevičius, and Prof. Irina Buyanova for taking the time to come to my defence.

Finally and importantly, I would like to thank the financial supports from China Scholarship Council (CSC), Royal Physiographic Society of Lund in Sweden, Guangzhou University (GU), Southern University of Science and Technology (SUSTech), and South China Normal University (SCNU).

Xianshao Zou

Lund, September 10th, 2020

List of Publications

This thesis is based on the following publications. All publications have been attached in their current state by the end of the thesis.

- I. **Zou, X.**; Li, C.; Su, X.; Liu, Y.; Finkelstein-Shapiro, D.; Zhang, W.; Yartsev, A. Carrier Recombination Processes in GaAs Wafers Passivated by Wet Nitridation. *ACS Appl. Mater. Interfaces* **2020**, *12* (25), 28360–28367.
- II. **Zou, X.**; Svensson, E.; Anttu, N.; Meng, J.; Lindgren, D; Su, X.; Sun, Y.; Wang, Z.; Zheng, K.; Zhang, W.; Pullerits, T.; Yartsev, A. Photoinduced Luminescence Measurements for Quantifying Carriers Recombination in GaAs/AlGaAs Core-shell Nanowires. *Manuscript*.
- III. Su, X.; Zeng, X.; Němec, H.; **Zou, X.**; Zhang, W.; Borgström, M. T.; Yartsev, A. Effect of Hydrogen Chloride Etching on Carrier Recombination Processes of Indium Phosphide Nanowires. *Nanoscale* **2019**, *11* (40), 18550–18558.
- IV. Zhang, W.; Zeng, X.; Su, X.; **Zou, X.**; Mante, P. A.; Borgström, M. T.; Yartsev, A. Carrier Recombination Processes in Gallium Indium Phosphide Nanowires. *Nano Lett.* **2017**, *17* (7), 4248–4254.
- V. Zeng, X.; Zhang, W.; **Zou, X.**; Su, X.; Yartsev, A.; Borgström, M. T. *In situ* Surface Passivation of Ga_xIn_(1-x)P Nanowires by Radially-grown Al_yIn_(1-y)P shells. *Manuscript*.
- VI. Hrachowina, L.; **Zou, X.**; Chen, Y.; Zhang, Y.; Barrigón, E.; Yartsev, A.; Borgström, M. T. Imaging the Influence of Oxides on the Electrostatic Potential of Photovoltaic InP Nanowires. *Submitted*.

My Contribution to the Publications

- I. I performed the wet passivation experiment with Chuanshuai Li, the PL QY and TRPL experiments, data analysis, discussion arrangement, and interpretation. I was responsible for writing the major part of the paper.
- II. I built and calibrated the absolute QY measurement setup, and performed the PL QY and TRPL experiments, data analysis, QY date modelling and fitting, interpretation, and discussion arrangement. I was responsible for writing the major part of the paper.
- III. I performed the PL QY and TRPL experiments, PL QY and TRPL data analysis, interpretation, and discussion. I contributed to the paper writing.
- IV. I performed the PL QY and TRPL experiments, PL QY and TRPL data analysis, and interpretation. I contributed to the paper writing.
- V. I performed the TRPL experiments, TRPL data analysis, interpretation, discussion, and comment. I contributed to the paper writing.
- VI. I performed the TRPL experiments, TRPL data analysis, interpretation, discussion, and comment. I contributed to the paper writing.

Publications are not included in the thesis

- I. **Zou, X.**; Wen, G.; Hu, R.; Dong, G.; Zhang, C.; Zhang, W.; Huang, H.; Dang, W. An insight into the excitation states of n-type small molecular semiconductor Y6. *Molecules, Just Accepted*.
- II. Wen, G.*; **Zou, X.***; Hu, R.; Chen, Z.; Zhang, W.; Dong, G. Study on the Chromophore Structure of Polymer Photovoltaic Material N2200. *Submitted*.
(*These authors contributed equally)
- III. **Zou, X.***; Dong, J.*; Zhang, K.; Lin, W.; Guo, M.; Zhang, W.; Wang, X. Effect of piezotronic on carrier recombination processes in InGaN/GaN multiple quantum wells microwire. *Manuscript*.
(*These authors contributed equally)
- IV. Li, C.; **Zou, X.**; Lin, W.; Mourad, H.; Meng, J.; Liu, Y.; Abdellah, M.; Guo, M.; Zheng, K.; Nordlander, E. Unveiling Charge and Energy Transfer Dynamics in a g-C₃N₄/CdSe quantum dot/iron carbonyl cluster Composite that enhances Photocatalytic Hydrogen Evolution. *Submitted*.
- V. Dong, J.; Zhang, K.; Wang, B.; **Zou, X.**; He, L.; Jiang, J.; Wang, Q.; Li, S.; Wang, X. Centimeter-Long III-Nitride Nanowires and Continuous-Wave Pumped Lasing Enabled by Graphically Epitaxial Lift-Off. *Submitted*.
- VI. Sun, H.; Liu, B.; Yu, J.; **Zou, X.**; Zhang, G.; Zhang, Y.; Zhang, W.; Su, M.; Fan, Q.; Yang, K.; Guo, H.; Gao, F.; Guo, X. Reducing Energy Loss via Tuning Energy Levels of Polymer Acceptors for Efficient All-Polymer Solar Cells. *Sci. China Chem.* **2020**, 1–8.
- VII. Liu, S.; Su, W.; **Zou, X.**; Du, X.; Cao, J.; Wang, N.; Shen, X.; Geng, X.; Tang, Z.; Yartsev, A.; Zhang, M.; Gruber, W.; Unruh, T.; Li, N.; Yu, D.; Brabec, C. J.; Wang, E. The Role of Connectivity in Significant Bandgap Narrowing for Fused-Pyrene Based Non-Fullerene Acceptors toward High-Efficiency Organic Solar Cells. *J. Mater. Chem. A* **2020**, 8 (12), 5995–6003.
- VIII. Tang, Y.; Liang, M.; Zhang, M.; Honarfar, A.; **Zou, X.**; Abdellah, M.; Pullerits, T.; Zheng, K.; Chi, Q. Photodetector Based on Spontaneously Grown Strongly Coupled MAPbBr₃/N-RGO Hybrids Showing Enhanced Performance. *ACS Appl. Mater. Interfaces* **2020**, 12 (1), 858–867.
- IX. Liang, M.; Lin, W.; Lan, Z.; Meng, J.; Zhao, Q.; **Zou, X.**; Castelli, I. E.; Pullerits, T.; Canton, S. E.; Zheng, K. Electronic Structure and Trap States of Two-Dimensional Ruddlesden–Popper Perovskites with the Relaxed Goldschmidt Tolerance Factor. *ACS Appl. Electron. Mater.* **2020**, 2 (5), 1402–1412.

- X. Zhang, W.; Hu, R.; Zeng, X.; Su, X.; Chen, Z.; **Zou, X.**; Peng, J.; Zhang, C.; Yartsev, A. Effect of Post-Thermal Annealing on the Performance and Charge Photogeneration Dynamics of PffBT4T-2OD/PC71BM Solar Cells. *Polymers (Basel)*. **2019**, *11* (3).
- XI. An, R.; Zhang, F.; **Zou, X.**; Tang, Y.; Liang, M.; Oshchapovskyy, I.; Liu, Y.; Honarfar, A.; Zhong, Y.; Li, C.; Geng, H.; Chen, J.; Canton, S. E.; Pullerits, T.; Zheng, K. Photostability and Photodegradation Processes in Colloidal CsPbI₃ Perovskite Quantum Dots. *ACS Appl. Mater. Interfaces* **2018**, *10* (45), 39222–39227.
- XII. Xu, X.; Li, Z.; Zhang, W.; Meng, X.; **Zou, X.**; Di Carlo Rasi, D.; Ma, W.; Yartsev, A.; Andersson, M. R.; Janssen, R. A. J.; Wang, E. 8.0% Efficient All-Polymer Solar Cells with High Photovoltage of 1.1 V and Internal Quantum Efficiency near Unity. *Adv. Energy Mater.* **2018**, *8* (1).

Abbreviations

$[N_e](t)$	Mobile carrier concentration
0D	Zero-dimension
1D	One-dimension
2D	Two-dimension
3D	Three-dimension
A	Trap-assisted recombination coefficient
A_1	Trapping rate which can be saturated
A_2	Trapping rate which cannot be saturated
AlGaAs	Aluminum gallium arsenide
AlInP	Aluminum indium phosphide
a-Si	Amorphous silicon
B	Bimolecular recombination coefficient
C	Auger recombination coefficient
CdTe	Cadmium telluride
CIGS	Copper indium gallium diselenide
CW	continuous wave
D	Density of nanowires
EO	Electro-optic
E_{photon}	Energy of one excitation photon
ESA	Excited-state absorption
FF	Fill factor
$G(t)$	Carrier generation rate
GaAs	Gallium arsenide
GaInP	Gallium indium phosphide
GaN	Gallium nitride
GaNAs	Gallium nitride arsenide
GSB	Ground-state bleach

HCl	Hydrogen chloride
HRTEM	High-resolution transmission electron microscopy
InP	Indium phosphide
IR	Infrared radiation
I_{sc}	Short-circuit current
k_g	Geminate recombination rate
k_{nr}	Rate of non-radiative recombination
k_r	Rate of radiative recombination
LDs	Laser diodes
LEDs	Light-emitting diodes
MMP	Maximum power point
MOVPE	Metal organic vapor phase epitaxy
N	Concentration of photogenerated charges
N_0	Concentration of background charges
N_e	Concentration of the free electrons
N_h	Concentration of the free holes
NREL	National renewable energy laboratory
NWs	Nanowires
PCE	Power conversion efficiency
PDs	Photo-detectors
$P_{Exc.}$	Excitation power
PL	Photoluminescence
PL QY	Photoluminescence quantum yield
PVs	Photovoltaics
QDs	Quantum dots
q_f	Fraction of filled traps
QWs	Quantum wells
RT	Room temperature

S/V	Surface volume ratio
SCs	Solar cells
SE	Stimulated emission
SEM	Scanning electron microscopy
SiO _x	Silicon oxide
SRV	Surface recombination velocity
SSPL	Steady-state photoluminescence
TA	Transient absorption
TCSPC	Time-correlated single photon counting
TEM	Transmission electron microscopy
TRPL	Time-resolved photoluminescence
TRTS	Time-resolved terahertz spectroscopy
U	Whole volume of the NWs
UV	Ultraviolet
V	Volume of NWs
V _{oc}	Open-circuit voltage
WZ	Wurtzite
ZB	Zincblende
$\Delta\sigma(t)$	Photoconductivity
η_{Abs}	Absorbance of the incident photons
μ_e	Electron mobility
μ_h	Hole mobility
τ	Lifetime
Φ	Absolute quantum yield
χ_{HCl}	Molar fractions of HCl

Chapter 1

Introduction

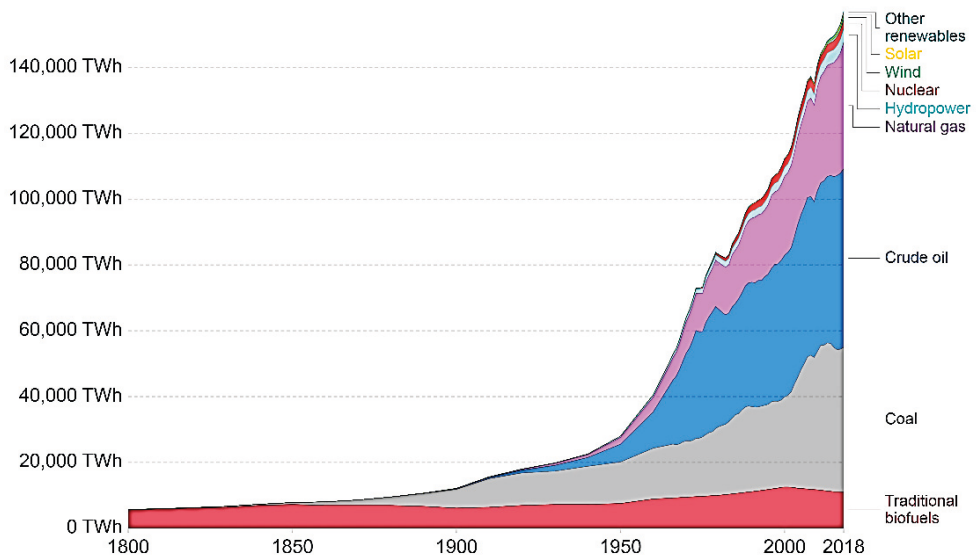
1.1 Background

In this section, the world's energy consumption, energy structure and environmental issues, as well as corresponding solutions, etc. will be addressed. The understanding and analysis of this section will lead us to the purpose of this thesis and the problem to be solved.

1.1.1 Current Situation of Energy Consumption

Global primary energy consumption

Global primary energy consumption, measured in terawatt-hours (TWh) per year. Here 'other renewables' are renewable technologies not including solar, wind, hydropower and traditional biofuels.



Source: Vaclav Smil (2017) and BP Statistical Review of World Energy

CC BY

Figure 1.1.1.

Global primary energy consumption. Reproduced with permission.¹ Copyright 2019, OurWorldInData and BP Statistical Review of World Energy.

Energy shortage is one of the most crucial problems in the 21st century. From 2010 to 2018, the global primary energy consumption has grown with the fastest rate of 2.9% in 2018. Although the consumption growth mainly comes via natural gas and renewable energy, the carbon emissions reached the fastest growth rate in the past seven years and increased by about 6×10^8 tons in 2018.¹ When we look at the structure of energy consumption in 2018 as shown in **Figure 1.1.1**, it is not hard to see that the traditional non-renewable energy sources such as oil, coal, and natural gas still dominate. Utilization of renewable energy source has grown tremendously compared to the past, but it has not kept up with the greater demands for the enormous energy consumption of modern society. This is, of course, an indication of the potential of renewable energies in the future energy consumption structure.

1.1.2 Problems in Global Energy Mix

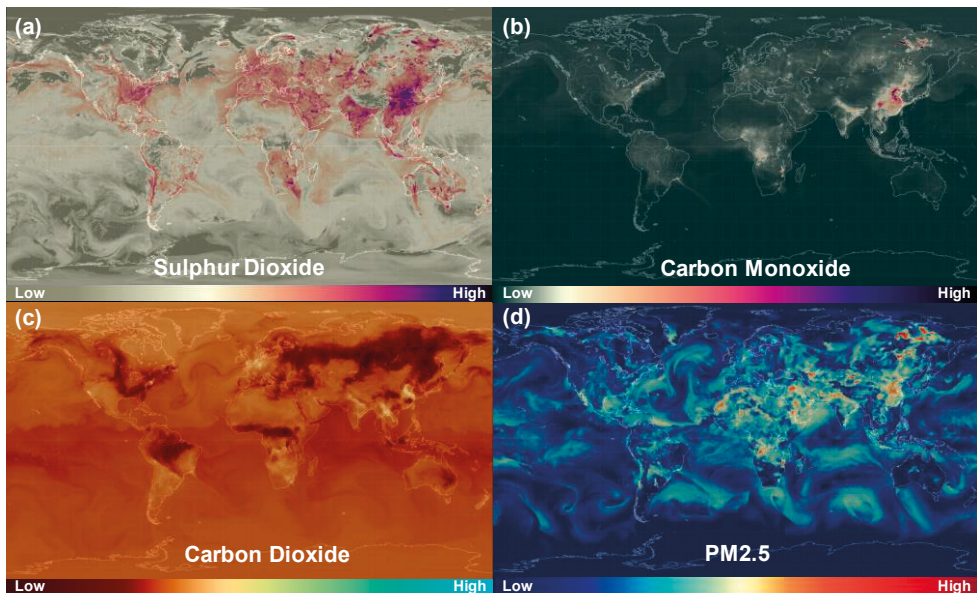


Figure 1.1.2. Concentration of (a) sulphur dioxide, (b) carbon monoxide, (c) carbon dioxide, and (d) PM2.5 close to the surface of the earth on July 14, 2020. Reproduced with permission. Copyright 2020, EarthWindMap and the data from the High Resolution Global Atmospheric Model (GEOS-5), the Global Modeling and Assimilation Office (GMAO), and the National Aeronautics and Space Administration (NASA).

For now, energy shortages could not threaten the survival of the human kind. The most severe problem may be caused by greenhouse gases and harmful particle matters, which are produced by burning fossil fuels. The events of the toxic smog in large cities like London smog and China smog are likely to be repeated for a

considerable period of time in specific regions. In some quickly developing countries with very high energy consumption such as China and India, emissions of the sulphur dioxide, carbon monoxide, carbon dioxide, and fine particulate matters like particles with size smaller than $2.5\ \mu\text{m}$ (called Particulate Matter $<2.5\ \mu\text{m}$ or PM $_{2.5}$) have led to the deterioration of air quality in those countries (see **Figure 1.1.2**). A series of greenhouse gases also have a humongous influence on ecology. The continued warming of the world is leading to the glaciers melting, sea levels rising, and loss of habitat and food shortages for animals. Extreme events in climate are also partly attributable to the high levels of greenhouse gas emissions. These effects have been more evident in recent years, with ice melting around the world, particularly at the poles of the planet, and global sea levels rising by 3.2 mm per year according to the report from the National Geographic. In some regions, there has been a marked increase in precipitation, but in contrast, others have become persistently dry, increasing the probability of forest fires. Frequent climate disasters as a result of these changes are threatening the survival of life.

1.1.3 Solutions to Optimize Energy Consumption Structure

To reduce greenhouse effect, production of harmful gases, and micro particulates emission led from fossil fuel combustion, using the renewable energy would be a good solution. In addition to nuclear energy, solar energy resource has a significant potential to become the main energy resource for our next generations. So far, the sun radiation as the largest renewable energy source in the world provides 1.2×10^{17} watts power to earth.² In 2018, however, the cumulative capacity of the installed optoelectronic conversion devices is about 5×10^{11} watts,³ which is just $\sim 0.0004\%$ of the sun energy that arrives to the surface of our planet. As a clean, inexhaustible, and not harmful energy source, solar energy is an extremely good candidate for human beings to supply our daily energy assumptions. Human beings have been harnessing solar energy for a long time through concentrating sun radiation for generating heat. But the need for energy goes far beyond simply heating. People need light at night, need air conditioner on hot summer days, and need computers for working and studying. The source of energy to make that happen is electricity. This led to the development of the solar cells (SCs), or photovoltaics (PVs), a kind of ideal devices for converting solar energy directly into electricity. However, human civilization has been working on improving the technology conversion of solar energy into electricity only for last few decades.

In the last decade, the PV industry has seen tremendous growth, especially in China. In 2019, China dominates the added SCs capacity (~ 30 MkW, 26.2%) and the cumulative SCs capacity (~ 205 MkW, 32.6%) in the global SCs capacity.⁴ In China, not only the SCs are used in some developed regions (like in Shenzhen as shown in **Figure 1.1.3a**) for power supply, but also the Chinese government innovatively

used the PVs for poverty alleviation. Like in Xinjiang province, every poor family possibly obtains about 6,000 CNY (~860 USD) per year via selling the surplus electricity to the power company.⁵ Even in some mountainous areas without enough sunlight, the low-income families can also benefit from the development of SCs. Such as in Zhulingcun Village, Ganzhou City, China, the government and the Chinese Academy of Social Sciences (CASS) helped 267 low-income families to build a SCs station (see **Figure 1.1.3b**) to supply them around 2,000 CNY (~300 USD) per family per year. The development of the PV industry not only can effectively reduce pollution, protect the environment, and improve the energy structure, but also plays an important role in promoting economic development, eradicating poverty and improving the life quality of residents.

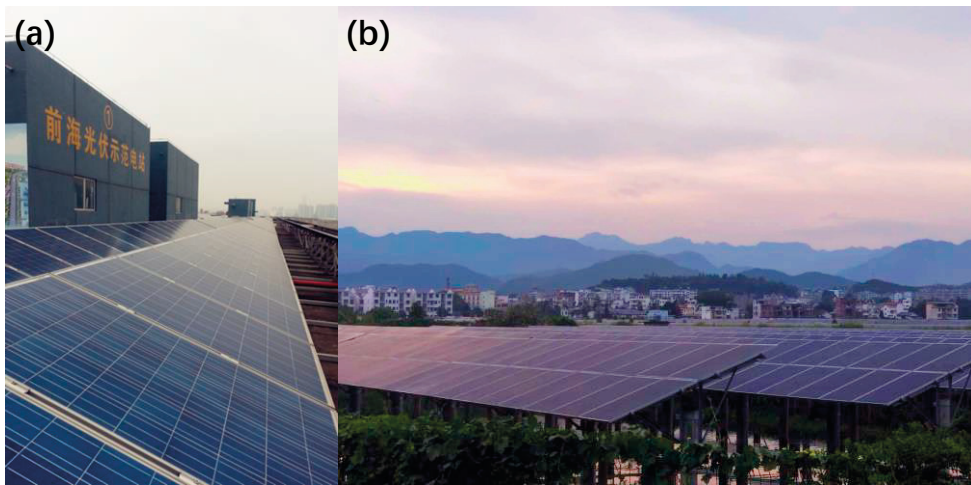


Figure 1.1.3. (a) A 1 MW PV project in Shenzhen, China. Copyright 2014, the author took on the 10th of March, 2014, at Qianhai Shenzhen-Hong Kong Cooperation Zone, Shenzhen, China. (b) A 30MW Fishery and Solar Complementary PV Power Generation Project in a remote countryside, Zhulingcun Village, Ganzhou City, China. Copyright 2019, the author took in Zhulingcun Village.

1.2 Technological Development of Solar Cells

SC is one kind of devices that can directly transfer the solar electromagnetic radiation to electric power. In 1839, the PV effect which also is known as the "Becquerel effect" was first discovered by a French physicist, Edmond Becquerel, through inserting metal rods into a conductive solution under light irradiation.^{6,7} Subsequently, the first functional SC with efficiency around 1% was developed by Charles Fritts through depositing a thin film gold on selenium in 1883.⁸ With the rapid development of solar technology, nowadays, SCs have progressed to the so-called "third-generation". The first-generation SCs usually using silicon as the fundamental material has been the most mature and most successful market dominant SCs type so far. However, the second-generation thin-film SCs including copper indium gallium diselenide (CIGS) SCs, cadmium telluride (CdTe) SCs, and amorphous silicon (a-Si) SCs, now are candidates to replace the first generation SCs, and becoming progressively dominating the market. Besides, nanostructure SCs, organic SCs, perovskite SCs, quantum dot SCs, and Dye-sensitized SCs as the third-generation of SCs are fabricated to overcome the Shockley-Queisser limit for single bandgap SCs, which is applicable to silicon wafer-based and the thin-film SCs.⁹ For comparison, these three SCs generations and the corresponding efficiency-cost projections are shown in **Figure 1.2.1a** and **Figure 1.2.1b**, respectively. It is obvious that in terms of efficiency and cost, state-of-the-art third-generation SCs is definitely the best solution so far!

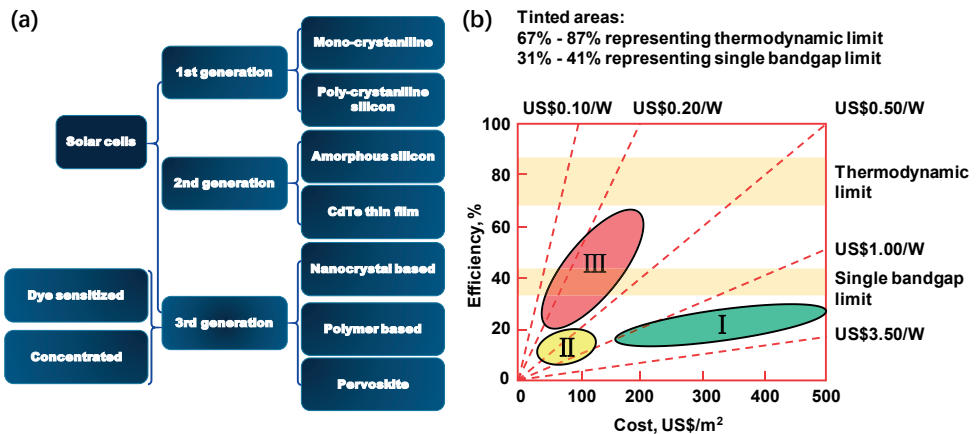


Figure 1.2.1.

(a) Three generations of SCs with their different type of SCs. (b) Efficiency and cost projections for first- (I), second- (II), and third- generation (III) PV technologies (wafer-based, thin films, and advanced thin films, respectively). Reproduced with permission.¹⁰ Copyright 2007, Elsevier.

From the best efficiencies of various types SCs reported in the National Renewable Energy Laboratory (NREL),¹¹ we find that this year, John F. Geisz et. al. in the NREL demonstrated a six-junction group III–V SCs with efficiencies of 47.1% and 39.2% under 143 suns and 1 sun, respectively.¹² This work got two record efficiencies which were measured under concentrated illumination and one sun illumination, presenting the extraordinary potential of SCs.

In some specific areas, such as energy supply systems in space, the power supply system is required to be sustainable, stable and lightweight. For example, in the application for the past decades, GaAs as a high stability and high charge mobility semiconductor has been the first used in single-junction GaAs SCs on the Soviet Union spacecrafts “Venera-2” and “Venera-3” launched in November 1965,¹³ and then it was applied in AlGaAs/GaAs SCs on the command module of MIR Space Station which was launched on March 13, 1986,¹⁴ due to the highly reliable performance and excellent radiation tolerance of the GaAs SCs in the high-temperature and high-energy particle radiation ambient environment. In addition to the multi-junction group III-V semiconductor SCs with the highest efficiency in the world, we, NanoLund, and our cooperater, Solvoltaics AB, also have got SCs efficiency records in InP and GaAs nanowires (NWs) SCs, respectively.^{15,16} This kind of third-generation SCs not only provides a lightweight solution to the problem of highly stable group III-V semiconductor-based SCs but also offers a potential to lower the materials consumption and thus the cost.

1.3 Principles of P-N Junction Solar Cells

The wide variety of SCs that have been invented one after another, the working principle of certain types of SCs has been described in detail in many reports, such as perovskite SCs,^{17–19} organic SCs,^{20–23} dye-sensitized SCs,^{24–28} copper indium gallium selenide SCs,^{29–31} plasmonic SCs,^{32,33} and quantum dots SCs.^{34–37} In this section, the working principle of inorganic p-n junction SCs will be highlighted.

In general, the basis of inorganic SCs is semiconductor materials, including silicon, germanium, gallium, and arsenide which have a conductivity between conductors and insulators. The electrical properties of semiconductors can be altered through adding external impurity atoms, which is called “doping”. If the dopant captures additional external electrons, leaving a hole in the valence band of the semiconductor as a result, this is called p-doping. Conversely, semiconductors are n-doped if the dopants lose their electrons and thus the conduction band obtains electrons. A single-junction SC is a simple junction composed of p-doped and n-doped semiconductors (see **Figure 1.3.1**). When these two types of semiconductor materials are combined, the electrons (“e”) will diffuse from the n-type semiconductor into the p-type semiconductor, and similarly, the vacancies of electrons (so-called holes, “h”) will diffuse from the p-type semiconductor into the n-type semiconductor. After diffusion and recombination of electron and hole carriers, an electric field is generated across the interface of p-type and n-type semiconductors in the direction from n-type to p-type. This built-in electric field working as a driving force to separate the photo-generated electrons and holes in space from the coulomb interaction is the most significant part of p-n junction SCs.

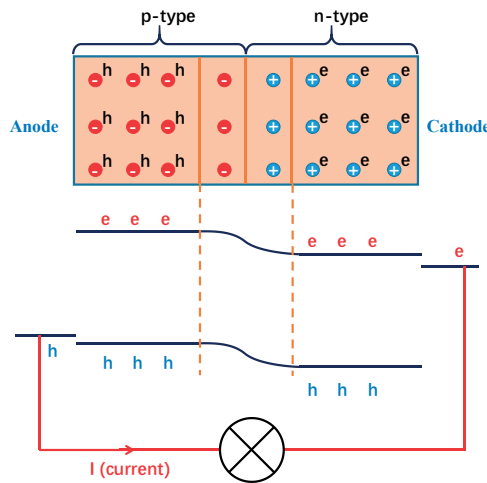


Figure 1.3.1. Schematic of the p-n structure and band structure of the single p-n junction SC.

To the optoelectronic conversion in a p-n junction SC, in brief, there are three main steps to convert the light to electricity. First, a SC absorbs the light and generates electron-hole pairs. These electrons and holes dissociate due to thermal fluctuations as the binding energy of the pair is much less than kT . Further, independent electrons and holes are separated by the built-in electric field at the p-n junction so that electrons move to the n-type and holes to the p-type semiconductors. Since the electrode has a work function that is the minimum energy necessary for an electron to escape from a metal surface, an electrode with a suitable work function has the ability to collect electrons and holes. Therefore, these electrons and holes in semiconductors can be finally collected by the cathode and anode, respectively. The difference of work function between cathode and anode can determine the open circuit voltage of the SCs. With an external circuit, the current travels from anode to cathode via a connected electric device.

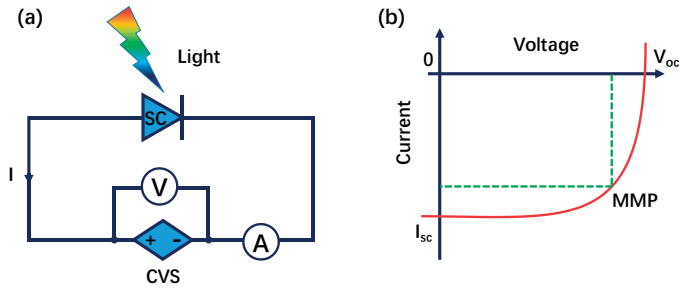


Figure 1.3.2. (a) Schematic of the I-V characteristic for SCs. (b) I-V curve.

Ordinarily, the open-circuit voltage (V_{oc}), short-circuit current (I_{sc}), maximum power point (*MMP*), fill factor (*FF*), and power conversion efficiency (*PCE*) from I-V characteristic curve are the most direct and key electric parameters to characterize the performance of a SC device. In general, the I-V characteristic curve is obtained through a test circuit as shown in **Figure 1.3.2a**, containing a controlled voltage source (CVS) with a voltmeter (V) and an ammeter (A). By adjusting the voltage of the CVS, the I-V curve (see **Figure 1.3.2b**) can be recorded by the voltmeter and ammeter. Obviously, to obtain these data, a complete SC device would need to be fabricated, which is a time-consuming and energy-intensive process for research work. Obviously, it is not friendly to researchers working on and improving the performance of SCs. Therefore, new techniques based on materials research should be developed to study the properties of optoelectronic materials. Through these novel techniques, researchers can predict the performance of the corresponding SCs based on the properties of the materials. In Section 1.8, optical study of the optoelectronic semiconductor will be presented as one of the techniques used for this purpose.

1.4 Group III-V Semiconductor Materials

Although the silicon PV technologies still dominate the worldwide SCs market, the group III-V materials like GaAs, InP, and GaInP have attracted significant interest because of their direct bandgap and high electron mobility. Their manufacturing cost has been further reduced by the improvement in the production processes of III-V semiconductors. This also offers a possibility of widespread use of these materials in modern research, industry, and people's daily life. Due to these advantages, group III-V semiconductors have extensive applications in electronic and optoelectronic devices, including not only SCs,^{38–42} but also light-emitting diodes (LEDs),^{43,44} laser diodes (LDs),^{45–49} and photo-detectors (PDs).^{50–52} In this thesis, three kinds of group III-V semiconductors, gallium arsenide (GaAs), indium phosphide (InP), and gallium indium phosphide (GaInP), will be addressed in relation to their SC applications.

In SC applications, particularly, GaAs is one of the most commonly used group III–V semiconductor materials. Although the majority of the SC systems are built based on silicon, in some application fields, GaAs has outperformed silicon. First, a thin GaAs film can absorb sunlight as well as much thicker silicon because of the higher absorption coefficient in the visible spectral ranges.^{53–56} In addition, GaAs has higher electron mobility, which can reduce charge recombination processes thus leading to higher SCs efficiency. Furthermore, GaAs can resist heat, moisture, and ionizing radiation, which makes it one of the best choices for space exploration.⁵⁷ Regarding InP, it is very similar to GaAs and is a good candidate to replace silicon in SC applications. Comparing to GaAs, InP has a larger absorption coefficient in visible light region, making it can harness more sunlight than GaAs. It also has an ideal bandgap of 1.35 eV close to the bandgap energy for obtaining the maximum PCE of SCs under AM1.5G terrestrial spectrum.^{56,58} Additionally, as InP is even more hard radiation-resistant than GaAs, it can be also used in high radiation fields.^{59,60} In contrast to the binary semiconductors, ternary GaInP materials have the advantage of the tunable bandgap via tuning the Ga/In composition. Depending on the composition of Ga, the bandgap of GaInP can be adjusted from 1.35 to 2.26 eV to meet the needs of the green-visible and near-infrared light absorption for device applications. GaInP is often used to be combined with other group III-V semiconductors, like GaAs, for tandem SCs to overcome the efficiency limit of single-junction SCs.^{61,62} Same as InP, GaInP materials have lower surface recombination or trap rate than GaAs.^{63–65} Therefore, it does not require extra surface passivation, which reflects the lower cost in materials synthesis and device manufacturing.

In conclusion, group III-V semiconductors have several advantages over silicon. This makes them an excellent alternative to silicon. We are looking forward to seeing their widespread use in technology, industry and life.

1.5 Group III-V NWs Semiconductor and Its Photovoltaic Applications

Nanoscience and nanotechnology have attracted growing attention and interest in the past decades due to their intriguing and special properties, such as lightweight, low driving power consumption, ultrasensitive, less influence of lattice mismatch and so on. Generally, nanomaterials have the size at least one-dimension in the range of 1 nm to 100 nm. Based on how many dimensions of materials are outside the nanoscale, nanomaterials can be classified as zero-dimension (0D) like quantum dots (QDs), one-dimension (1D) like NWs and nanotubes, and two-dimensions (2D) like thin film. As the size of semiconductors decreases, the energy levels gradually changes from continuous to discrete (see **Figure 1.5.1**) due to the confinement of the electronic wave function in the confined dimension.⁶⁶

Typically, as one kind of 1D materials, applications of NWs for SCs have several advantages, such as the fact that SCs with NW structures can reduce reflection, spatial separate, transport, and extract photo-generated charge carriers more efficiently than with bulk structure.^{15,67–69} Considering the advantages of group III-V materials, the corresponding NWs are prominent potential candidates for the next-generation SCs. Furthermore, because of the quantum confinement effects, the NWs exhibit distinctive electronic and optical properties. For example, quantum confinement effects in InP NWs can increase the bandgap, resulting in a shift of the PL emission peaks to higher energy when diameter of the InP NWs decreases. The tunable bandgap has the advantage in optimizing InP NWs for tandem SCs applications. Other applications of NWs LEDs and LDs offers possibility to tunable light sources.⁷⁰

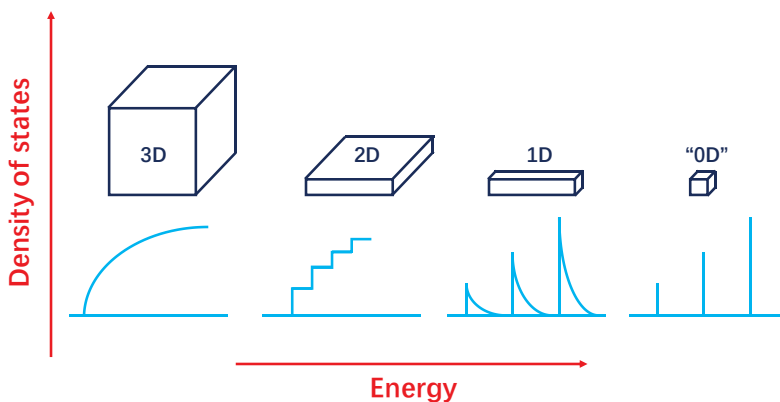


Figure 1.5.1.

Density of states in one band of a semiconductor as a function of dimension. Reproduced with permission.⁷¹ Copyright 2007, American Association for the Advancement of Science (AAAS).

In addition, the development of NWs-based SCs towards lower consumption of materials, which has the potential to lower the cost of PV conversion than planar devices.⁷² Admittedly, thin-film and nanoscale SCs are used to minimize the amount of materials used in SC applications. However, the utilization of thin films could reduce the absorption of light due to short absorption length and thus worsen the performance of SCs. In contrast, for NWs materials applied as SCs, the incident light concentration effect due to the waveguiding properties of NWs reduce reflection and then increase absorption efficiency, making the performance of these NWs SCs is even better than some SCs based on bulk materials.⁵⁸ In fact, by tailoring the length and diameter of NWs one can tune and optimize light absorption of the NWs based SCs.⁷³⁻⁷⁵ The lower materials consumption and favorable absorption that increase the power-to-weight ratio make the possibility to optimize a direction of portable applications, particularly in the space exploration field, such as providing the power supply to satellites and spacecraft.

More recently, SCs based on GaAs,^{16,76} InP,^{15,42,77} and GaAsP⁷⁸ NWs have been reported to have the PEC exceeding 10%, suggesting that these materials are promising building blocks for the next-generation of high-performance SC devices. However, the planar SCs, like for the GaAs with the bandgap of 1.45 eV, have the limiting un-concentrated illumination efficiency of ~29% according to the calculations assuming that electrons and holes recombine only radiatively.⁷⁹ According to the report from NREL,¹¹ the efficiency of single-junction GaAs solar has reached 27.8% which is very close to the efficiency limit. Although our collaborators from Solvoltaics AB, have developed NW-based SCs with the highest efficiency of 15.3%, which is the record in GaAs single-junction NW SCs around the world, the efficiency can still be improved further. For instance, improving surface quality therefore reduce trap density could one of the directions to increase the efficiency of SCs. Especially for the NWs-based SCs, the high surface-to-volume ratio (S/V) tends to result in high density of trap states on the surface leading to unwanted non-radiative recombination which deteriorates the performance of the NW SCs. Consequently, careful selection of surface optimization method and cautious treatment should be employed to minimize the surface defects without introducing more other defects as far as possible.

1.6 Passivation in Group III-V Semiconductor

The progress in group III-V technology has been impeded by a high density of states at the surface of semiconductors functioning as mobile charge trapping states, in particular in GaAs which has much higher surface trap states than InP. Under ambient conditions, an oxide layer is formed on the surface of GaAs, which is regarded to lead to charge trapping. Charge trapping reduces the free carrier lifetime and deteriorates the electronic properties of devices. In addition, the oxide layer is physically unstable and could be corroded over time, which could also worsen the performance of devices.

To reach the performance of the state-of-the-art GaAs-based optoelectronic devices, a variety of efficient surface chemical treatments have been developed. In general, these surface chemical treatments which are used to reduce trap density induced from the oxidation layer, dangling bonds, and defects on the surface of semiconductor are called “passivation”. After surface passivation of semiconductor, the trap density could be significantly reduced. One of the traditional but technically demanding passivation methods is an epitaxial growth, a process of growing a crystal on another crystal,⁸⁰ on the GaAs surface of a high bandgap layer, such as AlGaAs, GaP, Al₂O₃, and GaN. The encapsulation of GaAs by a wide-bandgap semiconductor not only creates energy barriers to localize the carrier within the NWs in the radial direction, but also reduces the surface trap density of the core semiconductors by reducing the dangling bond on the surface and preventing surface oxidation, thereby increasing the steady state PL intensity and slowing down the PL decay rate thus improving the performance of the GaAs-based devices.^{81,82} More than a dozen results show that this method can be used to successfully decrease the density of trap states in GaAs. Lars Samuelson’s group first compared the emission efficiency of GaAs NWs with- and without- GaInP shells and found that the passivation reduces surface states, leading to a PL improvement of 2 to 3 orders of magnitude.⁸³ Moreover, AlGaAs shell by Metalorganic Vapor Phase Epitaxy (MOVPE) and TiO₂ passivation shells through using a sol-gel chemistry method were also applied for increasing the PL intensity.^{84,85} Already early in 1977, people also reported the method of GaAs NW coating by a polymer polymethylsiloxane for successful surface passivating.⁸⁶

Michael B. Johnston and Laura M. Herz have used several polymers as protective layers for GaAs. Some of these polymer layers played a key role in enhancing the carrier lifetime (see **Figure 1.6.1**).⁸⁷

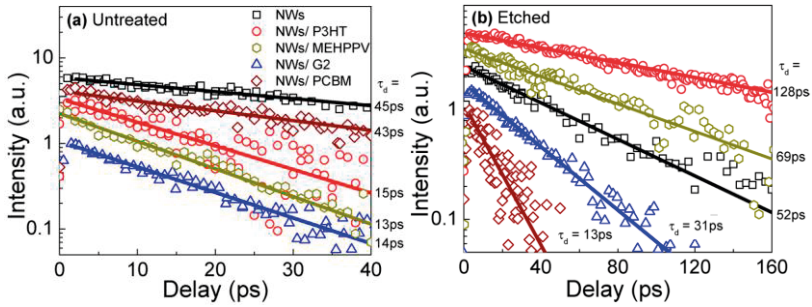


Figure 1.6.1.

PL transients of (a) untreated (o-) and (b) etched (e-) GaAs NWs and their blends with a range of organic semiconductors, measured at the emission energy of 1.52 eV, close to the band edge of GaAs at 10 K. The solid lines are the output of fitting these data with single-exponential decay functions of lifetime τ_d . Reproduced with permission.⁸⁷ Copyright 2012, American Chemical Society.

Several other passivation methods have been developed recently, with chemical wet passivation becoming one of the main choices because of the advantages of low-cost, easy-handle, and instrument-independent. Chemical passivation, such as sulfidation and nitridation via wet chemistry, is another conventional and inexpensive passivation approach. Sulfidation of the surface by wet chemistry improves the efficiency of group III-V SCs.⁸⁸ However, the sulfide layer is unstable under ambient conditions,⁸⁹ and a protective layer is needed to prevent the degradation of the sulfide layers over time. Instead, surface nitridation by the hydrazine-sulfide solution can form a GaN thin layer on the GaAs surface that acts as a more stable layer. Berkovits, V. L. et. al. proposed this method for bulk and NW GaAs.^{90–92} The GaN thin layer can protect GaAs surface against oxidation over a period of months and significantly improve the GaAs optical and electrical properties. The PL results in **Figure 1.6.2** reflect that the passivation via wet nitridation could reduce the density of trap states on the surface of GaAs by a factor of 6 while sulfide passivation only provides the factor of 2.

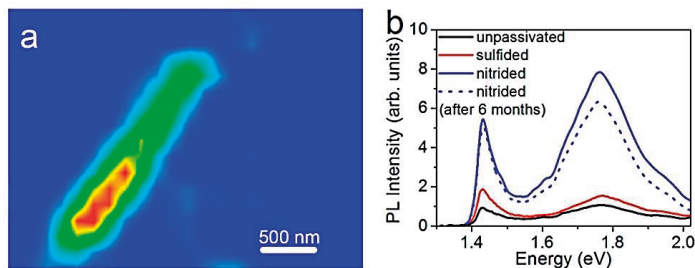


Figure 1.6.2.

(a) μ -PL intensity distribution (at wavelength $\lambda = 870$ nm, 300 K) over the surface of nitrided n-GaAs NW lying horizontally on a Si substrate covered by a Si_3N_4 film; (b) μ -PL spectra (300 K) taken from the middle section of the nitrided, sulfided, and unpassivated NWs. A μ -PL spectrum from a nitrided NW measured after six months of storage in ambient air is also presented. Reproduced with permission.⁹² Copyright 2014, American Chemical Society.

However, benefiting from the surface passivation used for reducing surface defects, we have to consider a possible lattice mismatch between the NWs and the passivation layers created by various methods. This lattice mismatch could lead to new and large number of defects that may deteriorate the performance of SCs and other optoelectronic devices. Besides, it is also important to note that surface passivation is not always needed for any semiconductor NWs. So far, researchers have found H_2S could passivate the surface of InP NWs during the MOVPE procedure.⁹³ To the intrinsic InP NWs, the surface of InP NWs almost do not affect the carrier lifetime.⁹⁴ We do not find a further way to passivate the intrinsic InP NW as it already has a very low recombination rate after epitaxial growth, and most passivation processes play a detrimental role in improving the performance of intrinsic InP NWs. But possibly it can be improved by some passivation. Up to now, people have not found a universal method to passivate intrinsic InP NWs to improve the performance. For doped InP NW, the doping level significantly affects the carrier lifetime.⁹⁴ Meanwhile, in SC devices, an insulating layer must be used to isolate the heterojunctions and the electrodes (see **Figure 1.6.3**). Therefore, suitable passivation layers are still needed to reduce non-radiative recombination caused by surface states in InP NWs.

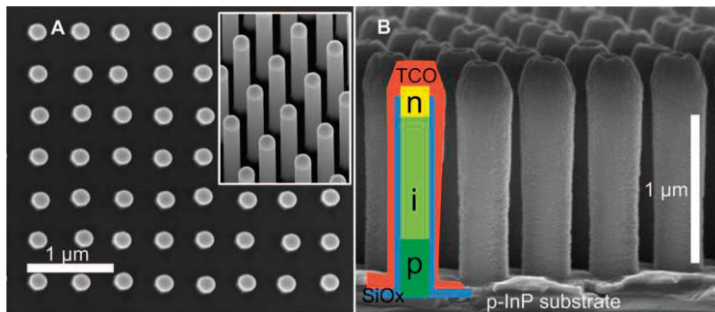


Figure 1.6.3.

Characterization of InP NW-array SCs: (A) 0° and 30° (inset) tilt scanning electron microscopy (SEM) images of as-grown NWs with a surface coverage of 12%. (B) SEM image of processed NWs. The superimposed schematics illustrate the silicon oxide (SiO_x , blue), TCO (red), and the p-i-n doping layers in the NWs. Reproduced with permission.¹⁵ Copyright 2013, American Association for the Advancement of Science.

Although surface passivation is especially relevant procedure for NWs with large S/V ratio, it is methodologically more straightforward to study the consequences of passivation for bulk materials, which actually often also need some passivation to improve their characteristics. In this thesis, a series of surface passivation processes of GaAs bulk wafer are studied to investigate how surface passivation affects the carrier recombination process in this material. The surface nitridation and Hydrogen Chloride (HCl) -solution-processed passivation significantly extend the lifetime of photo-generated carriers, which is attributed to reducing the density of non-radiative trapping centers as compared to naturally oxidized GaAs surface.

1.7 Photo-physical Processes in Group III-V NWs Semiconductor

Group III-V semiconductor NWs possess a great opportunity to become the next generation nanoscale PV devices in the future. The core feature of PV devices is related to the interaction with light and conversion the light energy into electrical energy. Therefore, understanding photo-physical processes in group III-V semiconductors provides the basis and shows direction for improving SCs to contribute to the widespread future applications of PVs. The photo-physical processes in NWs semiconductor may be quite different compared with bulk due to the possible two-dimension quantum confinement effects within NWs.^{95,96}

In solid-state physics, one atom has a nucleus and electrons which are spread around the nucleus in some orbitals with a certain energy. In semiconductor materials, a massive number of atoms interact with each other, and thus instead orbital description, researchers use description of quasi-continuous energy levels, known as energy bands. In general, the highest occupied band is the valence band and the lowest unoccupied band is the conduction band. The energy difference between these two bands is defined as the bandgap.

With regards to light, according to the wave-particle duality, it can be described as either a particle or a wave. When light is a wave, light is a kind of electromagnetic wave, which can be determined by wavelength or frequency, phase, and amplitude. From low to high frequency, light can be defined as radio wave, microwave, infrared region, visible region, UV region, X-ray region, and Gamma region as shown in **Figure 1.7.1**.

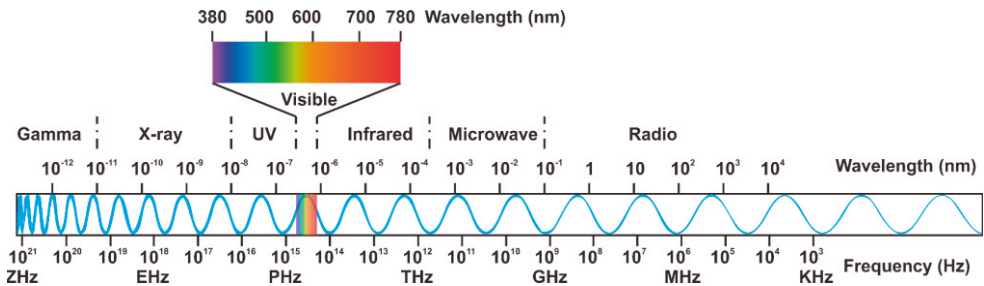


Figure 1.7.1.
The electromagnetic spectrum.

When light is a particle, it is defined as a photon with an energy of $h\nu$, where h is the Planck's constant, ν is the frequency of the light. In general, absorption of photons occurs by the excitation of electrons into a higher energy state or from valence to conduction band. Electrons and hole can be generated when a

semiconductor absorbs photons with the energy above the bandgap. After the semiconductor is photo-excited, the photo-generated electrons and holes are attracted to each other by the Coulomb interaction. This unit of bound together electron and hole is a so-called exciton. Generally, in an inorganic semiconductor, the temperature is higher enough that kT is larger than the exciton binding energy at room temperature so that electrons and holes can overcome the constraint of the binding energy to become free moving charge carriers.

Photo-generated charge carriers in the form of electrons and holes also cannot exist in the free form in semiconductor materials for a long period of time. They are supposed to recombine back to the steady-state condition or annihilate. In an ideal intrinsic semiconductor without defects (**Figure 1.7.2a**), after absorbing photons electrons are lifted to the conduction band and then relax to the bottom of the band via emitting phonons. These electrons then may return to the valence band by emitting photons with the energy equals to the energy of the bandgap. In the bandgap, electrons cannot come back to the valence band with emitting photons (E_{phonon}) because there are no available energy levels.

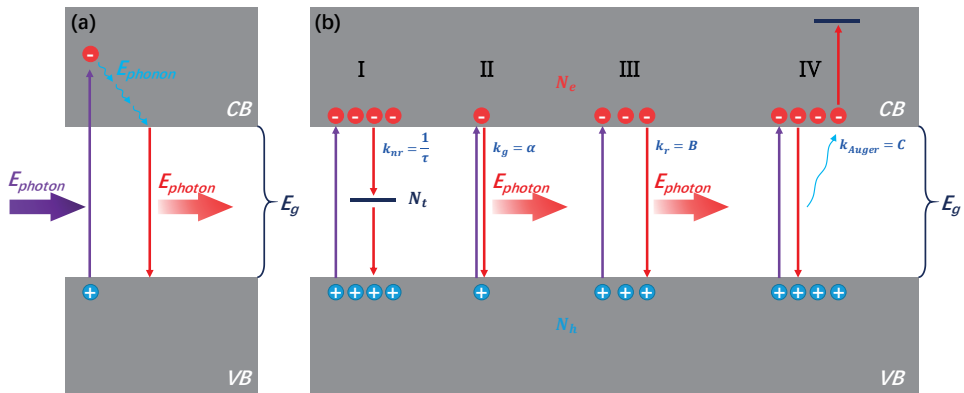


Figure 1.7.2. Schematic of recombination processes of the photogenerated charge carriers in semiconductors.

During the radiative recombination, the electrons must encounter holes before recombination can take place. Therefore, the radiative recombination (B) is a second-order process and thus the concentrations of electrons and holes changing with time ($\frac{dN}{dt}$) speeds up with the initial concentration of the free electrons (N_e) and holes (N_h). Naturally, electrons and holes are photo-generated simultaneously. So,

$$\frac{dN}{dt} = BN_eN_h = BN^2 \quad (1 - 1)$$

, where, B is the bimolecular recombination coefficient. However, in reality, semiconductor materials are not so perfect. The photo-generated carriers recombine

along more channels than just radiative recombination. Recombination processes can be classified according to these channels. The main recombination mechanisms in semiconductor materials are schematically shown in **Figure 1.7.2b**. If we consider recombination of an electron and a hole that are generated via absorption of a single photon or so to say from the same primary photo-generation then their recombination is called geminate recombination independently of is it radiative or non-radiative. Such recombination typically occurs in organic SCs because of the large binding energy between electron and hole in exciton.⁹⁷ For inorganic semiconductor materials, the binding energy is too small to maintain the electron and hole pair. However, in nano-materials, due to the size confinement effect, photo-generated carriers can be restricted in the nano-range so that they cannot move freely to encounter and recombine with other electrons or holes. So, it is possible that these charges recombine geminately, especially when the photoexcitation flux is low. $\frac{dN}{dt}$ can be written as a first-order recombination process,

$$\frac{dN}{dt} = k_g N \quad (1 - 2)$$

, where k_g is the geminate recombination coefficient.

In addition, non-radiative recombination mechanisms including Auger recombination and trap assisted recombination are two main processes that are also important for the performance of the semiconductor materials. The impurities might function as the non-radiative recombination centres resulting in the deterioration of the semiconductor performance. The rate of the trap assisted recombination ($\frac{1}{\tau}$) depends on the concentration of trap states and on the density of the photo-generated carriers. When the trap density is much larger than the concentration of photo-generated carriers, the recombination follows a first-order rate law:

$$\frac{dN}{dt} = \frac{N}{\tau} \quad (1 - 3)$$

Otherwise, if the concentration of photo-generated carriers is larger than the trap density, the trapping distance will be determined by the carrier density and trap density rather than the distance between traps. In this case, $\frac{dN}{dt}$ should be expressed as a second order reaction,

$$\frac{dN}{dt} = \frac{NN_t}{\tau} \quad (1 - 4)$$

, where N_t is the concentration of trap states.

Auger recombination, as a third-order recombination process, requires three free carriers to complete the process. For example, an excited electron recombines with a hole and subsequently transfers the energy to another electron. The recombination process is described as:

$$\frac{dN}{dt} = CN^3 \quad (1 - 5)$$

, where C is the Auger recombination coefficient.

For completeness, we need to include all these processes in the description of the carrier decay. Therefore,

$$\frac{dN}{dt} = G(t) - k_g N - BN^2 - CN^3 - \frac{N}{\tau} \quad (1 - 6)$$

, where $G(t)$ is the carrier generation rate, which is related to the excitation density of the pump light. Note that here we simplify the change of the photo-generated charges by trapping as a first-order process when the trap density is much higher than the photo-generated carriers.

Among these recombination processes, the trap-assisted recombination might be more important in nanoscale semiconductor materials due to the large S/V induced numerous defects on the surface.

1.8 Spectroscopy Study in Group III-V NWs Semiconductor

As compared to the traditional electric characterizations of NW materials such as I-V measurements, optical spectroscopy methods have several advantages such as no need for electrical contacts as the electron/hole pairs are generated by light and their evolution can be assessed by light as well. Spectroscopic characterisation of materials can be divided into steady-state spectroscopy and time-resolved spectroscopy in terms of measurement methods. The details of the used spectroscopic methods will be described in *Chapter 2*. In this part, a general spectroscopy studies in group III-V NWs semiconductor are reviewed.

1.8.1 Exciton Recombination

In group III-V semiconductors, excitons are generated after absorbing photons and then rapidly dissociate into free holes and electrons due to the very weak binding energy. When T is so small that kT is comparable or lower than the exciton binding energy (~ 4 meV), the exciton recombination will be the main radiative recombination.⁹⁸ In a bulk AlGaAs/GaAs heterostructure below 25K, the free or bound excitons are “frozen out” and then recombine radiatively at around 818 nm (1.516 eV) with a sharp PL emission peak,⁹⁸ meaning that the free excitonic emission locates at around 1.51~1.52 eV in bulk GaAs.⁹⁹ The exciton Bohr radius in GaAs materials is 12 nm.⁹⁹ If the width in any dimension is less than the exciton Bohr radius of GaAs nanostructure, the exciton annihilation could happen due to strong quantum confinement effects. Therefore, strong quantum confinement effects could happen when the diameter of NWs is smaller than the exciton Bohr radius in GaAs. In this study, the recombination lifetime of excitons in GaAs NWs at 5K measured by TRPL method is less than 80 ps, which is about one order of magnitude shorter than the lifetime in low temperature bulk GaAs/AlGaAs heterostructures. The shortening of the lifetime comes from the influence of defects in GaAs or at the interface between GaAs and AlGaAs.⁹⁹

1.8.2 Ultrafast Carrier Dynamics

The dynamics of photo-generated carriers could be very different in various group III-V semiconductors. A comparative study (**Figure 1.8.1**) of electronic properties of GaAs, InAs, and InP NWs has been presented by using an optical pump–terahertz probe spectroscopy.¹⁰⁰ A lifetime in the picosecond range was observed in GaAs NWs, (see **Figure 1.8.1a**) and was associated with the high trapping rate of photo-generated charge carriers at the surface, indicating that an appropriate passivation is

needed to improve the performance of the corresponding PV devices. On the contrary, the extremely long lifetime of free carriers in InP NWs (see **Figure 1.8.1c**) illustrates the low density of the trap states on the surface of InP NWs.

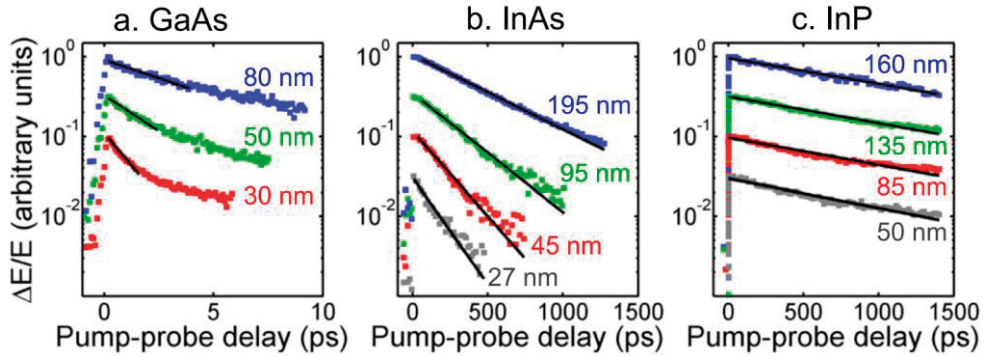


Figure 1.8.1.

Pump-induced change in terahertz electric field ($\Delta E/E$) at different pump-probe delays. (a) $\Delta E/E$ decays for 30, 50, and 80 nm diameter GaAs NWs, fitted with carrier lifetimes of $\tau = 1.3, 2.4$ and 4.7 ps, respectively. (b) $\Delta E/E$ decays for 27, 45, 95 and 195 nm diameter InAs NWs, fitted with carrier lifetimes of $\tau = 200, 290, 470$ and 660 ps, respectively. (c) $\Delta E/E$ decays for 50, 85, 135 and 160 nm diameter InP NWs, fitted with carrier lifetimes of $\tau = 1.18, 1.27, 1.30$ and 1.34 ns, respectively. These are scaled for clarity. The photoexcitation pump fluence was $10 \mu\text{J cm}^{-2}$. Straight lines are monoexponential fits to the decays at early times after photoexcitation. Reproduced with permission.¹⁰⁰ Copyright 2013, IOP Science.

1.8.3 Doping Correlated Carrier Recombination

In intrinsic and sulfur-doped InP NWs arrays, the recombination dynamics of photo-generated free carriers have been investigated by TRPL and TA method.¹⁰¹ The PL decay time and the integrated PL intensity were observed to decrease with increasing sulfur doping, which was attributed to the introduction of hole traps by sulfur dopant (**Figure 1.8.2a-c**). Similarly, as the level of Zn doping in GaAs NWs increases, we observed the PL decay becomes faster, which was interpreted that the electron trap density increases.¹⁰² However, in contrast to GaAs in the intrinsic InP NWs the stacking faults, twins, Zincblende-Wurtzite (ZB-WZ) polytypism, and the surface of InP NWs do not affect the carrier lifetime very much. This has been demonstrated by the similar TRPL and TA decays (see **Figure 1.8.2d**) indicating that the radiative recombination is the dominant recombination process in intrinsic InP NWs. This conclusion is in agreement with the long photoconductivity lifetime as was measured by optically pump-terahertz probe time-resolved spectroscopy.¹⁰³

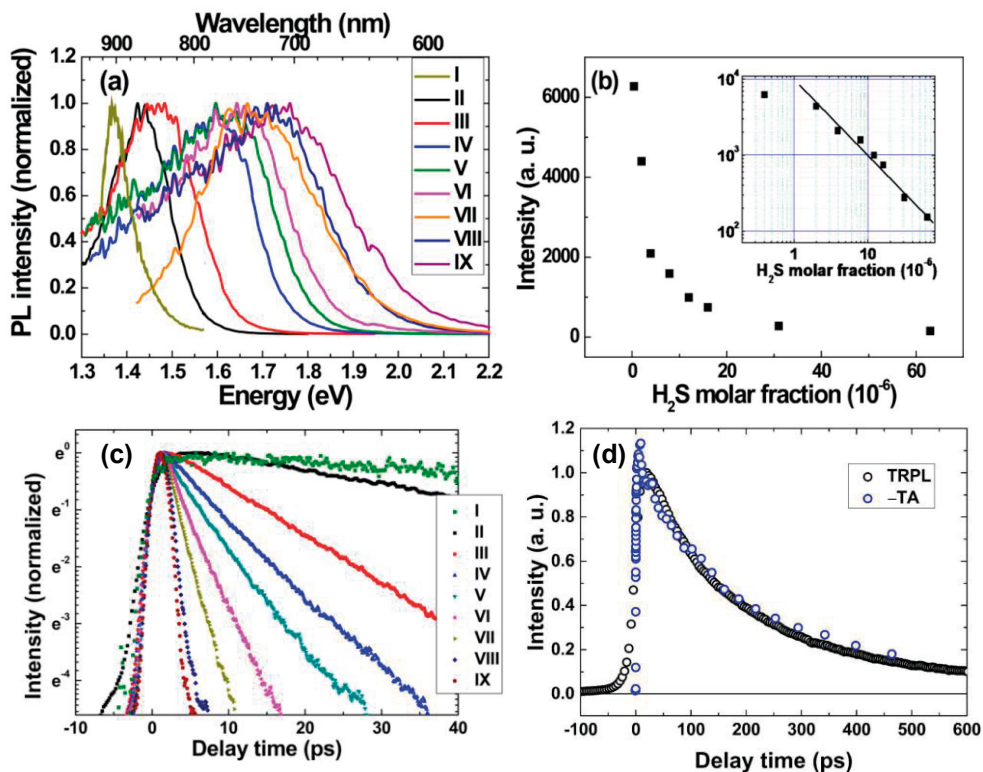


Figure 1.8.2.

(a) TRPL decay of InP NWs with different sulfur contents (increase from I to IX) as a function of time after photoexcitation at 400 nm (3.1 eV). The excitation photon flux is $7.8 \times 10^{12} \text{ cm}^{-2}$. (b) Time resolved photo-induced luminescence (excitation photon flux $6.2 \times 10^{12} \text{ cm}^{-2}$) and time resolved transient absorption (excitation photon flux $6.3 \times 10^{12} \text{ cm}^{-2}$) decays of sample I (TA, 850 nm (1.46 eV); TRPL, 850 nm). To compare with TRPL, TA signal is reversed and normalized. Reproduced with permission. Copyright 2015, American Chemical Society.

1.8.4 Surface Passivation

In contrast to InP materials, processes occurring at the surface of GaAs NWs have a significant influence on the photo-generated charge carrier dynamics. In order to passivate the surface defects, a layer of AlGaAs has been grown on the GaAs core NW. The steady state PL of AlGaAs passivated GaAs increases by about 20 times compared to bare GaAs.^{104,105} The carrier recombination processes in aerotaxy-grown GaAs NWs have also supported these observations.¹⁰⁶ The shell passivation effect and Zn doping influence were evaluated through TRPL and TA spectroscopy studies (see **Figure 1.8.3**). In addition, GaNAs can also be grown on the surface of GaAs NWs by nitrogen plasma. The exciton and free carrier recombination dynamics in GaAs/GaNAs core/shell NWs have been studied. Radiative recombination of localized excitons dominates the PL decay at low temperature whereas at high temperature, it is determined by free carriers recombination.¹⁰⁷

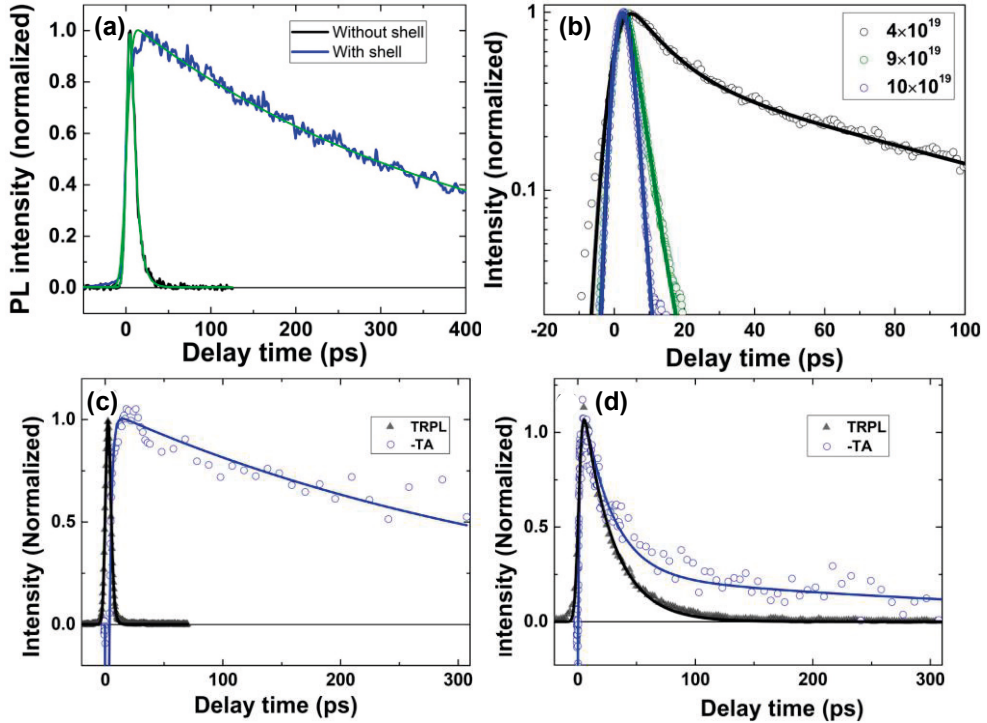


Figure 1.8.3. (a) TRPL decays of intrinsic GaAs NWs with (blue) and without (black) AlGaAs shell at 1.505 eV under excitation at 3.1 eV and measured at 77 K. Green lines represent mono-exponential fitting curves. (b) TRPL decay of GaAs/AlGaAs NWs grown with varied hole doping concentrations as a function of time measured at 1.505 eV after photo-excitation at 3.1 eV at 77 K. Solid lines represent mono-exponential fitting curves. TRPL and TA decays of (c) Zn-doped (hole doping concentration of $1 \times 10^{20} \text{ cm}^{-3}$) and (d) intrinsic GaAs/AlGaAs NWs at 300 K. Solid Reproduced with permission.¹⁰⁶ Copyright 2016, IOP Science.

Another method of passivation, wet treatment, has also been spectroscopically proven to be a promising passivation effect. The TRPL study of bulk GaAs has also been presented in relation to different wet passivations and AlGaAs encapsulation procedures. Comparing to the simple removing the oxidized layer on the surface, called deoxidation, AlGaAs capped GaAs and GaAs treated by 1.0M 4-Cl-thiophenol in CCl_4 for 30 min have a very good passivation effect and the lifetime of the PL decay becomes slower after the treatments.¹⁰⁸ In GaAs NWs, two frequently used passivation methods, sulfidation and nitridation, have been applied for GaAs NWs. The increase of the PL intensity by 2 and 6 times has been observed after sulfidation and nitridation, respectively. This increased PL was interpreted as the decrease of the trap density 2 and 6 times by using surface recombination approach.⁹² In the thesis, carrier recombination processes in bulk and NW group III-V semiconductors are described.

Chapter 2

Experimental Methods

In this thesis, we will present the outcomes of the study by a varies spectroscopy methods of the photophysical processes in optoelectronic materials. In particular, we will focus on the understanding of the carrier recombination processes in nanostructured Group III-V semiconductor materials. In this section, we will introduce the spectroscopy methods used for our measurements, such as steady-state absorption, steady-state and time-resolved photoinduced luminescence, absolute photoluminescence quantum yield, transient absorption and time resolved terahertz spectroscopy.

2.1 Steady-state Spectroscopy

2.1.1 Steady-state Absorption

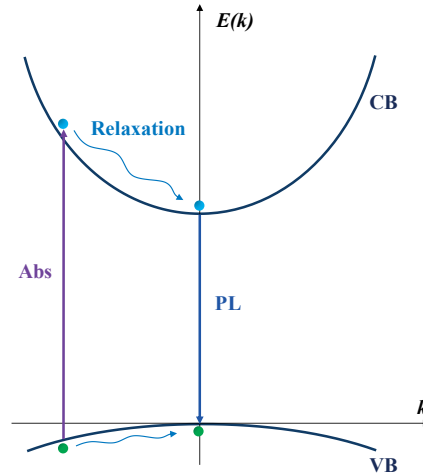


Figure 2.1.1. Schematic diagram of the absorption and emission processes in a direct bandgap semiconductor.

The absorption of light by semiconductors has different mechanisms, such as interband absorption, exciton absorption, free charge carrier absorption and so on. In the semiconductor studies, absorption edge of a semiconductor provides information about the bandgap and the states close to the conduction and valence bands.¹⁰⁹

Figure 2.1.1 shows the schematic diagram of the absorption and emission processes in a direct bandgap semiconductor. When a photon is incident on and absorbed by a semiconductor material, it transfers an electron from the valence band to the conduction band, while leaves a hole in the valence band. Then, the electron and hole relax to the bottom of the conduction band and the top of the valence band, respectively. The charge pair could recombine radiatively with emitting a photon or could recombine non-radiatively, in particular via trapping at some trap centres.

Absorption is the first step related to the performance of many optoelectric devices, such as PV materials, for which the performance is significantly affected by the absorption efficiency of a semiconductor. In general, the absorption can be measured by an absorption spectrometer (see **Figure 2.1.2a**). The absorption of inorganic semiconductors can be described by Beer-Lambert law (see **Figure 2.1.2b**), which

$$A = \log_{10} \left(\frac{I_0}{I} \right) = \alpha l \quad (2 - 1)$$

, where A is the absorption, I_0 is the incident light, I is the transmission light, $\frac{I_0}{I}$ is the absorbance, α is the absorption coefficient which describes the intensity attenuation of the incident light pass through a semiconductor, and l is the optical path length.

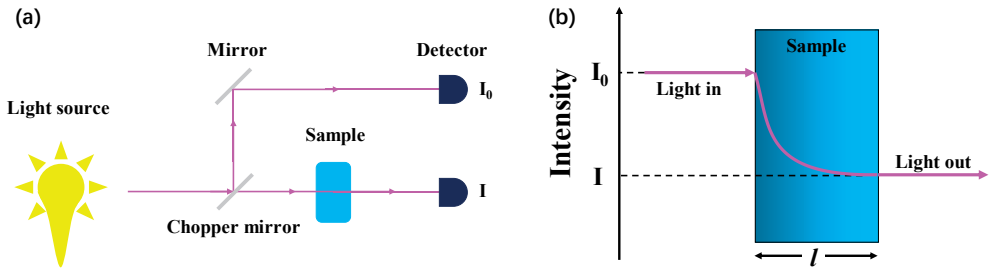


Figure 2.1.2. (a) Simple schematic diagram of the absorption spectrometer. (b) Schematic diagram of the absorption of light in a sample with thickness of l .

Figure 2.1.2b shows the absorption of an incident light in a bulk semiconductor that has a thickness of l . Since the incident light intensity will decrease with the increase of the depth (see the pink line), the absorbed photon density will be accordingly reduced with the depth of the material.

For the NW array, the absorption also correlates with the characteristics of the array besides the intrinsic properties of the bulk materials. These characteristics include the diameter and length of NWs, and the distance of NWs, which is usually called pitch among NWs. For the application of NW arrays in SCs, a critical step is to increase the absorption of a NW array via optimizing the light in-coupling of NWs.

Inorganic bulk materials and NW array typically have reflection and/or scattering at the surface of the material, thus the regular absorption measurements based on the light transmission is not sufficient for these materials. Usually, an absorption spectrometer with an integration sphere is needed for the accurate absorption measurement.

In our work, the Lambda 1050 UV/VIS/NIR absorption spectrometer from PerkinElmer was employed for the absorption measurement of the NWs. A simple structure of the equipment is shown in **Figure 2.1.2a**. The transmission mode is usually applied for the measuring the solution samples, while the integration sphere is used for measuring solid samples, such as for measuring absorption of NWs in

this work. **Figure 2.1.3a** shows a representative absorption spectrum of polymer embedded GaAs core-shell NWs array measured by the instrument. The shape of the absorption spectrum is similar to that reported for GaAs NWs (see **Figure 2.1.3b**).¹¹⁰

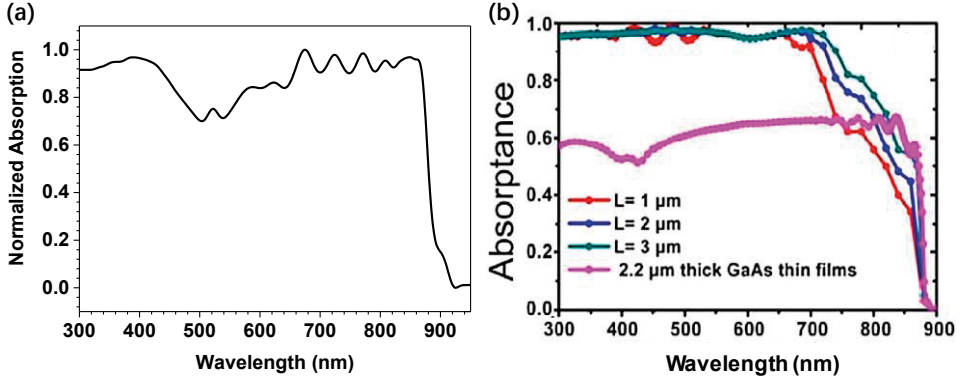


Figure 2.1.3.

(a) Normalized absorption spectrum of AlGaAs/GaAs core-shell NWs array. (b) Calculated absorbance of GaAs NWs with different lengths of 1 to 3 μm . The pink curve shows the absorbance of a 2.2- μm -thick GaAs thin film. Reproduced with permission.¹¹⁰ Copyright 2011, SpringerOpen, BioMed Central Ltd.

2.1.2 Steady-state Photoluminescence and Absolute Quantum Yield

In group III-V semiconductors, PL is typically emitted due to recombination of free (mobile) electrons and holes, thus the recombination depends on the concentrations of both electrons and hole, thus it should be considered as a bimolecular process. Steady-state and time-resolved PL have become the well-accepted characterization methods that can provide a detailed description of the processes within the materials of interest. In particular, PL quantum yield (PLQY or Φ) measurement is a useful steady-state technique that is naturally coupled with the description of the thermodynamic limit of photovoltage in PVs.

Φ is defined as the ratio between the number of emitted photon and the number of absorbed photons; thus it can be expressed as:

$$\Phi = \frac{N_{em}}{N_{ex}} \quad (2 - 2)$$

In molecular physics, the PL quantum yield (Φ) can be expressed as:

$$\Phi = \frac{k_r}{k_r + k_{nr}} \quad (2 - 3)$$

Here, k_r is a radiative recombination rate and k_{nr} is a non-radiative recombination rate.

Based on the discussion in **Section 1.7** and the ABC model of recombination which was developed for describing the excess carriers restore to the thermal equilibrium,^{111,112} the QY can be written as

$$\Phi = \frac{BN^2}{AN + BN^2 + CN^3} \quad (2 - 4)$$

under the steady-state condition. In this model, N is the concentration of photogenerated carriers, BN^2 is the radiative recombination rate, and AN and CN^3 are nonradiative recombination rates. If charge trapping dominates carrier recombination processes, i.e., $AN \gg BN^2 + CN^3$, the QY can be expressed as

$$\Phi = \frac{B}{A}N \quad (2 - 5)$$

In this case, the QY is linearly dependent on the carrier concentration.

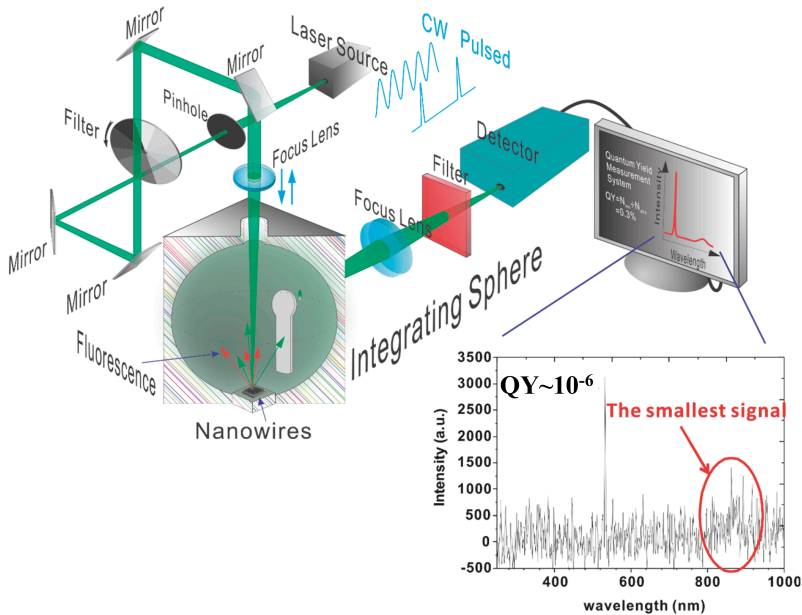


Figure 2.1.4.
Schematic picture of the quantum yield measurement system.

For our studies, we have constructed a PL quantum yield set-up, which was employed for measuring the steady state PL and the PL quantum yield of the bulk

and nanostructured semiconductors. The scheme of the setup is shown in **Figure 2.1.4**. The PL quantum yield system includes an integrating sphere (HORIBA, Quanta-φ, F3029), continuous wavelength (CW) laser sources with the wavelength of 780 nm and a spectrometer (AvaSpec-ULS2048-USB2-UA-50). The excitation light intensity can be changed through adjusting the excitation power and the diameter of the excitation spot at the sample under investigation. The output of the signal was collected by two 1 in. quartz lenses of 50 mm focal length and focused on the input slit of the spectrometer. Some suitable glass absorption filters were used to avoid the over-exposure of spectrometer at the excitation wavelength. The measured spectrum with and without the sample were calibrated by using a reference light source (Ocean Optics, LS-1-CAL), and thus we accounted for the factors such as reflection index of the integrating sphere, sensitivity of the spectrometer and the collection efficiency of the optical paths. By changing the area of the irradiation on the sample, the QY of NW array under fluence from 9 mW/cm² (the equivalent of ~1/4 sun) up to 400 W/cm² (the equivalent of ~0.1M suns) can be measured. The measured PL QY of the samples has been employed for analysing carrier recombination processes in group III-V semiconductors, by combining with the time-resolved spectroscopy study.

2.1.3 Models for Analysing Carrier Recombination by PLQY

1. The effect of background carriers.

During the semiconductor growth process, various impurities are inevitably introduced. The presence of impurities can significantly affect optical properties of semiconductors. These background carriers introduced by some of the impurities will be involved in both radiative and non-radiative recombination of photogenerated charges in semiconductors. Let's assume that the geminate recombination and the Auger recombination are negligible to simplify the modelling. In the simplest case, we assume that there is no preferential long-lived trapping of one carrier type (like electron or hole trapping) and that the background charges are all free. These free background charges will contribute to the bimolecular recombination. Therefore, the **Equation 1-6** can be rewritten as

$$\frac{dN}{dt} = G(t) - AN - B(N + N_0)N \quad (2 - 6)$$

, where N_0 is the concentration of the background carriers. In this case, the recombination contribution from the bimolecular recombination can be separated into BN^2 and BN_0N . According to **Section 2.1.2**, the QY is

$$\Phi = \frac{B(N + N_0)N}{AN + B(N + N_0)N} = \frac{B(N + N_0)}{A + B(N + N_0)} \quad (2 - 7)$$

under the steady-state conditions. When the concentration of the background charges (N_0) is much larger than that of the photo-generated charges (N), the quantum yield under low excitation density will be intensity independent.

$$\Phi \approx \frac{BN_0}{A + BN_0} \quad (2 - 8)$$

The contribution of the background charges to recombination can be negligible when the concentration of the photo-generated charges becomes much larger than that of the background charges. If so, the quantum yield dependence on the excitation density should approach unity, as in the following equation:

$$\Phi \approx \frac{BN}{A + BN} = 1 - \frac{1}{A + BN} \quad (2 - 9)$$

The theoretical QY of the semiconductor materials depends on the irradiation density, as shown in **Figure 2.1.5a**.

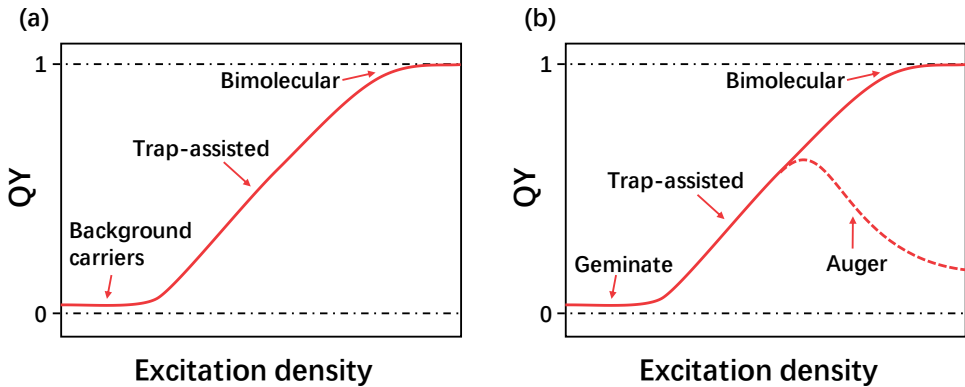


Figure 2.1.5. Theoretical quantum yield of semiconductor materials depends on the irradiation density when (a) consider and (b) neglect background carriers. The quantum yield is a constant under very low excitation density, and then increases linearly, finally decreases significantly due to Auger recombination.

2. The effect of geminate recombination

If the density of the background carriers is small, or if they are not free they do not contribute significantly to the radiative recombination process. In this case, under

the steady-state conditions, the carrier generation rate $G(t)$ is equal to the recombination rate. If we do not consider the Auger recombination,

$$G(t) = k_g N + AN + BN^2 \quad (2 - 10)$$

Here, $G(t)$ comes from the photogeneration since the thermal charge generation rate is negligible (it can result in about $2.25 \times 10^6 \text{ cm}^{-3}$ at 300K for an ideal intrinsic GaAs materials w/o unintentional doping) as presented by J. S. Blackmore et al.^{113,114} As a result, $G(t)$ can be estimated by using the number of absorbed photons only. Therefore,

$$G(t) = \frac{\eta_{Abs.} \cdot P_{Exc.}}{V \cdot E_{Photon}} \quad (2 - 11)$$

, where, $\eta_{Abs.}$ is the absorbance of the incident photons. $P_{Exc.}$ is the excitation power, V is the volume of NWs excited by the incident light, and E_{Photon} is the energy of one excitation photon.

From **Section 2.1.2**, the QY can be expressed as the ratio of the radiative rate and all recombination rate, which represents the ratio of the number of emitted photons to the number of absorbed photons. The rate of free charge carrier disappearance due to charges recombination in the NWs array can be represented as in **Equation 1-6**. Therefore, under the steady-state condition, the QY can be represented as

$$\Phi = \frac{k_g N + BN^2}{(k_g + A)N + BN^2} = \frac{k_g + BN}{k_g + A + BN} \quad (2 - 12)$$

When the concentration of the photogenerated charges is extremely low, these rate components which contain a product of the charge concentration, N , are negligible. Thus, the quantum yield can be written as:

$$\Phi = \frac{k_g}{k_g + A} \quad (2 - 13)$$

Apparently, the quantum yield is constant, which is irrelevant to the photo-generated charges. With the increase of the irradiation density, but not up to exceedingly high level, the concentration of photo-generated carriers grows linearly but the Auger recombination is not yet evident. In this case, both geminate and bimolecular recombination contributed to the radiative recombination. However, apparently the trap-assisted non-radiative recombination still dominates the overall recombination, which results in a negligible impact of the geminate and bimolecular recombination. The quantum yield, therefore, can be expressed as:

$$\Phi = \frac{k_g + BN}{k_g + A} = \text{Cons.} + \frac{B}{A}N \quad (2 - 14)$$

, which exhibits a linear intensity dependence on the concentration of carriers.

Further, the bimolecular recombination is significant and non-negligible when the bimolecular recombination is comparable to or even larger than the trap-assisted recombination. The quantum yield is approaching the following expression:

$$\Phi = \frac{k_g + BN}{k_g + A + BN} = 1 - \frac{A}{k_g + A + BN} \quad (2 - 15)$$

However, that will not happen since the Auger recombination occurs under the exposure of extremely intensive incident irradiation. Thus, the quantum yield should decrease as a function of $1/N$, like

$$\Phi = \frac{B}{B + CN} \quad (2 - 16)$$

instead of approaching unity.

According to the description above, it is expected that the quantum yield with increase of the incident light density should be first intensity independent, then increase linearly and then undergo a dramatic decrease, as shown in **Figure 2.1.5b**.

2.2 Time-resolved Spectroscopy

2.2.1 Transient Absorption (TA)

Transient absorption is one type of the pump-probe spectroscopies. It can account for the photo-generated carriers in studied materials with several advantages, such as good temporal resolution and high signal-to-noise. This technique has been extensively used to study, in particular, excited states and photo-generated carrier dynamics in metal-centered porphyrins and carbene complexes.¹¹⁵ In recent years, transient absorption spectroscopy was also employed for studying the photophysical processes in semiconductor NWs.

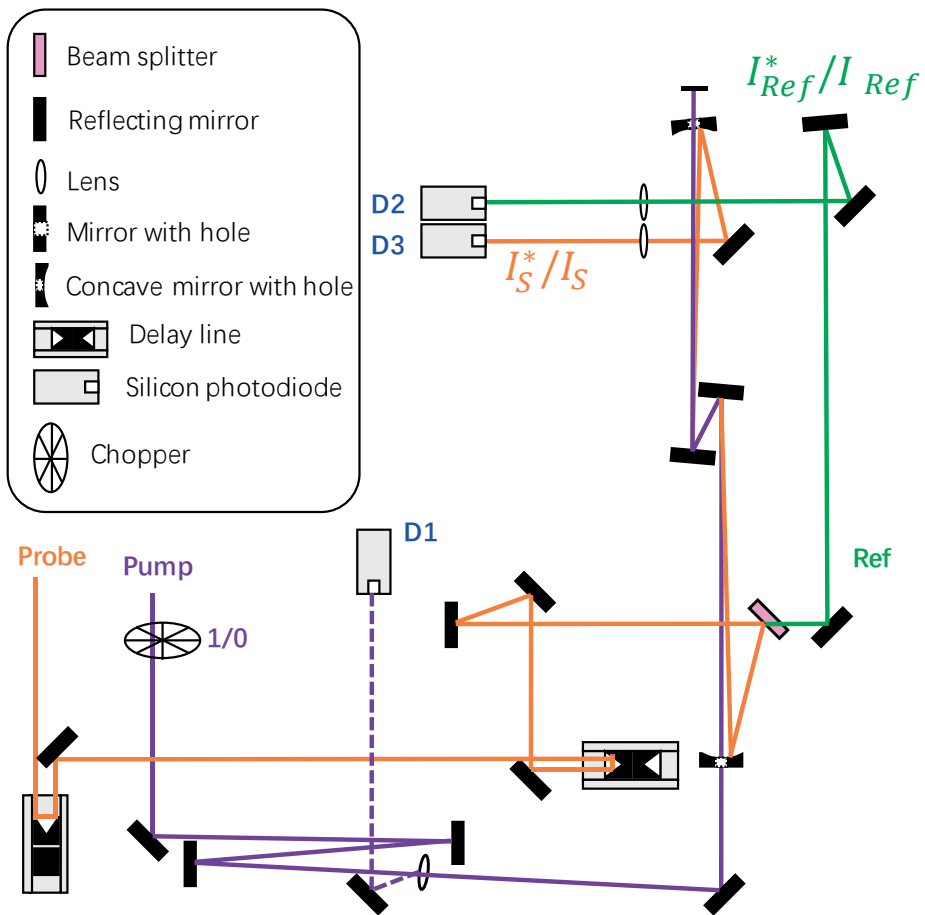


Figure 2.2.1. Schematic diagram of an experimental transient absorption system.

The schematic diagram of the transient absorption system can be found in **Figure 2.2.1**. First, the pump light passes through a mechanical chopper that can be varied between ON (1) or OFF(0) states for controlling the excitation of a sample. The transient absorption is determined by the difference of absorption of the excited and unexcited states, which can be expressed as:

$$\Delta A = A^* - A \quad (2 - 17).$$

where A^* and A are the absorption under the pumped and unpumped situation, respectively. According to the Beer-Lambert law and the Equation 2-1, the absorption can be converted into

$$A = -\log T = -\log\left(\frac{I_0}{I}\right) \quad (2 - 18).$$

Then, the absorption difference can be written in terms of the light intensity:

$$\Delta A = -\left[\log\left(\frac{I_S^*}{I_R^*}\right) - \log\left(\frac{I_S}{I_R}\right)\right] \quad (2 - 19)$$

, or

$$\Delta A = -\log\left[\frac{I_S^*}{I_R^*} \times \frac{I_R}{I_S}\right] \quad (2 - 20)$$

, where I_S^* and I_S are the signal light intensity that the detector received from the probe light passing through the sample with and without pump light; I_R^* and I_R are the reference light that is measured with and without the pump conditions. Generally, if the probe laser is stable,

$$I_R^* = I_R \quad (2 - 21)$$

Then,

$$\Delta A = -\log\left(\frac{I_S^*}{I_S}\right) \quad (2 - 22)$$

However, in order to reduce the fluctuations of the laser, the measurements of I_R^* and I_R are needed.

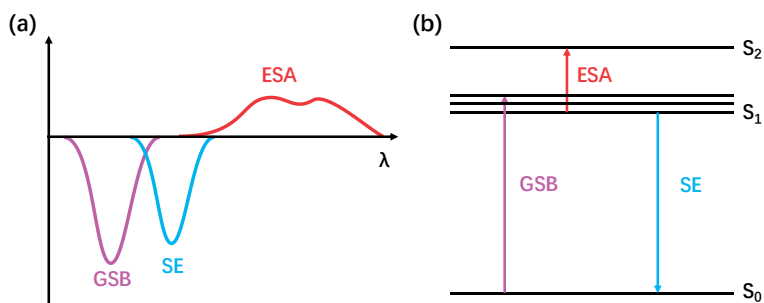


Figure 2.2.2.
Schematic diagram of the composition of signals in TA spectrum.

The following processes usually contribute to transient absorption (**Figure 2.2.2**): (1) ground-state bleach (GSB). When illuminating molecules by a pump light, some of these molecules can be transferred to the excited states. At this moment, the ground states absorption of the pumped sample is less than that of the un-pumped sample. As a result, the detected intensity of probe light for the pumped sample shall be larger than that for the un-pumped sample, and ΔA shows a negative signal in the wavelength range of the steady state absorption. (2) stimulated emission (SE). For the stimulated emission, it occurs when photons pass through excited molecules. In this case, the excited molecule can be converted back to the ground state via stimulated emission. Consequently, the intensity of the transmitted probe light in the case of the pumped sample in the emission spectral range shall be higher than that for the un-pumped sample. Thus, stimulated emission will contribute to ΔA as a negative signal as well. (3) excited-state absorption (ESA). The excited-state absorption significantly refers to the population of the excited molecules. So, the excited molecules absorb photons and thus the detected signal is smaller than that for the un-pumped sample, resulting in a positive ΔA in the ESA wavelength range.

Generally, the transient absorption spectra are collected at every delay time between the moment of excitation and the moment of probing by controlling a delay line (see **Figure 2.2.1**). So, at different wavelengths, the contribution of GSB, SE, and ESA could be different.

In the past few years, TA has been used to study the carrier behavior in group III-V semiconductor NWs as it can reveal the decay of the overall photo-generated charge carriers in semiconductor materials. Wei et al. used the TA method to study the charge recombination processes in Zn doped and intrinsic aerotaxy-grown GaAs/AlGaAs core-shell NWs.¹⁰² In that study, they concluded that most of the photo-generated carriers recombine non-radiatively in Zn-doped GaAs/AlGaAs core-shell NWs by comparing the time-resolved PL and TA. Besides, they find that the charge trapping process is suppressed significantly in intrinsic GaAs/AlGaAs NWs.

2.2.2 Time-resolved Terahertz Spectroscopy (TRTS)

As we know from **Figure 1.7.1**, the spectral range of the terahertz (THz) radiation is around $300\ \mu\text{m}$, corresponding to a photon energy of $\sim 4\ \text{meV}$. This energy is so low that it corresponds to the quantum transitions of the translation of the energy. Therefore, the mobile charges are accelerated by absorption of THz. Recently, TRTS has been applied to study the photoconductivity dynamics in a semiconductor with a sub-picosecond time resolution.^{116–118} Photoconductivity usually arises from generation of mobile electrons and holes.¹¹⁹ For many group III-V semiconductors, electron mobility (μ_e) is significantly higher than hole mobility (μ_h).^{120,121} In those cases, the photoconductivity, $\Delta\sigma(t)$, primarily reflects the concentration of the photo-generated electrons, and thus, TRTS can be used for analysing the photogenerated electron dynamics.

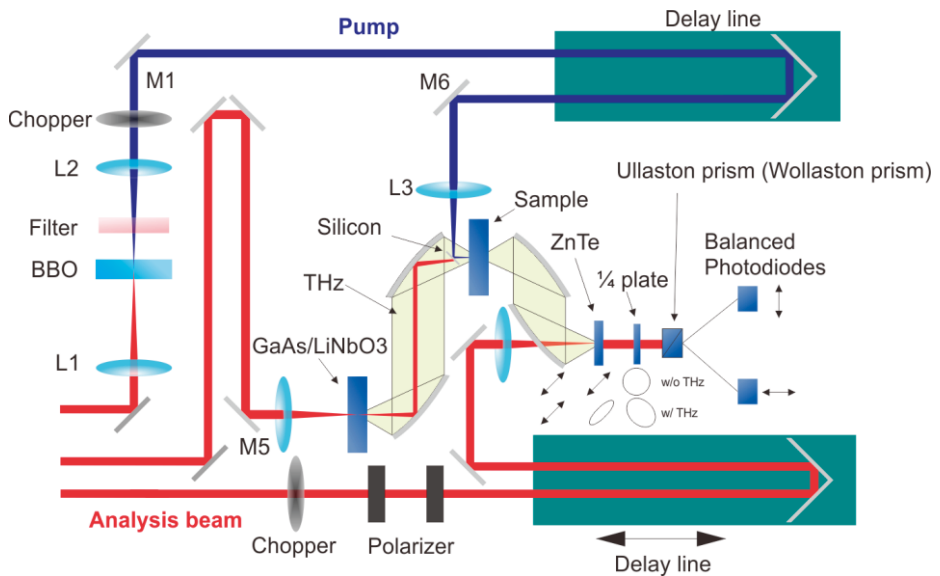


Figure 2.2.3.
Schematic diagram of an experimental TRTS system.

Figure 2.2.3 shows the THz setup. The output of a femtosecond pulsed laser is divided into a pump beam, THz generation beam and an analysis beam by beam splitters. Usually, the THz probe beam is generated via an optical rectification by focusing a femtosecond laser pulse on non-linear materials. The THz generation theory was given by Chuang et al.¹²² Generated THz wave is focused on the sample at the same spatial position as the pump. After the sample, the THz pulse is going through, and the pump light is blocked by a silicon wafer to eliminate the impact of the pump on the detection of the THz pulse. As a result of sample excitation, photogenerated carriers are generated.

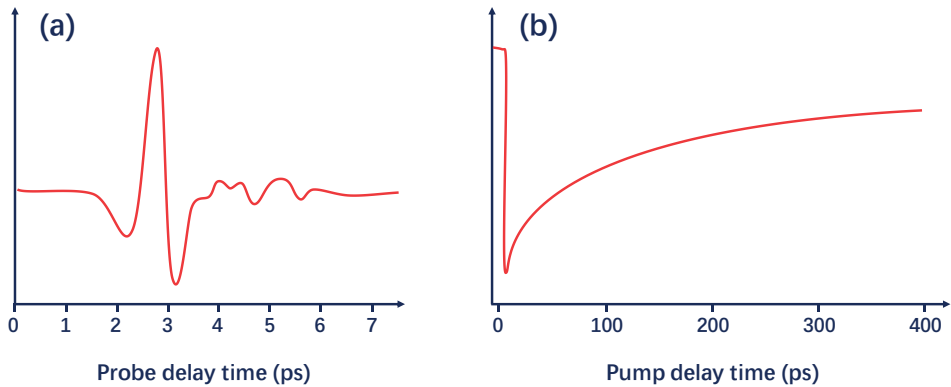


Figure 2.2.4.
 (a) THz probe scan and (b) TRTS pump scan.

In general, the THz time-domain signal caused by the optical pump can be measured by moving the delay line for the analysis beam. This process is called “*Probe scan*” as shown in **Figure 2.2.4a**, and it can record the entire THz spectrum at a fixed delay time between optical pump and THz probe. Another process named “*Pump scan*”, as shown in **Figure 2.2.4b**, is used to resolve the dynamics of the THz signal at a fixed point on the THz waveform. Typically, the delay line of the *Probe-scan* path is fixed at the maximum of the THz time-domain signal, then the evolution of the THz amplitude with time can be obtained by moving the delay line of the pump optical path, and the dynamics of the carrier in the sample can be studied.

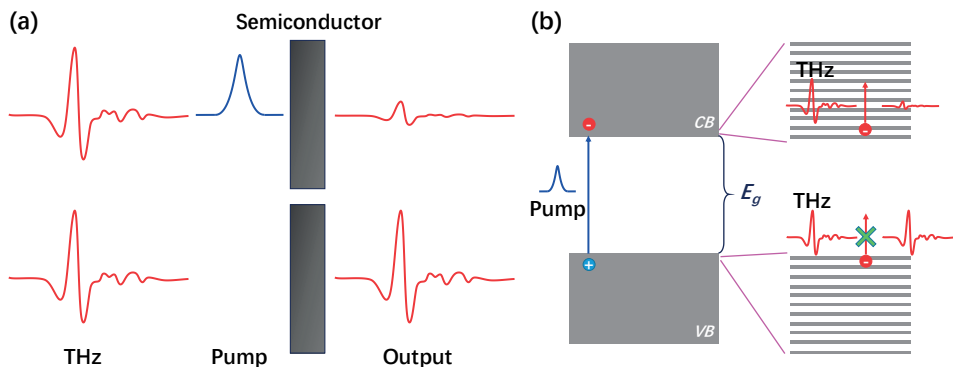


Figure 2.2.5.
 (a) The THz wave interacts with semiconductor w/ and w/o pump. (b) The physical mechanism of the interaction between THz wave and electrons in semiconductor w/ and w/o pump.

In the absence of pump, the THz wave cannot interact with an ideal semiconductor because all electrons are located in the valance band while the THz wave cannot excite electrons to a higher energy level (See **Figure 2.2.5**). In contrast, if the THz wave arrives after the pump pulse, the photogenerated free carriers attenuate the THz electric field due to the absorption of the mobile electrons.

After transmitting through the sample, the THz pulse is collected and focused by an elliptical mirror on the detector crystal ZnTe. A probe (detection) laser pulse is focused on this ZnTe as well and overlaps with the THz pulse in space and time. The Free space electro-optic (EO) sampling technique is utilized to probe the electric field of the THz pulse.^{123,124} Finally, the optical properties of semiconductors at THz frequencies can be recorded.

2.2.3 Time-resolved Photoluminescence (TRPL)

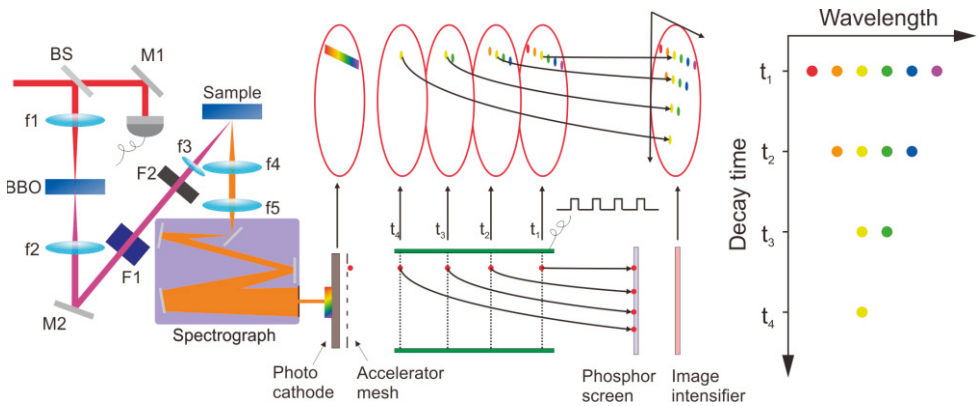


Figure 2.2.6. Schematic diagram of the streak camera TRPL system.

TRPL has been widely used to characterize semiconductor optoelectronic materials due to its non-contact testing.^{49,76,96,105,106,113–119} Several types of techniques are available to obtain temporal and spectral information related to the PL emission of semiconductor, such as time-correlated single photon counting (TCSPC) and streak camera.^{94,132,133} In this thesis, the streak camera is the most used method for measuring TRPL of our samples. **Figure 2.2.6** shows the schematic diagram of the streak camera. A laser at 800 nm with a repetition rate of 81 MHz and a pulse duration of 100 fs is the excitation source and is focused on the sample. If needed, frequency-doubled light (400 nm) was used for excitation. The PL signal is collected and focused on the input slit of a spectrograph by two quartz plano-convex lenses. The output PL light from the spectrograph is sent to the photocathode in the streak camera, which then converts the incident photons into photoelectrons. Subsequently,

these photoelectrons are accelerated by an electric field between the photocathode and the accelerator mesh. These electrons enter an electric field with high-speed sweep and then arrive to a phosphor screen. Finally, the TRPL pattern with temporal and spectral information is displayed on an image intensifier.

In general, TRPL measures the decay of the free charge carrier concentration. Alternatively, the TA and TRTS signals are sensitive to the overall population of the photo-generated charge carriers and to the mobile carriers, respectively. In order to understand the physical mechanism of photo-generated carriers in semiconductors better, these time-resolved spectroscopic techniques are usually combined together.

Chapter 3

Results & Discussion

3.1 Carrier Recombination Processes in GaAs Bulk Wafers Passivated by Wet Nitridation

As has been introduced above, carrier dynamics in bulk semiconductor of group III-V could be very different to the NW-based semiconductors of the same type. To see the case, we begin with studying carrier recombination in GaAs wafers. As surface contributes significantly to the fate of charge carriers, we consider several GaAs samples with surface processes affected by various treatments, in particular by wet passivation. Comparing to the passivation by means of overgrowth of a wide-bandgap semiconductor layer, chemical wet treatment is an inexpensive passivation approach.^{134–137} We aim at the passivation methods when a layer of GaN close to a monolayer is formed at the GaAs surface through surface nitridation by using hydrazine-sulfide solution. This thin layer can protect the crystal surface against oxidation over a period of months and can significantly improve the GaAs optical and electrical properties.⁹² However, a comprehensive description of the processes influenced by nitride passivation, especially carrier recombination have not been studied and understood in detail before our study.

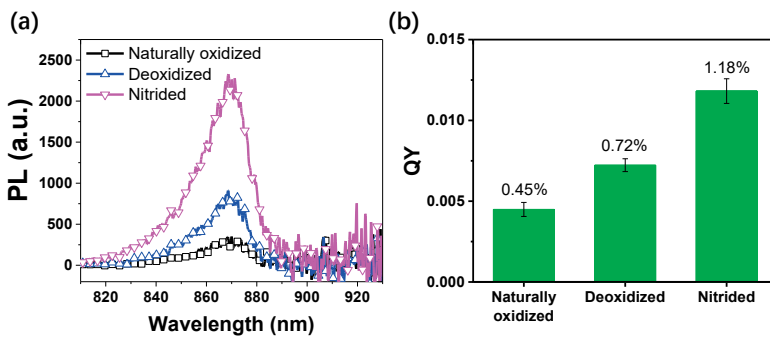


Figure 3.1.1.

(a) Time-integrated PL spectra of GaAs wafers with naturally oxidized, deoxidized and after 10 min nitridation treatment under photoexcitation at 1.6 eV. The excitation photon flux was 1.9×10^{13} photons cm^{-2} pulse⁻¹ for these PL spectra measurements. (b) Absolute PL QY of GaAs wafers with naturally oxidized, deoxidized and after 10 min nitridation treatment under photoexcitation at 1.6 eV. QY of the GaAs after nitridation is ~ 2.6 times higher than that of naturally oxidized GaAs and ~ 1.6 times higher than of the deoxidized GaAs. The excitation intensity was 1.8×10^{21} photons s^{-1} cm^{-2} .

First, intrinsic (unintentionally doped) GaAs wafers were prepared in three forms: naturally oxidized, deoxidized, and wet nitrided. To evaluate the overall surface treatment effect, we compared the time-integrated PL emission method to study these GaAs wafers, as shown in **Figure 3.1.1a**. We observed that the time-integrated PL intensity of the deoxidized (chlorine terminated) and the nitrided wafer is about 2.5 times and 7.5 times larger than that of the naturally oxidized samples, indicating that surface deoxidation and nitridation do reduce the non-radiative recombination processes.

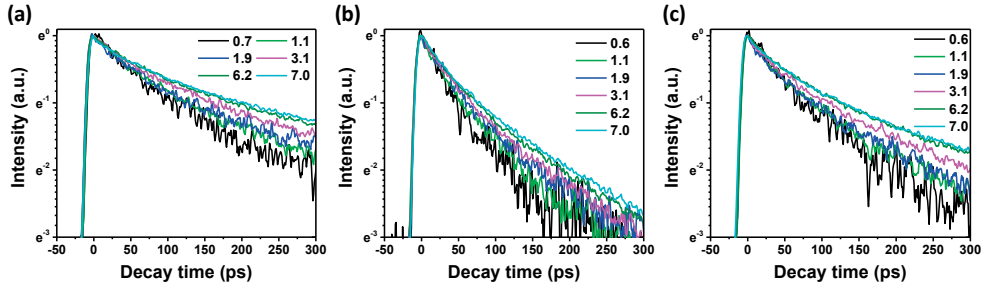


Figure 3.1.2. Normalized TRPL kinetics of (a) the GaAs after 10 min nitridation, (b) the natural oxidized GaAs, and (c) the deoxidized GaAs under varied excitation fluencies from 0.7 to 7.0×10^{13} photons cm^{-2} pulse $^{-1}$ at 1.6 eV.

Then, we analyzed TRPL kinetics to understand the processes related to recombination of photogenerated charge carriers. In **Figure 3.1.2**, via analysis of the TRPL kinetics of 10 min nitride treated, naturally oxidized, and deoxidized GaAs under varied excitation photon flux we observe that TRPL decays slower with increasing excitation fluency. In general, the radiative recombination, non-radiative Auger recombination, and trap-assisted non-radiative charge recombination with traps can lead to the decay of photogenerated carriers.^{101,117,138} Besides, spatial separation of mobile electrons and holes due to the built-in electric field close to the surface could also result in reduction of the radiative recombination rate.¹³⁹ However, it is worth noting that the spatially separated by this electric field photo-generated charges are still mobile. Therefore, they can recombine radiatively.

From the previous discussion in **Section 1.7**, both Auger recombination and radiative recombination processes should lead to a faster PL decay with increasing concentration of photogenerated charges. Thus, TRPL kinetics in our case are most likely dominated by the charge trapping processes. As is apparent from **Figure 3.1.2**, the PL decay cannot be fitted by a single exponential function. This could be related to an inhomogeneous distribution of trap energy and thus trapping rates in the samples.

In relation to the spatial separation of photogenerated electrons and holes, which could result from the surface pinning,¹⁴⁰ charges with a certain polarity will compensate the surface field when they drift to the surface of the GaAs wafer. Therefore, the contribution of early fast PL decay should decrease with an increase of the excitation fluence (injection level). On longer time scale, however, spatial separation of mobile charges should be reduced, resulting in their faster recombination at the long time, which is opposite to the observed dependency of the PL decay on the excitation intensity.

Further, if the observed PL decay is dominated by charge trapping, the slowing down PL decay with the injection level can be understood via trap filling. Specifically, at low excitation fluence the charge carriers are efficiently captured by empty traps. This leads to a fast PL decay. As the fluence increases, some of the traps are filled with photo-generated charges at the arrival of the next excitation pulse. As a result, the charge trapping rate decreases and PL decays slower.

Furthermore, we can distinguish the role of charge trapping and spatial separation in the PL dynamics through an absolute PL quantum yield (QY) measurement (**Figure 3.1.1b**). Spatial separation of photo-generated mobile charges should not reduce QY even if it slows down radiative recombination. Nevertheless, for all studied samples, we record QY at the level of 1%. Therefore, we believe that trapping processes dominate the dynamics of photogenerated charges, leading to their efficient non-radiative recombination.

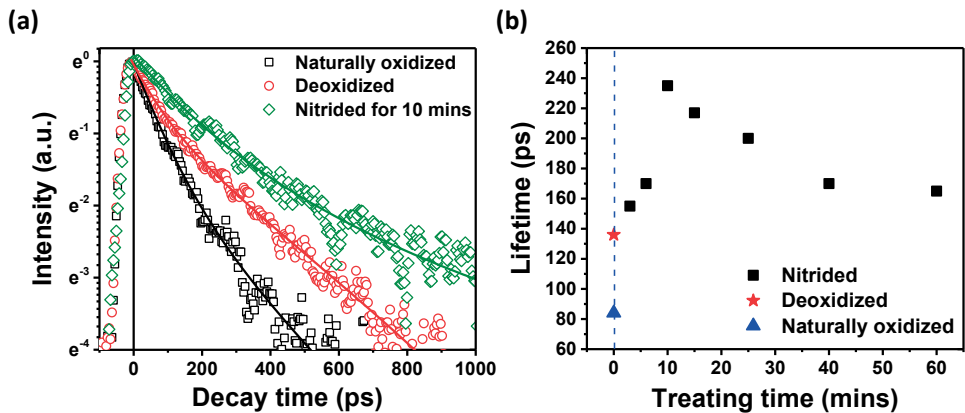


Figure 3.1.3.

(a) Normalized TRPL kinetics and (b) PL decay times of the GaAs wafer after naturally oxidized, deoxidized, and nitride surface with the varied nitridation time. The excitation photon energy and flux were 1.6 eV and 1.9×10^{13} photons cm^{-2} pulse⁻¹, respectively. Solid lines are the fitting curves based on double-exponential functions. In the **Figure 3b**, TRPL decay time is quantified via 1/e methods.

Figure 3.1.3b shows the PL decay times of the GaAs wafer after naturally oxidized, deoxidized, and nitride surface with the varied nitridation time. First, at the fluency of 1.9×10^{13} photons cm^{-2} pulse $^{-1}$ after 1.6 eV excitation, we find that the PL lifetime of GaAs after the best nitridation (see **Figure 3.1.3a**) is ~ 225 ps, which is 1.6 times longer than for the deoxidized GaAs (~ 140 ps) and 2.8 times longer than for the naturally oxidized sample (~ 80 ps). Second, we find that PL decay time of the nitride GaAs depends on the nitridation time in such a way that it initially increases and then decreases. The reason could be that a certain nitridation time is required to fully convert the GaAs surface,⁹² whereas an excessive nitridation could introduce new traps caused by the high GaAs/GaN lattice mismatch that may appear after the overgrowth of a thick GaN layer.⁹² Furthermore, SH^- anions could penetrate into the chemisorbed layer at longer nitridation and break the short-range order of the overlayer,³⁵ which could also create new trapping centers.

Further, we find that the ratio (naturally oxidized : HCl treated : best nitrided) of integrated spectra intensity (1 : 2.5 : 7.5) and the ratio of the absolute QY values (1 : 1.6 : 2.6) are not the same. We attribute this to the different types of excitations used: 80 MHz short pulse excitation used for time-integrated TRPL spectra and continuous wave (CW) excitation in the case of absolute QY measurements. Since the integrated spectra are obtained by the short pulse excitation, the instantaneous photon density could be much higher than that when the CW laser is used, leading to the trap filling effect. We interpret our results such as both surface deoxidation and nitridation have a stronger passivating effect on the non-filled traps.

Furthermore, when we compare the ratio of intensities of time-integrated spectra (1 : 2.5 : 7.5) and of time-resolved PL decays (1 : 1.6 : 2.8), we observe much more pronounced passivation effect on the time-integrated spectra. We associate this observation with the faster decay that was not resolved in TRPL experiment. Following this assignment, we have to conclude that the fast decay is passivated more efficiently under deoxidation and nitridation.

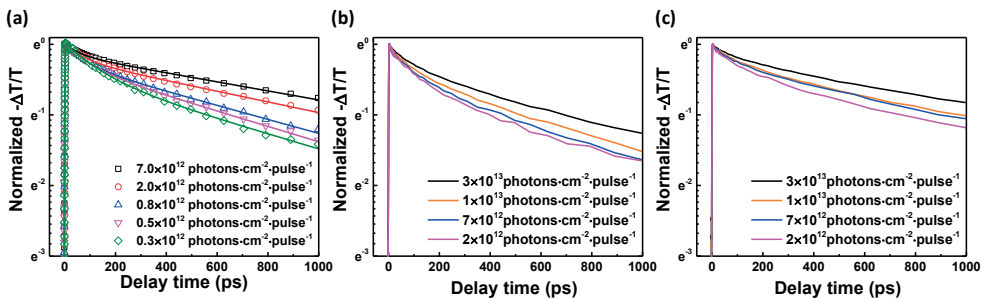


Figure 3.1.4. Normalized photoconductivity ($\Delta\sigma$) kinetics of (a) GaAs with 10 min nitridation, (b) the natural oxidized GaAs, and (c) the deoxidized GaAs under varied excitation fluencies after photoexcitation at 1.6 eV.

To investigate the dynamics of photoconductivity, we conducted TRTS measurements on the same samples. **Figure 3.1.4** shows TRTS kinetics of all GaAs wafers under varied excitation fluence. Obviously, photoconductivity $\Delta\sigma(t)$ decays non-exponentially, and the decay slows down with the increasing excitation fluence. Similar to the discussion on the TRPL data we argue that the slowing down of the $\Delta\sigma(t)$ decay with increased excitation is not coming from the non-linear recombination processes such as bi-molecular radiative and the third-order Auger recombination.

To investigate how surface nitridation influences electron recombination processes, we compare photoconductivity kinetics of GaAs wafers with the surface being naturally oxidized, deoxidized, and optimally nitrided at the same excitation fluence. In **Figure 3.1.5**, we show that the photoconductivity lifetime of the GaAs after nitridation (~ 1310 ps) is 3.1 times and 1.8 times longer than that of the naturally oxidized and deoxidized samples, respectively, suggesting that GaAs surface nitridation can effectively reduce the concentration of the electron traps and thus of the electron trapping rate.

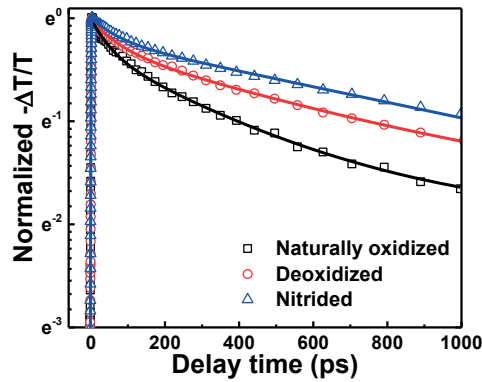


Figure 3.1.5.

Normalized $\Delta\sigma(t)$ kinetics of GaAs wafers after surface naturally oxidized, deoxidized and nitrided with 10 min treatment. The excitation photon energy and flux were 1.6 eV and 2×10^{12} photons cm^{-2} pulse $^{-1}$, respectively. Solid lines are fitting curves based on double-exponential functions.

In the **Section 2.2.2**, we have shown that TRTS is selectively sensitive to time-dependent $\Delta\sigma(t)$ of the sample and hence to the product of time-dependent carrier mobility $\mu_e(t)$, and the concentration of mobile carriers, $[N_e](t)$. In general, both of $\mu_e(t)$ and $[N_e](t)$ depend on the overall charge recombination or electron trapping which may not lead to charge recombination because charges can be de-trapped. In detail, $[N_e](t)$ will decay because mobile electrons recombine with mobile holes. Mobile electrons will recombine with trapped hole as well if they can encounter

with each other by the traps at the same place and then recombine instantaneously. Besides, trapped electrons can be de-trapped if they are trapped by shallow traps. So, $[N_e](t)$ will change because of the charge de-trapping processes. To $\mu_e(t)$, it depends on the concentration of mobile charges due to charge-charge scattering. Therefore, when the concentration of charges decreases, the mobility can arise. Furthermore, the trapping and de-trapping processes could also reduce $\mu_e(t)$ because electrons can be in traps for some time. Thus, slowing down of the $\Delta\sigma(t)$ decay at high excitations may be related to both slower disappearances of $[N_e](t)$ compared to that at low excitation and to slower decay and even to increase of $\mu_e(t)$ with time at higher excitations. Therefore, we consider these two contributions to the $\Delta\sigma(t)$ dynamics.

First, we assume that $\mu_e(t)$ does not change with time and excitation intensity. Then, similar to the considerations used for analysis for the excitation dependent TRPL dynamics, the $\Delta\sigma(t)$ effect can be associated with the mobile electrons trapping. A significant long-time photoconductivity is observed at all excitations and in all GaAs samples, indicating that not all electrons are trapped up to 1 ns delay time. This could result from a slow charge recombination, moderate electron trapping due to a relatively small number of traps, or from a non-negligible de-trapping process of the electrons, which results in establishing the equilibrium of trapped and mobile electrons.¹¹⁷ With the trap filling effect, the trapping rate decreases whereas the de-trapping rate may stay unchanged. The proportionality of $\Delta\sigma(t)$ to the concentration of the overall carriers varies with the delay time. First, we assume that the electron trapping by deep traps is fast. If all of the carriers are trapped by deep traps, $\Delta\sigma(t)$ will be zero. The possible reason for the long-lived $\Delta\sigma(t)$ could be that some of the deep traps are filled. But after that, $\Delta\sigma(t)$ will not change. Therefore, the electron trapping by deep traps cannot be a very fast process to match the wxperimental observation. Similarly, if reaching trapping – de-trapping equilibrium is very fast, $\Delta\sigma(t)$ will not change after that. So, reaching the trapping – de-trapping equilibrium should not be a very fast process neither. Furthermore, the apparent difference of the $\Delta\sigma(t)$ dependence on excitation for the GaAs surface with different treatments is consistent with the conclusion that electron traps are associated with the GaAs surface and that their density varies under the exploited treatments.

Second, we assume that $[N_e](t)$ does not change with time. From the TRPL result, we concluded that the concentration of mobile electrons and holes decreases with time in a concerted manner. On the other hand, the small PL yield values indicate that only a minor part of the photo-generated charges recombine radiatively. Thus, we can assume that most of mobile electrons are not involved in PL and the PL decay is dominated by the reduction of the mobile hole concentration. Using the above assumption, we have to assign the observed deceleration of the $\Delta\sigma(t)$ dynamics to $\mu_e(t)$, which then has to decay slower at higher excitations. However, this outcome is highly improbable as the carrier scattering processes should be more

efficient with the increase of their concentration.¹³⁸ Therefore, as each of the scattering processes is expected to be faster at higher excitations, we should expect faster decay of $\Delta\sigma(t)$ due to increasing scattering contrary to the observed trend.

Finally, the observed effect can be a combination of the decay of $[N_e](t)$ and the variation of $\mu_e(t)$. To examine a possible contribution of $\mu_e(t)$, we first assume that $[N_e](t)$ decay is independent of the excitation density and $[N_e](t)$ is proportional to the excitation density at any delay times. Then the observed slowing down of $\Delta\sigma(t)$ should be associated with the increase of $\mu_e(t)$ as $[N_e](t)$ decreases. Contrary to this expectation, the observed that $\Delta\sigma(t)$ increases linearly with the excitation density both at early and late delays (see **Figure 3.1.5a**) and late (**Figure 3.1.6b**) suggesting a constant $\mu_e(t)$ over the presented range of excitations, which largely covers the density range used when slowing down of $\Delta\sigma(t)$ was observed, see **Figure 3.1.6a**. We note here that at even higher excitations, $\Delta\sigma(t)$ does not change linearly with the excitation density at early and late delay times, see **Figure 3.1.6c, d**.

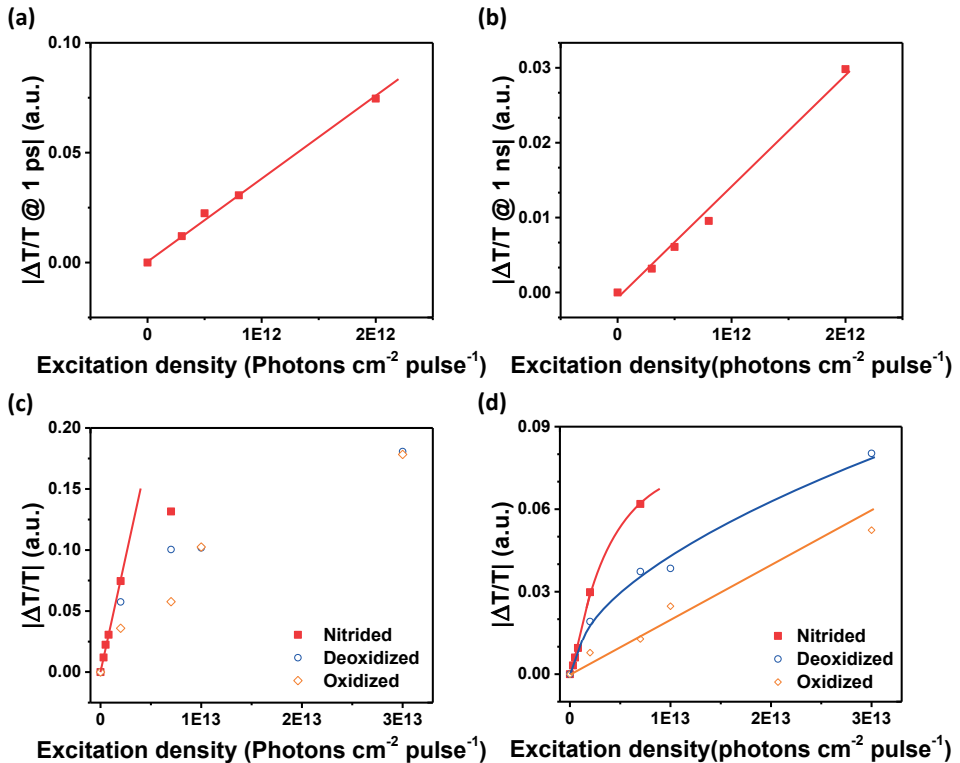


Figure 3.1.6.

Photoconductivity of GaAs with 10 min nitridation measured at the delay time of (a) ~1 ps and (b) ~1 ns, after photoexcitation at 1.6 eV under varied excitation fluencies. Photoconductivity of GaAs with 10 min nitridation, deoxidized and naturally oxidized measured after photoexcitation at 1.6 eV under varied excitation fluencies at (c) ~1 ps delay time and (d) ~1 ns delay time.

To the nitride sample, the signal measured over the first four points at both 1 ps and 1 ns can be fitted by a linear function. The slope of the $\Delta\sigma(t)$ dependency on $[N_e](t)$ at 1 ns actually increases with time by $\sim 30\%$ compared to the 1 ps delay (see **Figure 3.1.6a, b**). Such an increase with time of $\mu_e(t)$, which is excitation independent at each delay, seems unreasonable, implying that the observed $\Delta\sigma(t)$ behavior is most probably related to $[N_e](t)$ decay function that changes with time as discussed earlier. It is possible that $\mu_e(t)$ does contribute to the $\Delta\sigma(t)$ decay changes as well, but it appears reasonable to assign most of the decay to $[N_e](t)$ dynamics.

Besides, it is worth to consider the influence of charge diffusion, which could also reduce the concentration of mobile electrons and thus increase their mobility, μ_e . We note here that surface modification should not affect the bulk of GaAs. Spatial distribution of photo-generated charge and thus their diffusion should not depend on the excitation density (within the linear excitation conditions) and on the status of the surface. Therefore, an identical effect of diffusion is expected for all GaAs samples independent on the surface treatment, which is in a clear disagreement with the experimental observations, see **Figure 3.1.5**. Thus, we conclude that the dynamics of $[N_e](t)$ is mainly responsible for the observed retardation of $\Delta\sigma(t)$ decay with excitation density.

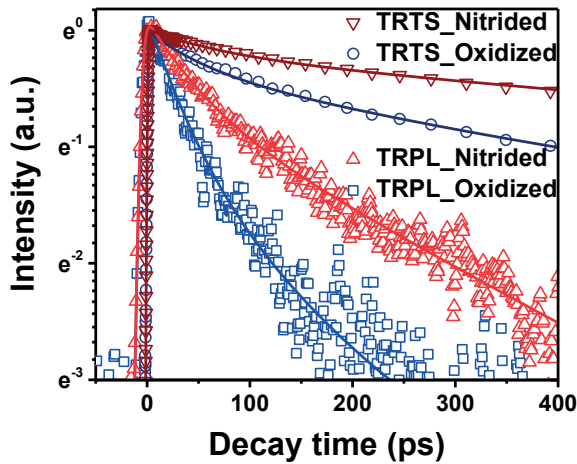


Figure 3.1.7.

Normalized photoconductivity and PL kinetics of GaAs with naturally oxidized and 10 min nitridation after photoexcitation at 1.6 eV. The excitation photon flux in TRPL was 7×10^{12} photons \times cm $^{-2}$ \times pulse $^{-1}$, and in TRTS it was 2×10^{12} photons \times cm $^{-2}$ \times pulse $^{-1}$.

Further, TRPL and THz kinetics of GaAs with modified surfaces at similar excitation fluencies have been compared, as shown in **Figure 3.1.7**. We find that PL decays much faster than photoconductivity in GaAs with naturally oxidized and

nitride surface (~ 140 ps and ~ 400 ps versus ~ 420 ps and ~ 1310 ps, respectively). As discussed above, photoconductivity decay is at least partially associated with the mobile electron trapping, while PL decay depends on both electron and hole trapping. Much faster PL decay implies that PL dynamics is dominated by the hole trapping process.

In general, the Surface Recombination Velocity (SRV) is frequently used to describe the process when charges generated in materials move to the materials surface where they instantly recombine either with each other or with trapped charges. However, in this study, we find that PL decay is not dominated by charge recombination. Moreover, since the mobility of electrons is much higher than that of holes, electron trappings process should dominate the SRV extracted from optical measurements. However, we find that the disappearance of mobile holes is faster than that of electrons. Therefore, we think that the process at the surface should be re-interpreted. From PL dynamics, charge trapping rather than recombination can be extracted. Therefore, “surface recombination velocity” should be better re-named as “surface trapping velocity”.

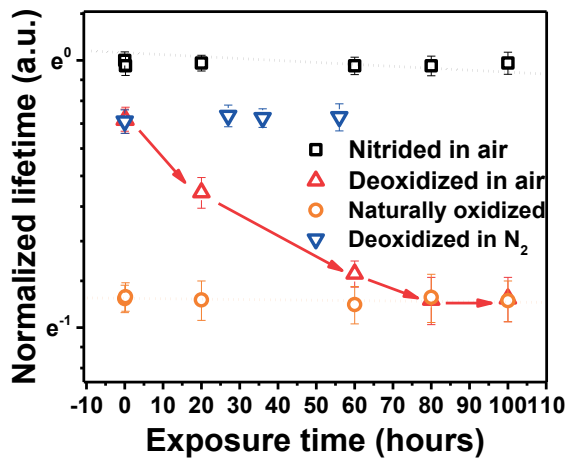


Figure 3.1.8. PL lifetime of deoxidized, naturally oxidized and nitrided GaAs as a function of exposure time in air or nitrogen.

Figure 3.1.8 shows PL decay measured after varied time of the GaAs exposure to air and to N₂. First, we came to an unexpected conclusion that the GaAs surface deoxidized by HCl is resistant to air exposure because of the slow decay of the lifetime in 80 hours. The measured time is opposite to the traditional believe that surface oxidation occurs nearly instantly.^{142,143} The slower oxidation time should be related to the replacement of chlorine at the surface of GaAs by oxygen, which

apparently takes time. After surface nitridation, we have not observed any measurable change of the PL lifetime during 80-hour exposure to air. Apparently, surface nitridation results in resistive passivation of the GaAs surface, which could be of significant importance for multiple applications of GaAs crystals.

In conclusion, we have investigated the effect of wet passivation in GaAs wafer by deoxidation and nitridation. Physical mechanisms of photo-generated carriers are studied in naturally oxidized, deoxidized, and nitrided GaAs wafer by means of time-resolved and steady-state spectroscopy. We found that the trap-assisted non-radiative recombination dominates the overall recombination process. The hole trapping process in this study dominates PL quenching. After optimized nitridation of GaAs (100), hole and electron trapping rates reduce compared to naturally oxidized GaAs by factors of 2.6 and 3, respectively. The nitrided GaAs (100) can resist air over at least one hundred hours. This study not only demonstrates efficient chemical and electronic passivation by nitridation but also dwells on the details of the carrier recombination processes at the surface of GaAs (100).

3.2 Carrier Dynamics in Core-shell AlGaAs/GaAs NWs array

As a relatively common means of passivation, AlGaAs is often grown on the surface of GaAs to reduce the contribution of the charge trapping process. Here, we account for our study where carrier recombination behaviour in GaAs/AlGaAs core-shell NWs array was studied by steady-state and time-resolved PL methods.

GaAs/AlGaAs NW arrays were grown on p-type GaAs wafer by using the MOVPE method. The NWs had a length of $\sim 2.8 \mu\text{m}$, a diameter of $\sim 0.23 \mu\text{m}$, and a pitch of $\sim 0.5 \mu\text{m}$, which were characterized using SEM (**Figure 3.2.1a** and **Figure 3.2.1b**). The NW arrays with this growth parameter exhibit outstanding absorption characteristics. The absorption spectrum and the absorbance at 780 nm were measured by an integrating sphere installed in the absorption spectrometer and PL emission spectrometer. As is shown on **Figure 3.2.1c**, the absorption of the AlGaAs/GaAs core-shell NWs array was above 1.2 O.D. in the range of 250 to 875 nm, corresponding to the absorbance of $\sim 94\%$. With this absorbance, $\sim 44\%$ of the photons from AM1.5 solar radiation should be absorbed. In addition, the excitation intensity dependent absorption spectra in **Figure 3.2.1d** shows that the absorbance of the NW array is independent on the excitation power at 780 nm in the fluence range of 9 mW/cm^2 to $400,000 \text{ mW/cm}^2$, showing extremely absorption characteristics under high-intensity light.

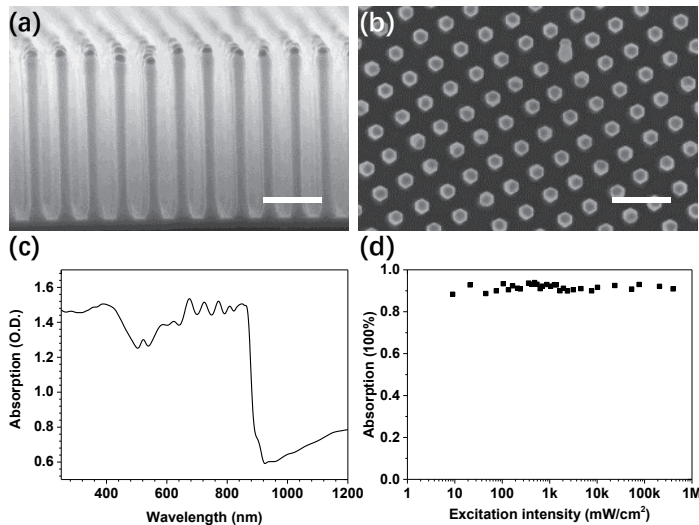


Figure 3.2.1.

(a) Side and (b) top-view scanning electron microscopy graphs of GaAs/AlGaAs NWs with a density of $4 \times 10^8 \text{ cm}^{-2}$ grown by the MOVPE method. The scale in the figure is $1 \mu\text{m}$. (c) Absorption of the NWs from 250 nm to 1200 nm. (d) Absorbance of the NWs at 780 nm under the excitation from smaller than 10 mW/cm^2 to $400,000 \text{ mW/cm}^2$.

To determine the composition of Al in the shell, steady-state PL was measured, as shown in **Figure 3.2.2**. The PL spectrum exhibits two emission peaks, at ~ 1.42 eV and ~ 1.80 eV. The ~ 1.42 eV peak is consistent with the bandgap of GaAs, and thus can be attributed to the emission from GaAs core. Then, the emission of ~ 1.80 eV peak can be attributed to the emission from AlGaAs shell. According to the correlation between Al composition and PL emission energy, the Al composition (x) can be calculated by $E_g(x) = 1.422 \text{ eV} + 1.2475 \text{ eV} \cdot x$. So, x is ~ 0.3 .¹⁴⁴⁻¹⁴⁶

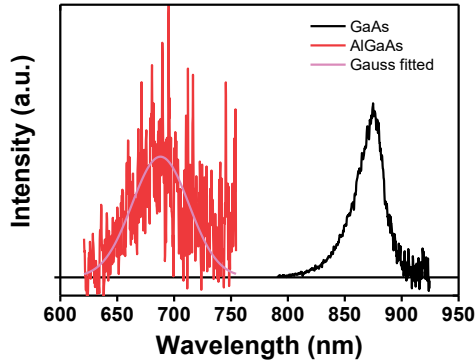


Figure 3.2.2. GaAs and AlGaAs integrated PL emission. Note here the emission of AlGaAs is zoomed in.

To have a better understanding of carrier recombination dynamics of GaAs/AlGaAs NWs, we measured TRPL kinetics under varies excitation fluence, as shown in **Figure 3.2.3**. We find that the kinetics can be approximated by a bi-exponential decay function. Both decay components are independent on excitation when the excitation is lower than 4.5×10^{10} photons \cdot cm $^{-2}$ \cdot pulse $^{-1}$, while the fast decay component slows down and the slower decay component becomes faster when the excitation fluency exceeds 2.5×10^{11} photons \cdot cm $^{-2}$ \cdot pulse $^{-1}$. Here, we attribute the fast recombination to charge trapping of minor carriers at the interface of the core-shell structure due to the surface electric field that is induced by the background charges. The background charges that are trapped at the interface could induce a surface electric field, and thus induce a band bending. This electric field could promote the drift of minor carriers towards the interface followed by their trapping. The trapped charges then weaken the surface electric field, so that charge drift and trapping become slower. The influence of surface electric field could be weakened when the concentration of photo-generated charges is high, and thus the electric field-driven charge trapping could be slower. Therefore, we observe the faster decay component becomes slowing down with excitation fluency. The slower decay component could be induced by charge trapping without surface electric field and/or bimolecular

carrier recombination processes. For the kinetics at the lowest excitation density, we find that the kinetics are independent with excitation power, thus the slower decay component would be dominated by carrier trapping without the electric field rather than by the bi-molecular recombination that has to depend on the charge concentration and therefore on the excitation fluence.

By fitting the kinetics by bi-exponential decay functions, we get a charge trapping rate without a surface electric field, which is $3.45 \times 10^8 \text{ s}^{-1}$. We should note that surface electric field-induced charge trapping may be not pronounced at the steady-state irradiation conditions due to the long-lived trapped charges and continuous absorption of photons. Actually, using the literature data, we expect ~ 100 background charges in each NW. When the excitation density of the CW irradiation is larger than 1 W/cm^2 , the photogenerated carriers can compensate the electric field induced by the background charges if the trapped charge lifetime is 10 ns. Experimentally, we find that the fast decay in TRPL starts to saturate when the excitation fluency is about $4.5 \times 10^{10} \text{ photon cm}^{-2} \text{ pulse}^{-1}$, which is corresponding to ~ 110 photons absorbed in one NW after a pulse irradiation. This leads to the conclusion that the fast PL decay is caused by the electric field generated by background carriers. Therefore, the charge trapping process without surface electric field could contribute to the steady-state irradiation conditions. With the increase in the excitation fluence, bimolecular recombination would become pronounced, as the probability for meeting of free electrons and holes increases, and thus the slower component becomes faster.

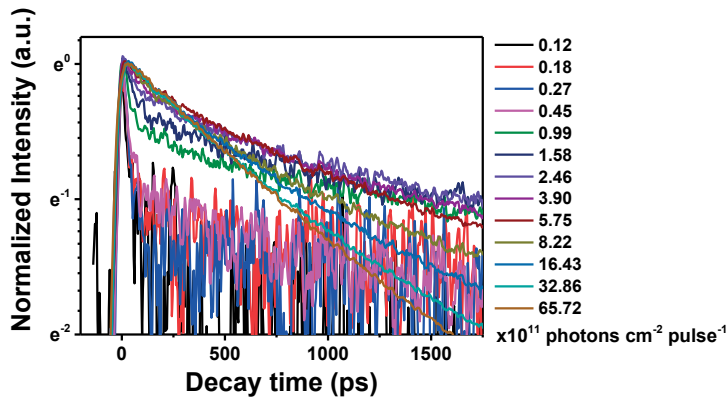


Figure 3.2.3.

TRPL kinetics of GaAs core in GaAs/AlGaAs NWs at indication excitation fluency after photoexcitation at 1.59 eV.

Then, a series of absolute PL quantum yield measurements of as-grown GaAs/AlGaAs NW array at a wide range of excitation density using an integration sphere method was conducted. **Figure 3.2.4** shows the PLQY of the NW array under

varied excitation fluency. We find that PLQY has a complicated fluency dependence: at the low fluence ($<300 \text{ mW/cm}^2$), it is independent of excitation fluency; at excitation fluency higher than 10k mW/cm^2 it increases linearly; between 300 and 400k mW/cm^2 , we observe a non-linear increase.

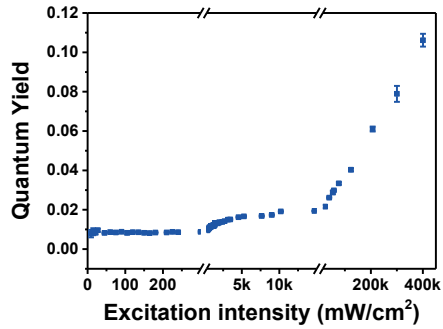


Figure 3.2.4. PL QY of GaAs/AlGaAs core-shell NWs under varies excitation fluency after photoexcitation at 780 nm.

From the discussion in the **Section 2.1.3** we concluded that, when the excitation density is very small, the geminate recombination of photo-generated carriers or recombination of photo-generated carriers and background free carriers could dominate the QY. First, we used the model of the background carriers (see **Figure 3.2.5a**) to describe this behaviour. Obviously, this model is in disagreement with our experimental results. Therefore, the background carriers should not contribute to the radiative recombination when the excitation density is low. Most probably the background carriers are not free due to trapping and thus cannot contribute to radiative recombination.

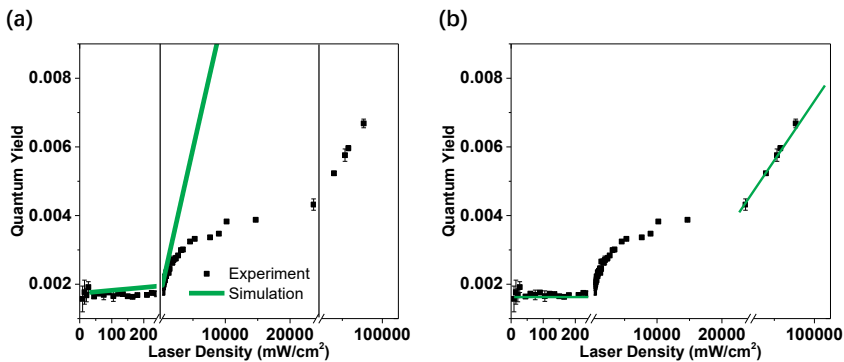


Figure 3.2.5. Experiment and simulation results of PLQY vs excitation laser density depending on (a) the background carriers model and (b) the geminate recombination model.

Then, a model, which includes geminate radiative recombination was applied to explain the trend of the QY dependence at various excitation density. Although at low excitation and at high excitation density, the model can fit the experimental data very well, the transition region between the geminate recombination and bimolecular recombination dominated regions cannot be fitted (see **Figure 3.2.5b**). We concluded that more complex carrier recombination processes, such as charge trapping and trap filling processes,¹⁴⁷ should be considered in this region.

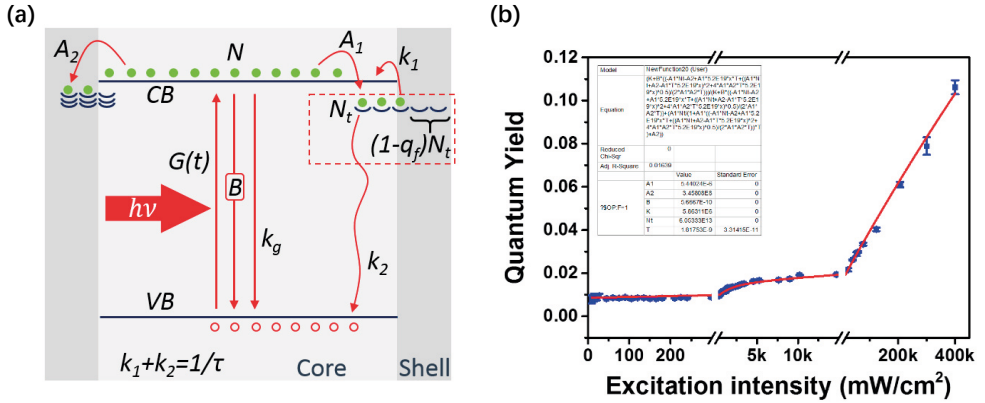


Figure 3.2.6.

(a) Schematic of carrier generating, trapping, and recombination processes. (b) Experiment and simulation results of PLQY vs excitation laser density depending on the geminate recombination model with trapping and trap filling processes.

This trap filling effect also has been reported previously when the carrier density was very high, leading to a PL decay time increasing with increasing the irradiance.¹⁴⁸ However, in our QY experiments, the QY is still very low after the trap filling effect, meaning that although one kind of trap states is filled, probably some other traps cannot be filled easily due to their large density or fast non-radiative recombine process, which involves trapped charges. So, as follows from the previous expression for QY modelling (see **Equation 2-4**), we should add the geminate radiative and at least two kinds of trap-assisted non-radiative recombination processes. In these two trap-assisted recombination processes, one kind of traps can be relatively easily filled but another one kind is not easily filled (see **Figure 3.2.6a**). Then, the QY expression is modified as

$$QY = \frac{k_g + BN}{k_g + BN + A_1 N_t (1 - q_f) + A_2} \quad (3 - 1)$$

, where k_g (s⁻¹) is the geminate recombination rate; A_1 (cm³ s⁻¹) and A_2 (s⁻¹) are the trapping rates which can and cannot be saturated, respectively; N_t (cm⁻³) is the

concentration of the trap states to be filled; and q_f is the fraction of filled traps. q_f is a function of N , $q_f = f(N)$ such that

$$\frac{dq_f}{dt} N_t = A_1 N N_t (1 - q_f) - \frac{q_f}{\tau} N_t \quad (3 - 2)$$

Then,

$$\frac{dq_f}{dt} = A_1 N (1 - q_f) - \frac{q_f}{\tau} \quad (3 - 3)$$

Under the steady-state conditions, $\frac{dq_f}{dt} = 0$.

So,

$$AN(1 - q_f) = \frac{q_f}{\tau} \quad (3 - 4)$$

Then,

$$q_f = \frac{A_1 N \tau}{1 + A_1 N \tau} \quad (3 - 5)$$

Then, Substitute **Equation 3-5** to **Equation 3-1**:

$$QY = \frac{k_g + BN}{k_g + BN + \frac{A_1 N_t}{1 + A_1 N \tau} + A_2} \quad (3 - 6)$$

, where N can be expressed as a function of $G(t)$. Under the steady-state conditions, the carrier generation rate $G(t)$ is equal to the recombination rate. In this case, $G(t) = \frac{dN}{dt}$, therefore,

$$G(t) - A_1 N N_t (1 - q_f) - A_2 N - k_g N - BN^2 = 0 \quad (3 - 7)$$

Here, $G(t)$ (mW/cm^3) can be estimated by the number of photons that NWs absorb at different excitation flux (F (mW/cm^2)). The NW density (D) and the volume of one NW (V) are

$$D = 4 \times 10^8 \text{ cm}^{-2} \quad (3 - 8)$$

and

$$V = \pi r^2 l = 1.7 \times 10^{-13} \text{ cm}^3 \quad (3 - 9)$$

The Absorbance (η_{Abs}) of the NWs array in the range of excitation intensities, which were used in QY measurement is:

$$\eta_{Abs} = 90\% \quad (3 - 10)$$

The photon energy at 780 nm is

$$E_{Photon} = h \frac{c}{\lambda} = 2.55 \times 10^{-19} \text{ J} \quad (3 - 11)$$

Let's set $P_{Exc.}$ (mW) as the power of the excitation light, A (cm²) as irradiated area, U (cm³) as the whole volume of the irradiated NWs. So, the carrier generation rate $G(t)$ (s⁻¹ · cm⁻³) is:

$$\begin{aligned} G(t)(s^{-1} \cdot \text{cm}^{-3}) &= \frac{\eta_{Abs.} \cdot P_{Exc.}(mW)}{V(\text{cm}^3) \cdot E_{Photon}(J)} \\ &= \frac{\eta_{Abs.} \cdot F(\text{mJ} \cdot \text{s}^{-1} \cdot \text{cm}^{-2}) \cdot A(\text{cm}^2)}{U(\text{cm}^3) \cdot D(\text{cm}^{-2}) \cdot A(\text{cm}^2) \cdot E_{Photon}(J)} \\ &= \frac{\eta_{Abs.} \cdot F(10^{-3} \text{ J} \cdot \text{s}^{-1} \cdot \text{cm}^{-2}) \cdot A(\text{cm}^2)}{U(\text{cm}^3) \cdot D(\text{cm}^{-2}) \cdot A(\text{cm}^2) \cdot E_{Photon}(J)} \\ &= 5.2 \times 10^{19} \times F (\text{mW} \cdot \text{cm}^{-2}) \end{aligned} \quad (3 - 12)$$

The **Equation 3-7** can be re-written as:

$$G(t) = 5.2 \times 10^{19} (\text{cm}^{-1}) \times F = k_g N + BN^2 + A_1 NN_t (1 - q_f) + A_2 N \quad (3 - 13)$$

Because of the domination of the non-radiative recombination,

$$G(t) \approx A_1 NN_t (1 - q_f) + A_2 N \quad (3 - 14)$$

Set $G = G(t)$ and substitute **Equation 3-5** to **Equation 3-14**,

$$G = \frac{A_1 N_t N}{1 + A_1 N \tau} + A_2 N \quad (3 - 15)$$

Then, N can be presented as the following equation as a function of G :

$$N(G) = \frac{-(A_1 N_t + A_2 - A_1 \tau G) + \sqrt{(A_1 N_t + A_2 - A_1 \tau G)^2 + 4A_1 A_2 \tau G}}{2A_1 A_2 \tau} \quad (3 - 16)$$

Substrate **Equation 3-16** to **Equation 3-6** and do the fitting. The result is shown in **Figure 3.2.6b**, getting the parameters of A_2 , B , and k_g as shown in **Table 3.2.1**. Meanwhile, the relation between N_t , A_1 , and τ is obtained as well ($A \cdot N_t = 3.24 \times 10^8 \text{ s}^{-1}$, $N_t / \tau = 3.32 \times 10^{22} \text{ cm}^{-3} \cdot \text{s}^{-1}$).

In the QY experiment, a dominated trap filling effect happens in the range from ~ 300 to $\sim 10\text{k}$ mW/cm² as shown in **Figure 3.2.6b**. So, from **Equation 3-12**, the photo-generated carrier rate at 300 mW/cm² is

$$G(t)_{start} = \frac{\eta_{Abs.} \cdot P_{Exc.}}{V \cdot E_{photon}} = 1.56 \times 10^{22} \text{ cm}^{-3} \cdot \text{s}^{-1} \quad (3 - 17)$$

With q_f increases, the trapping process becomes saturated due to trap filling. So, the generation rate of photo-generated carrier at 10k mW/cm² is

$$G(t)_{end} = \frac{\eta_{Abs.} \cdot P_{Exc.}}{V \cdot E_{photon}} = 5.2 \times 10^{23} \text{ cm}^{-3} \cdot \text{s}^{-1} \quad (3 - 18)$$

When traps just start to be filled, $q_f = 0$, then both trapping processes contribute.

$$G(t) \approx A_1 N N_t + A' N \quad (3 - 19)$$

So, the density of photo-generated carriers is:

$$N \approx \frac{G(t)_{start}}{A_1 N_t + A_2} = \frac{1.56 \times 10^{22} \text{ cm}^{-3} \cdot \text{s}^{-1}}{(3.24 + 3.45) \times 10^8 \text{ s}^{-1}} = 2.3 \times 10^{13} \text{ cm}^{-3} \quad (3 - 20)$$

With increasing N , traps are gradually filled to $q_f = 1$, then the A_2 trapping process dominated the carrier depopulation,

$$G(t) \approx A_2 N \quad (3 - 21)$$

So, the density of photo-generated carriers become

$$N \approx \frac{G(t)_{end}}{A_2} = \frac{5.2 \times 10^{23} \text{ cm}^{-3} \cdot \text{s}^{-1}}{3.45 \times 10^8 \text{ s}^{-1}} = 1.5 \times 10^{15} \text{ cm}^{-3} \quad (3 - 22)$$

, meaning that (A_1) trap filling happens in the following range of $N = 2.3 \times 10^{13} \sim 1.5 \times 10^{15} \text{ cm}^{-3}$, and then the (A_1) trap density, N_t , is estimated in the range of $10^{13} \sim 10^{15}$

cm^{-3} as trap-assisted recombination is the most efficient way in carrier recombination processes in AlGaAs/GaAs core-shell NWs array as is indicated by the extremely low QY. Here, the trap density is in agreement with the published trap density in GaAs NWs ($1 \times 10^{13} \sim 1.2 \times 10^{15} \text{ cm}^{-3}$).^{149,150} Because N_t , A_I , and τ are coupled in the fitting procedure, independently on the N_t , the dependence of N and q_f to the excitation density is the same at different N_t . According to the range of N_t , we can estimate A_I and τ as shown in **Table 3.2.1**.

Table 3.2.1.

Fitting parameters of QY traces in **Figure 3.2.6b** by using the geminate recombination model with trapping and trap filling processes.

A_2	B	k_g
$3.45 \times 10^8 \text{ s}^{-1}$	$5.67 \times 10^{-10} \text{ cm}^3 \cdot \text{s}^{-1}$	$5.86 \times 10^6 \text{ s}^{-1}$
N_t	A_1	τ
$10^{13} \sim 10^{15} \text{ cm}^{-3}$	$3.24 \times 10^{-7} \text{ cm}^3 \cdot \text{s}^{-1} \sim 3.24 \times 10^{-5} \text{ cm}^3 \cdot \text{s}^{-1}$	$10^{-10} \text{ s} \sim 10^{-8} \text{ s}$

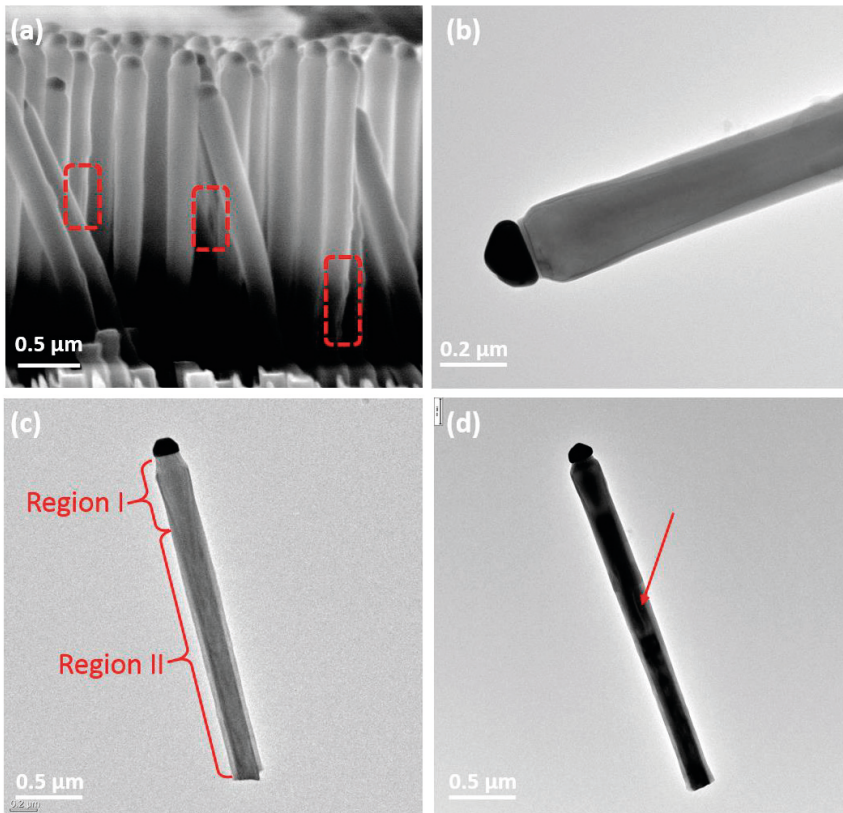


Figure 3.2.7.

(a) SEM and (b)-(d) TEM of AlGaAs/GaAs core-shell NW.

Finally, to understand the nature of traps in GaAs/AlGaAs NWs, we characterized the structure of the NWs via SEM. In **Figure 3.2.7c**, the thickness of the AlGaAs shell in the Region I and Region II is less than 10 nm and approximately 50 nm, respectively. Usually, a thicker AlGaAs shell can suppress the non-radiative recombination processes more efficiently. However, when the thickness of AlGaAs is too large, the defect can be formed inside the AlGaAs shell¹⁵¹ as shown in the **Figure 3.2.7a, d**. The non-single exponential PL decay may result from an inhomogeneous distribution of surface traps in energy and space along the NWs. For the AlGaAs/GaAs core-shell NW shown in the **Figure 3.2.7d**, we have observed a good crystallinity that comes from the diffraction patterns along the NW (see **Figure 3.2.8**). With the good AlGaAs passivation, most of the interface traps could be passivated, resulting in the trap filling effect in the QY measurements. However, thick AlGaAs may deteriorate the lifetime of the free carriers due to formation of defects in AlGaAs, resulting in a larger number of trap states which are hardly to be filled. Alternatively, thick AlGaAs can break the short-range order of the GaAs core and then generate more trap states at the interface.¹⁵¹

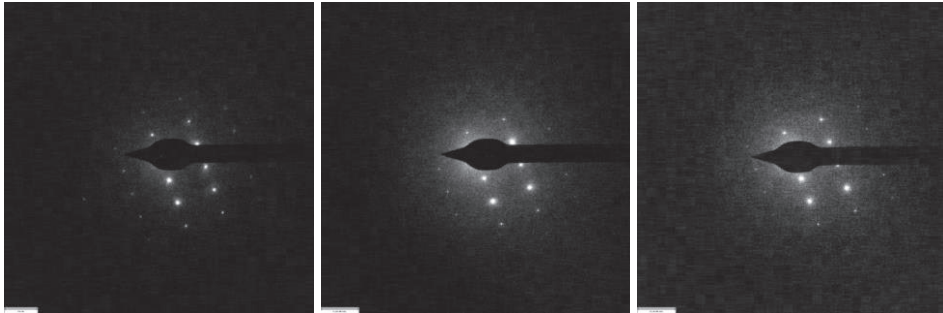


Figure 3.2.8. Diffraction patterns at head, body and tail of the GaAs NW in **Figure 3.2.7d**, respectively.

In summary, in this study, we report for the first-time observation of a geminate recombination in the group III-V semiconductor NWs. A physical model that includes bimolecular and geminate recombination that dominate radiative recombination processes at high and low excitations separately was applied for explaining varies excitation fluence dependence of PL QY. The bimolecular recombination rate of $5.67 \times 10^{-10} \text{ cm}^3 \cdot \text{s}^{-1}$, the geminate recombination rate of $5.86 \times 10^6 \text{ s}^{-1}$, the trap density of $10^{13} \sim 10^{15} \text{ cm}^{-3}$, and the trap lifetime in the range of $10^{-10} \text{ s} \sim 10^{-8} \text{ s}$ were extracted. Furthermore, three kinds of trapping processes were found in GaAs/AlGaAs core-shell NWs. The trapped background charges induced surface electric field that promote the photogenerated carriers towards the interface

where they are trapped, leading to a fast decay of PL. Although one kind of traps could be filled at the steady-state irradiation conditions, low QY in this excitation range suggests that trapping processes still dominates because the other trapping channels are still very active. A trapping rate of $3.45 \times 10^8 \text{ s}^{-1}$ for the trap that cannot be filled and another trapping rate of $3.24 \times 10^{-7} \text{ cm}^{-3} \cdot \text{s}^{-1} \sim 3.24 \times 10^{-5} \text{ cm}^{-3} \cdot \text{s}^{-1}$ for traps that can be filled are used in our model. This study prompts us to rethink trapping and recombination behaviours of the photogenerated carrier in NWs semiconductor materials due to the confinement effect of nanoscale-size NWs on carrier dynamics.

3.3 Growth Improvement in InP NWs by Hydrogen Chloride Etching

In situ etching of InP NWs by using HCl was found to suppress radial growth and to improve the morphology and PL of the NWs. Here, we investigate the dynamics of photo-generated charge carriers in a series of InP NWs grown with varied HCl fluxes. First, InP NW arrays were grown by using metal organic vapor phase epitaxy (MOVPE) method. The SEM pictures of 6 InP NW arrays grown with different molar fractions of HCl (χ_{HCl}) in the gas phase with tri-methylindium (TMIn) at molar fractions of $\chi_{\text{TMIn}} = 7.4 \times 10^{-5}$ and phosphine (PH_3) at molar fractions of $\chi_{\text{PH}_3} = 6.92 \times 10^{-3}$, ranging from 0 to 8.5×10^{-5} , are shown in **Figure 3.3.1**, suggesting that the morphology of the as-grown NWs is significantly affected by χ_{HCl} .

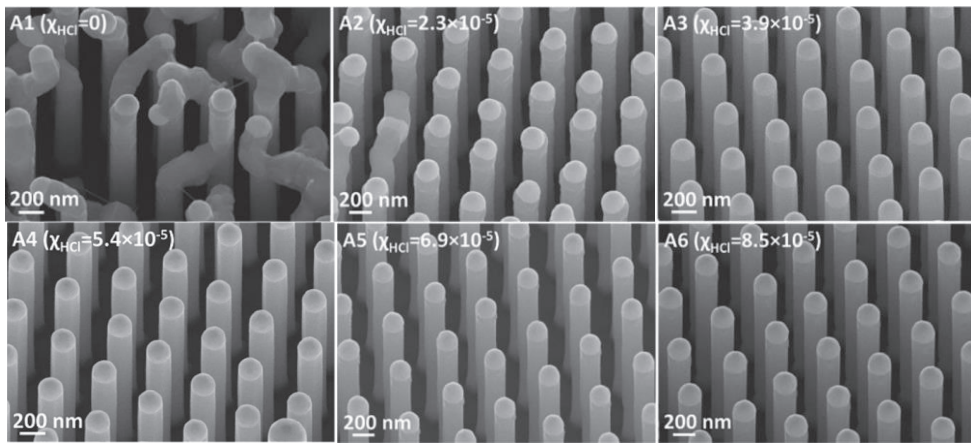


Figure 3.3.1. SEM images of the InP NWs grown with different HCl molar fractions. The images were recorded at an angle of 30° toward the normal plane of the substrate.

In order to investigate the carrier recombination processes with different HCl etching, the TRPL was studied in as-grown NWs and in the NWs embedded in a polymer matrix. We used excitation from both top and bottom sides of the NW arrays when considering the direction of the NW growth. First, in **Figure 3.3.2** it is shown that the PL decay is qualitatively similar in as-grown and polymer-embedded NWs, suggesting that the photo-physics of NWs is nearly unaffected by the presence of the polymer. Apparently, the PL decay is the slowest for the NWs with a HCl molar fraction of $\chi_{\text{HCl}} = 5.4 \times 10^{-5}$, whereas it speeds up as the HCl molar fraction becomes higher.

To distinct the recombination of mobile charge carriers in as-grown InP NWs, the PL decay under different excitation fluence was investigated as shown in **Figure**

3.3.3. In this study, when the excitation fluence changes two times, the PL decay almost stays unchanged, implying that the PL decay is not dominated by the second and third order processes in the employed excitation range. Therefore, the dominated process could be a first-order and intensity-independent charge trapping. However, in **Figure 3.3.3b**, we find that the PL decay becomes slightly faster at higher excitation fluency, indicating that there is a possible minor contribution of the radiative recombination in the PL dynamics. This trend can be seen only when the trapping rate is relatively slow as the PL decay is ~ 10 times slower than that of other two samples ($\chi_{\text{HCl}} = 0$ and 8.5×10^{-5}) judging by the $1/e$ amplitude decrease.

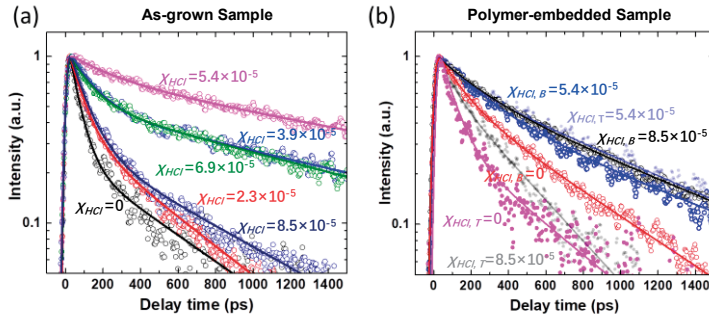


Figure 3.3.2.

(a) Spectrally integrated PL kinetics of InP NW arrays grown with different HCl molar fractions after photoexcitation at 400 nm. The excitation photon flux was 9×10^{11} photons per cm^2 per pulse. (b) Spectrally integrated PL kinetics of InP NW arrays embedded in the polymer, after photoexcitation at 780 nm of the top (T) and bottom (B) of the NW arrays. Symbols: measurements. Closed and open symbols correspond to the kinetics for the Top or the Bottom of the NW arrays, respectively. Lines: fits by biexponential decay functions.

Note here that all the measured PL decays can be fitted by a bi-exponential decay function. This may be associated with a distribution of trapping rates as we discussed in the previous studies.

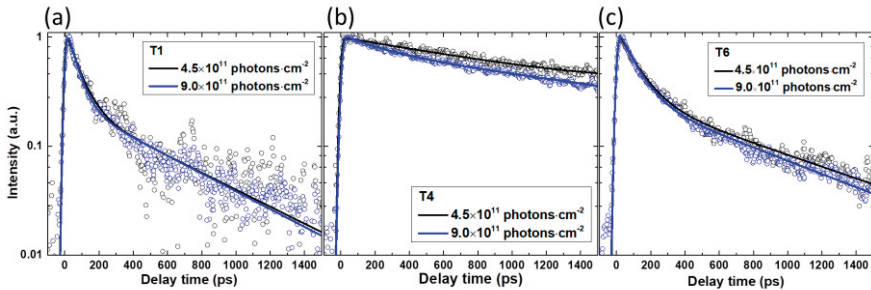


Figure 3.3.3.

Spectrally integrated TRPL decays of the as-grown InP NWs with HCl molar fractions of (a) $\chi_{\text{HCl}} = 0$, (b) 5.4×10^{-5} , and (c) 8.5×10^{-5} during the NW growth under excitation at 400 nm at the indicated excitation densities. Symbols: measurements (the intensities are normalized by the excitation power). Lines: fits by bi-exponential decay functions.

As shown in **Figure 3.3.2b**, the TRPL decay does not depend on the excitation orientation of the polymer-embedded InP NW with the HCl molar fractions of 5.4×10^{-5} . We interpreted this observation as related to a uniform trap density along the NWs. However, we observed an orientation dependence for other HCl fluxes, indicating that traps are inhomogeneous along the NW length under using these HCl etching fluxes. Therefore, we conclude that $\chi_{\text{HCl}} = 5.4 \times 10^{-5}$ in this series of NWs introduces the lowest density and homogeneously distributed traps.

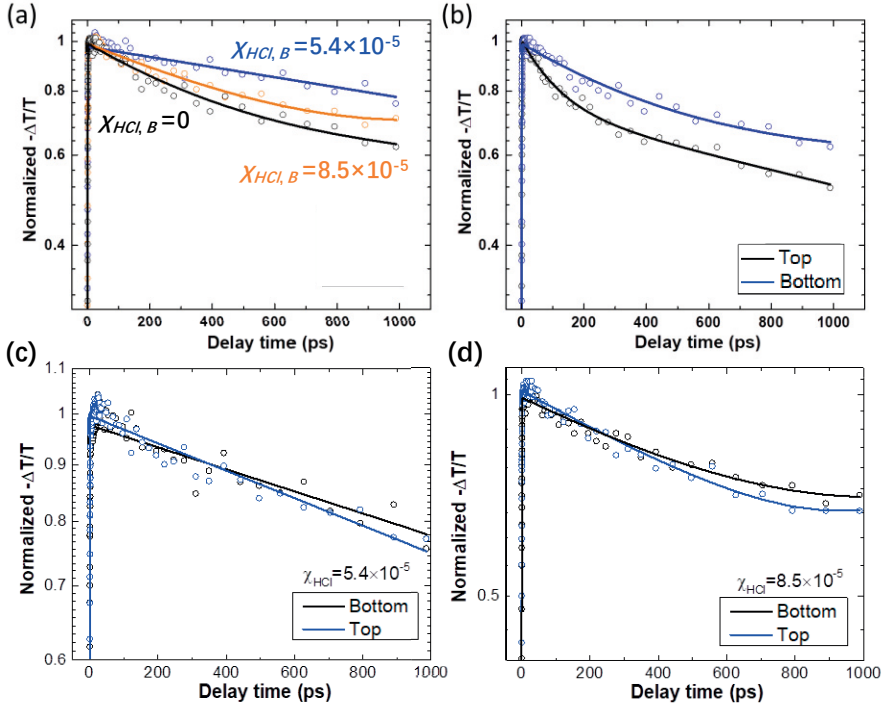


Figure 3.3.4.

Normalized transient THz transmittance kinetics of the selected InP NW arrays embedded in the polymer, excited at 800 nm with the flux of 4.6×10^{12} photons per cm^2 per pulse. (a) Excitation from the bottom side. (b) Comparison of the signal upon excitation from the top and bottom sides of the sample prepared without HCl etching. Symbols: measurements. Lines: bi-exponential fits. TRTS kinetics of InP NWs with HCl etching of (c) $\chi_{\text{HCl}} = 5.4 \times 10^{-5}$ and (d) 8.5×10^{-5} after photoexcitation via polymer side (Top) and NWs side (Bottom). The InP NWs are embedded in FC polymer. The excitation wavelength is 800 nm.

To distinguish the contribution of electron trapping and hole trapping processes, TRTS is used to selectively probe the dynamics of electrons (see **Figure 3.3.4**). Before that, we first verified the normalized TRTS under excitation fluences of 2.1×10^{12} and 4.6×10^{12} photons per cm^2 per pulse as shown in **Figure 3.3.5a**. The intensity-independent decay indicates that the bimolecular and Auger recombination at these excitations are not dominant.

From the comparison of varied χ_{HCl} , we find that the decay of the THz signal is the slowest for $\chi_{\text{HCl}} = 5.4 \times 10^{-5}$ when excited from the bottom side of the array. The TRTS decay in the etched NWs is nearly independent of the excitation direction (**Figure 3.3.3c, d**). However, the decay of non-etched NWs is faster when excited from the top than from the bottom (see **Figure 3.3.3b**). This could be that associated with the different morphology at the top and bottom of the NWs (**Figure 3.3.1**).

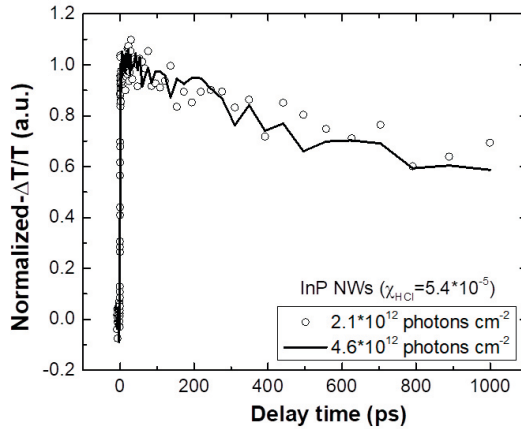


Figure 3.3.5.

Photoconductivity kinetics of InP NWs with HCl etching of $\chi_{\text{HCl}} = 5.4 \times 10^{-5}$ under the indicated excitation densities. The excitation wavelength is 800 nm.

Since TA reveals the decay of the overall photo-generated charge carrier population in the material, we studied the kinetics of TA for the NWs grown under optimal conditions in **Figure 3.3.6**. Comparing with the other two time-resolved techniques, we find that the TA decay is similar to the TRTS decay but much slower than the PL decay. The difference between TA kinetics and the dynamics of TRPL implies that non-radiative recombination is the dominant channel of the overall recombination of photo-generated charges. This is supported by the measurements of the absolute PL quantum yield (QY) at the level of $\sim 5 \times 10^{-4}$, which was measured by an integrating sphere. Meanwhile, most of photo-charges remain in the NWs long after the radiative recombination decay is over and therefore can only recombine non-radiatively (see **Figure 3.3.6**). Furthermore, these long-lived mobile charges are electrons. Since the TRTS and TA kinetics are very similar, we conclude that the mobility of electrons does not change on the nanosecond time scale. Therefore, the PL decay should be dominated by the hole trapping. The TRTS and TA decay rates have similar HCl etching influence trend to the TRPL with different HCl

etching conditions, and the scheme of the charge carrier recombination processes is shown in **Figure 3.3.7**.

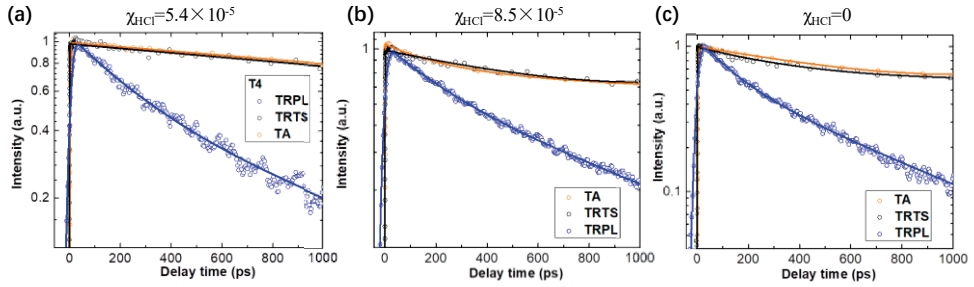


Figure 3.3.6. Comparison of transient THz transmittance, TRPL and TA (all normalized to the peak value) in InP NWs (a) $\chi_{\text{HCl}} = 5.4 \times 10^{-5}$, (b) $\chi_{\text{HCl}} = 8.5 \times 10^{-5}$, and (c) $\chi_{\text{HCl}} = 0$. Symbols: measurements. Solid lines represent the exponential fits.

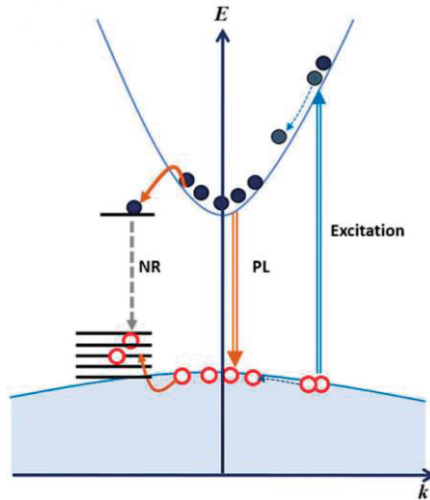


Figure 3.3.7. Scheme of charge carrier recombination processes in HCl in situ etched InP NWs. Double curved lines represent the photoexcitation and emission processes; dark yellow curved lines represent the carrier trapping processes; dotted curved lines represent the charge relaxation processes; 'NR' represents the nonradiative recombination process; straight horizontal lines represent the trap states.

In the $\chi_{\text{HCl}} = 5.4 \times 10^{-5}$ sample as shown in **Figure 3.3.3b**, we observed a pronounced excitation dependence, and the TRTS in **Figure 3.3.5** shows that the photo-generated carriers do not undergo any substantial decay due to bimolecular or Auger recombination up to an excitation fluence of $\sim 10^{12}$ photons per cm^2 per pulse. Therefore, the observed dependence in TRPL measurements is related entirely to the hole trapping dynamics. Meanwhile, the trap filling effect results in

the disappearance of the fast decay at high excitation density for $\chi_{\text{HCl}} = 5.4 \times 10^{-5}$ sample. Since we did not see any trapping saturation in the other NWs, we think that the trap density in those NWs is higher.

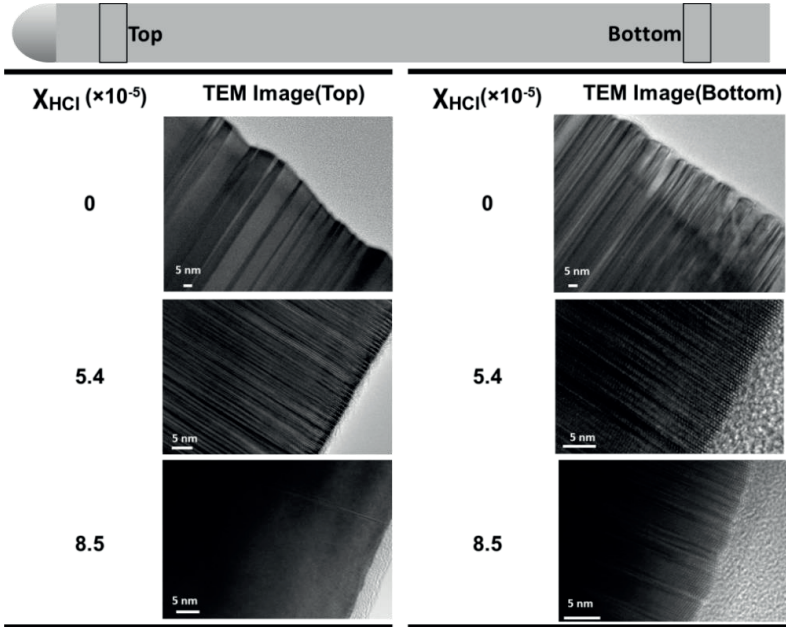


Figure 3.3.8. TEM images of the InP NW with HCl etching of (a) $\chi_{\text{HCl}}=0$, (b) $\chi_{\text{HCl}}=5.4 \times 10^{-5}$ and (c) $\chi_{\text{HCl}}=8.5 \times 10^{-5}$ at the top and bottom of the NWs. The top position was chosen away from the neck region and the bottom - away from the NW break region.

Summarizing the analysis of the TEM data (**Figure 3.3.8**), we find less stacking faults at the top of the NWs than at the bottom. However, the PL quenching is more pronounced at the top of the NWs. The bottom of the NWs has the lowest stacking fault density because of no etching are applied during the NWs growing process. Meanwhile, the PL decay of these NWs excited from the bottom side is slower than excited from the top. Therefore, we conclude that it is not stacking faults, but surface-related defects which are essential for the hole trapping.

In conclusion, we found a pronounced retardance of the carrier trapping process in InP NWs when regulating the NW growth by the HCl etching. The predominantly non-radiative recombination of photo-generated charges that we observed, even after optimal HCl etching, suggests that surface passivation can be exploited to allow further improvements in future NW-based devices. It is important to note that the optimization of carrier recombination must be properly characterized by a thorough examination of charge carrier dynamics and by absolute measurements of photoluminescence quantum yields (or both), but only not by means of a relative increase of the PL intensity.

3.4 Carrier Recombination Processes in $\text{Ga}_x\text{In}_{1-x}\text{P}$ NWs

Ga composition in the growing process of $\text{Ga}_x\text{In}_{1-x}\text{P}$ NWs plays for characteristics of semiconductor optoelectronic devices made of these materials. In this section, we investigated NWs with varied Ga composition in $\text{Ga}_x\text{In}_{1-x}\text{P}$ and studied the radiative and non-radiative recombination, and the photoconductivity dynamics of the photo-generated charge carriers in $\text{Ga}_x\text{In}_{1-x}\text{P}$ NWs by means of SSPL, TRPL, TRTS, and TA methods.

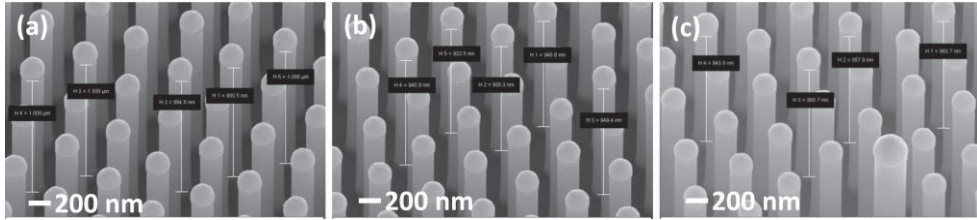


Figure 3.4.1. SEM images of as-grown (a) $\text{Ga}_{0.35}\text{In}_{0.65}\text{P}$, (b) $\text{Ga}_{0.43}\text{In}_{0.57}\text{P}$ and (c) $\text{Ga}_{0.54}\text{In}_{0.46}\text{P}$ NW arrays.

The $\text{Ga}_x\text{In}_{1-x}\text{P}$ NWs grown by metal organic vapor phase epitaxy (MOVPE) have similar diameter and length, which is independent of the Ga composition (see **Figure 3.4.1**).

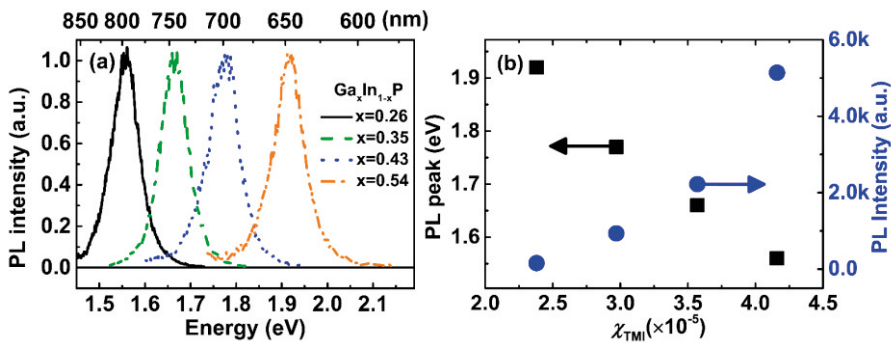


Figure 3.4.2. (a) Normalized time-integrated PL spectra of as grown $\text{Ga}_x\text{In}_{1-x}\text{P}$ NW arrays with varied TMI molar fractions after photoexcitation at 3.1 eV. (b) PL emission energy and intensity of as grown $\text{Ga}_x\text{In}_{1-x}\text{P}$ NW arrays as a function of the TMI molar fraction measured under the same effective excitation.

The maximum PL intensity shows a close to linear correlation to the TMI molar fraction as we see from the dependence of the PL measurement for $\text{Ga}_x\text{In}_{1-x}\text{P}$ NWs with varied Ga composition (**Figure 3.4.2a, b**). The composition of x in $\text{Ga}_x\text{In}_{1-x}\text{P}$ can be calculated as shown in **Figure 3.4.2a**.¹⁵²

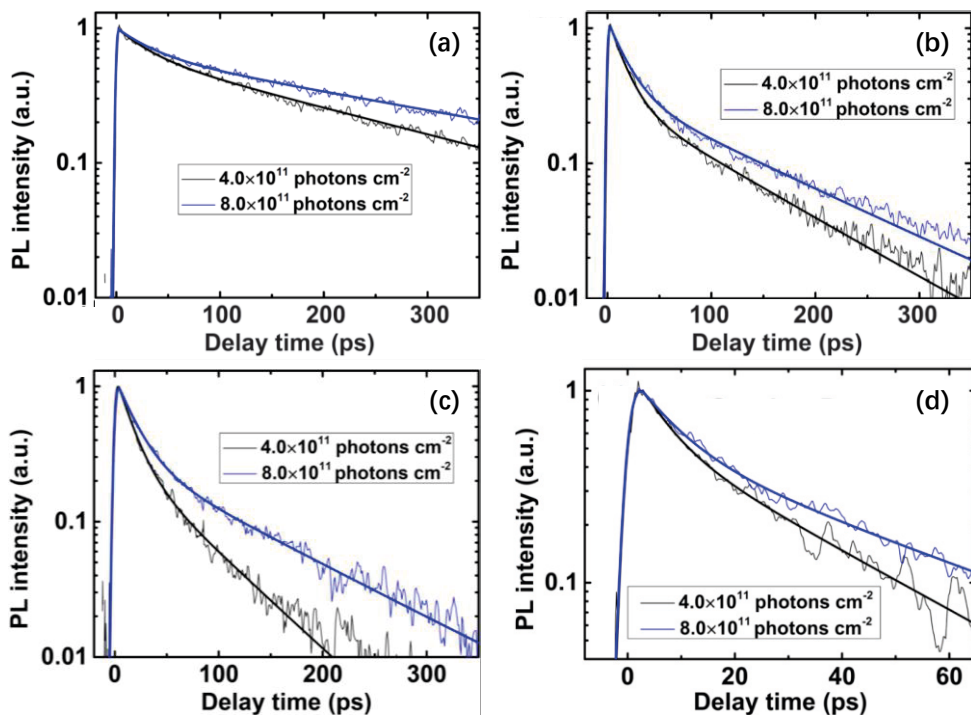


Figure 3.4.3.

TRPL decays of as grown (a) $\text{Ga}_{0.26}\text{In}_{0.74}\text{P}$, (b) $\text{Ga}_{0.35}\text{In}_{0.65}\text{P}$, (c) $\text{Ga}_{0.43}\text{In}_{0.57}\text{P}$, and (d) $\text{Ga}_{0.54}\text{In}_{0.46}\text{P}$ NW arrays at the indicated photo-excitation fluencies after photoexcitation at 3.1 eV. The kinetics were fitted by two exponential decay functions.

The TRPL kinetics of $\text{Ga}_x\text{In}_{1-x}\text{P}$ NWs for varied x have been analysed to understand the physical mechanisms related to the recombination dynamics of the photo-generated charge carriers. In **Figure 3.4.3**, slower PL decay at higher excitation power suggests that the TRPL kinetics of $\text{Ga}_x\text{In}_{1-x}\text{P}$ NWs are dominated by charge trapping and trap filling effect rather than by bimolecular or Auger recombination. This agrees with a low QY of $\sim 10^{-6}$ for the as-grown $\text{Ga}_{0.43}\text{In}_{0.57}\text{P}$ NW array at the CW excitation flux equivalent to ~ 300 suns. Faster PL decay with increasing x in **Figure 3.4.3** indicates that the trapping rate of electrons or holes or both types of carrier increases with increasing x in $\text{Ga}_x\text{In}_{1-x}\text{P}$ NWs. According to the energy diagram shown in **Figure 3.4.4**, PL emission is a bimolecular radiative recombination process, which is related to the momentary distribution of mobile electrons and holes. Therefore, the increasing of Ga composition may lead to a faster trapping rate and thus to the faster PL decay.

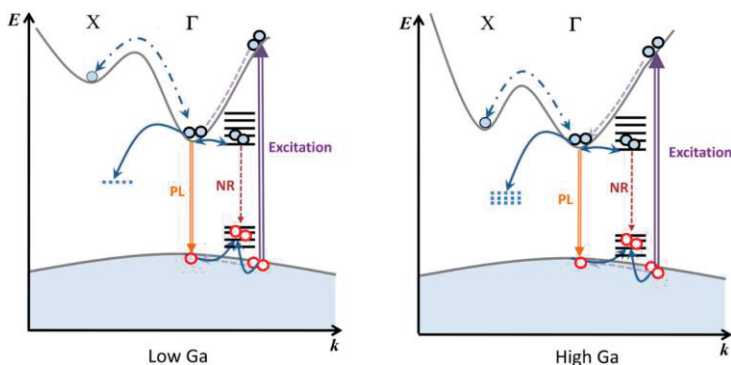


Figure 3.4.4.

Schematic of charge recombination processes in $\text{Ga}_x\text{In}_{1-x}\text{P}$ NWs with low and high Ga compositions used in our study. Double curved lines represent photoexcitation and emission processes; blue curved lines represent carrier trapping–detrapping processes; dashed-dotted curved lines represent the coupled electron scattering between X and Γ valleys; dashed curved lines represent charge relaxation processes; “NR” represent nonradiative recombination process; straight lines represent trap states. In the NWs with high Ga compositions, the deep trap (dotted lines) density is higher than that in low Ga composition NWs, resulting in faster decay of TRTS at early time.

Similar to the excitation intensity dependent TRPL, **Figure 3.4.5b** clearly shows that the photoconductivity decay slows down with increased excitation fluences. Based on the excitation dependences, we attribute this TRTS dynamics to the increase of the electron concentration or of the electron mobility. However, with increasing of the free photo-generated charge carrier concentration, more efficient charge–charge scattering should lead to lower charge mobility. Thus, the TRTS dynamics is caused by the contribution of trapping of electrons combined with the trap filling. Note here that the TRTS signal is still notable at the delay times at about 1 ns, indicating that the photo-generated electrons still have high mobility at this delays.

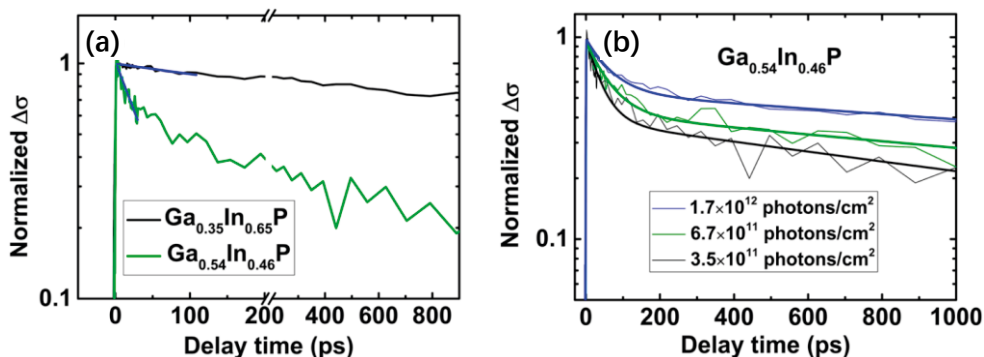


Figure 3.4.5.

(a) Normalized photoconductivity kinetics of $\text{Ga}_{0.35}\text{In}_{0.65}\text{P}$ and $\text{Ga}_{0.54}\text{In}_{0.46}\text{P}$ NWs after photoexcitation at 3.1 eV at a fluence of 3.5×10^{11} photons cm^{-2} pulse $^{-1}$, blue lines are monoexponential fits to the decays at early times after photoexcitation. (b) Normalized photoconductivity kinetics of $\text{Ga}_{0.54}\text{In}_{0.46}\text{P}$ NWs at indicated photoexcitation fluences after photoexcitation at 3.1 eV, the kinetics were fitted by two-exponential decay functions.

TA kinetics reflects the dynamics of electrons, holes, or the sum of charge carriers depending on the probe photon energy. From **Figure 3.4.6a**, TA kinetics suggests that the overall concentration of photo-generated charges decay faster at higher Ga composition.

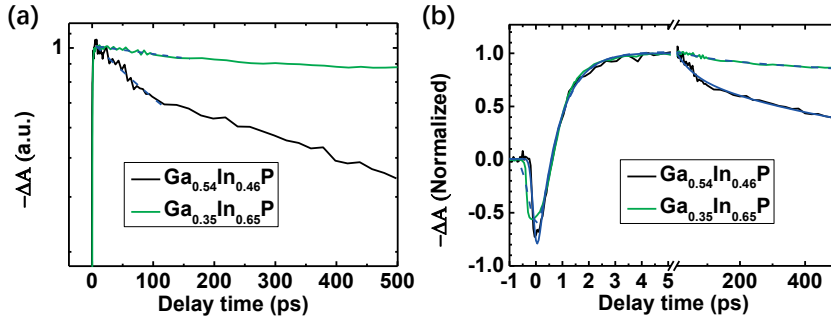


Figure 3.4.6.

(a) The absorption recovery dynamics (decay of the negative TA) of $\text{Ga}_{0.54}\text{In}_{0.46}\text{P}$ and $\text{Ga}_{0.35}\text{In}_{0.65}\text{P}$ NWs embedded in first contact polymer after photoexcitation at 2.3 eV at a fluence of $\sim 4 \times 10^{11}$ photons cm^{-2} pulse $^{-1}$. The dashed lines are fitting curves based on mono-exponential decay functions at early timescales. (b) The absorption recovery dynamics (decay of the negative TA) of $\text{Ga}_{0.54}\text{In}_{0.46}\text{P}$ and $\text{Ga}_{0.35}\text{In}_{0.65}\text{P}$ NWs embedded in first contact polymer after photoexcitation at 2.3 eV at a fluence of $\sim 4 \times 10^{11}$ photons cm^{-2} pulse $^{-1}$. The dashed lines are fitting curves based on mono-exponential decay functions at early timescales.

In the slow decay components of TRTS and TA decay shown in **Figure 3.4.7**, we find that the slow decay components are very similar.

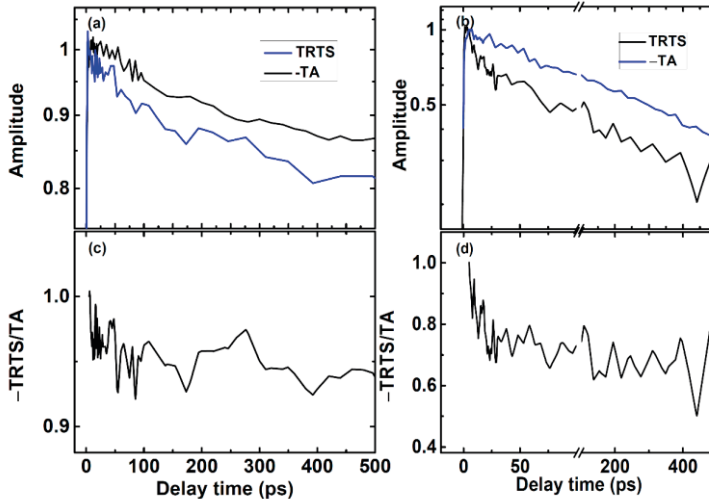


Figure 3.4.7.

Normalized TRTS and TA kinetics of (a) $\text{Ga}_{0.35}\text{In}_{0.65}\text{P}$ and (b) $\text{Ga}_{0.54}\text{In}_{0.46}\text{P}$ NWs embedded in CFPC. Normalized $-\text{TRTS}/\text{TA}$ kinetics of (c) $\text{Ga}_{0.35}\text{In}_{0.65}\text{P}$ and (d) $\text{Ga}_{0.54}\text{In}_{0.46}\text{P}$ NWs embedded in CFPC.

If we assume that TA kinetics reflect only photo-generated charge density, we can assess the change in relative electron mobility by dividing the normalized $\Delta\sigma$ by the normalized TA intensity (see **Figure 3.4.7c, d**). Note here that this procedure is not appropriate for the first 5 ps as the TA signal shows some rise (see **Figure 3.4.6b**) but it is not realistic that the concentration of photo-generated charges rise further after the pump pulse. In the TA measurement, the negative signal implies the absorption bleach effect. In this case, two components could be considered: a decrease of absorption due to the state filling in conduction and valence bands and the bleach of a possible trap state absorption. Therefore, neither photo-generated electrons nor holes have predominant contribution to the TA signal. Obviously, some weaker positive signal, such as intra-band absorption of electrons and holes or absorption of trapped charges, may contribute to the measured kinetics, but unfortunately, we cannot identify it. In addition, the negative signal could result from the stimulated emission as well. However, via comparison of TA and TRPL dynamics, we do not see similar decay in TA and TRPL signal. Since the TA decay is much faster than the TRPL decay, we conclude that only a small part of photogenerated charges recombine radiatively. In **Figure 3.4.7**, distinctly, for $x = 0.35$, the mobility experienced a $\sim 5\%$ decay on ~ 100 ps time scale (see **Figure 3.4.7c**). However, for $x = 0.54$, a $\sim 20\%$ faster mobility decay on sub-20 ps time scale is observed in **Figure 3.4.7d**.

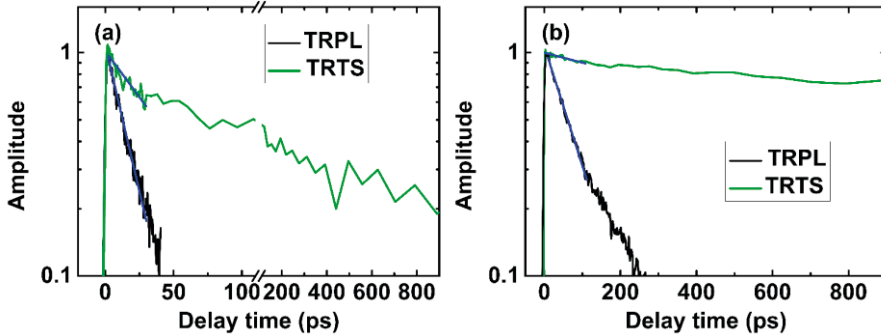


Figure 3.4.8. Normalized TRTS and TRPL kinetics of (a) $\text{Ga}_{0.54}\text{In}_{0.46}\text{P}$ and (b) $\text{Ga}_{0.35}\text{In}_{0.65}\text{P}$ NWs embedded in first contact polymer. Blue lines are fitting curves based on mono-exponential functions.

To rationalize the observation of the slow decay of electron mobility in relation to trapping, the density of electron trap states associating with trapping and de-trapping processes must be considered. As shown in **Figure 3.4.3**, if the temperature is high enough, the electrons could leave the shallow traps and become mobile. Meanwhile, the mobile charges will be predominately trapped by the deepest trap states.

After comparing TRPL and TRTS kinetics at similar excitation (see **Figure 3.4.8**), we find that early TRPL decays are much faster (about 3 and 12 times, respectively) than the early TRTS decay for $x = 0.54$ and 0.35 , respectively. As TRTS decay is

associated with the decrease of the product of concentration and mobility of electrons, the TRPL decay is too fast for the decay of the electron concentration or their trapping; thus, it has to be induced by the hole trapping. Moreover, we do not see PL at long times, indicating that trapped holes most probably cannot escape from the deep traps. We conclude that hole trapping is much faster than electron trapping in $\text{Ga}_x\text{In}_{1-x}\text{P}$ NWs. Moreover, only a small part of photo-generated charges recombines radiatively, which agrees with the low PL QY of 10^{-6} .

Apparently, the hole and electron trapping processes strongly depend on the composition of Ga. The increase of Ga composition may result in a deep trap formation because of the Ga vacancies. Deep traps have higher driving force leading to a faster charge trapping. Besides, the Ga-dependent material constituent variation could cause decrease of the electron mobility. Alloy scattering and direct-to-indirect band gap transition could be two possible scattering processes. When Ga composition is in the range of 0 - 0.5, randomly positioned Ga atoms and Ga clusters due to segregation of Ga and In could significantly decrease the mobility. To the band gap transition induced scattering, like in **Figure 3.4.4**, electrons in the conduction band locate in the Γ -valley and X-valley for direct bandgap and the indirect bandgap, respectively. The difference in scattering rate between these two valleys could be the reason of the mobility change. To investigate the scattering contribution from these two mechanisms, we used Harrison & Hase's model¹⁵³ and Macksey's model¹⁵⁴ to study scattering due to the alloy and direct-to-indirect bandgap transition as shown in **Figure 3.4.9**. We find that the direct-to-indirect bandgap transition model matches our experimental data better.

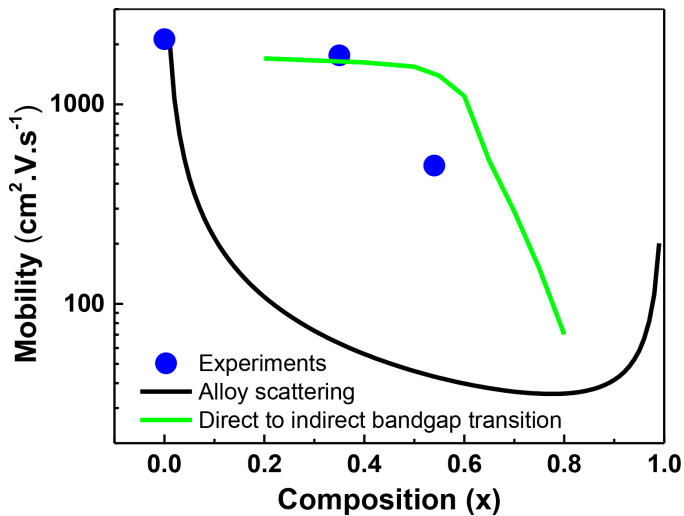


Figure 3.4.9. Experimentally obtained mobility as a function of Ga composition x , and mobility calculated from alloy scattering and direct to indirect bandgap transition.

To summarize, we have investigated the dependence between Ga composition and the recombination dynamics of photo-generated charges in $\text{Ga}_x\text{In}_{1-x}\text{P}$ NWs. The fast PL decay is due to an efficient trapping process of the photo-generated holes. The mobile photo-generated electrons have a much longer lifetime than that observed in PL. Furthermore, we proposed that an electron trapping observed as slowing down of the early photoconductivity decay with excitation fluence. We concluded that the overall decay of photo-generated charge concentration is dominated by the non-radiative recombination. Comparing the decays of photoconductivity and transient absorption, we assessed the electron mobility dynamics and considered diffusion of photo-generated electron in the NWs over a spatial and energetic distribution of shallow trap states to rationalize the slower (~ 100 ps) part of the electron mobility decay. The fast hole- and electron- trapping rates and the non-radiative recombination rate are all strongly dependent on Ga composition in $\text{Ga}_x\text{In}_{1-x}\text{P}$ NWs, in agreement with the expected formation of deep traps under increased Ga composition. The strong dependence of the early time electron mobility on Ga composition in $\text{Ga}_x\text{In}_{1-x}\text{P}$ NWs most probably originates from the direct-to-indirect bandgap transition.

3.5 Surface Passivation of $\text{Ga}_x\text{In}_{(1-x)}\text{P}$ NWs by $\text{Al}_y\text{In}_{(1-y)}\text{P}$

The surface states in $\text{Ga}_x\text{In}_{(1-x)}\text{P}$ are important for their optoelectronic properties. The passivation approaches such as growing a wide-bandgap semiconductor shell,^{39,155–158} wet treated surfaces,^{159,160} and ex-situ deposition of a dielectric layer^{161–163} have been developed to reduce the surface trap density. In this study, growth of $\text{Al}_y\text{In}_{(1-y)}\text{P}$ was done as an *in situ* surface passivation layer for $\text{Ga}_x\text{In}_{(1-x)}\text{P}$.

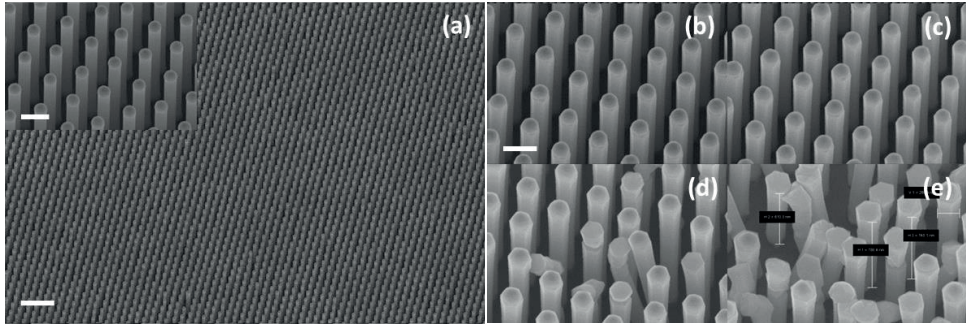


Figure 3.5.1. (a) SEM images of $\text{Ga}_{0.41}\text{In}_{0.59}\text{P}/\text{Al}_y\text{In}_{(1-y)}\text{P}$ core-shell samples. The scale bar is 2 μm ; the inset shows a zoomed-in area with a scale bar of 400 nm. SEM images of the samples with (b) $\text{Al}_{0.26}\text{In}_{0.74}\text{P}$, (c) $\text{Al}_{0.36}\text{In}_{0.64}\text{P}$, (d) $\text{Al}_{0.48}\text{In}_{0.52}\text{P}$, (e) $\text{Al}_{0.55}\text{In}_{0.45}\text{P}$ shell. The scale bar is 400 nm.

First of all, $\text{Ga}_x\text{In}_{(1-x)}\text{P}$ NW arrays were grown by metal-organic vapor phase epitaxy (MOVPE) method. Two series of samples were grown for studying the effect of the Al composition and thickness of the shell layers on the surface of $\text{Ga}_x\text{In}_{(1-x)}\text{P}$ NWs, respectively. **Figure 3.5.1** shows the SEM images of (a) $\text{Ga}_x\text{In}_{(1-x)}\text{P}$ core and $\text{Ga}_x\text{In}_{(1-x)}\text{P}/\text{Al}_y\text{In}_{(1-y)}\text{P}$ core-shell NWs with Al composition of (b) 0.26, (c) 0.36, (d) 0.48, and (e) 0.55.

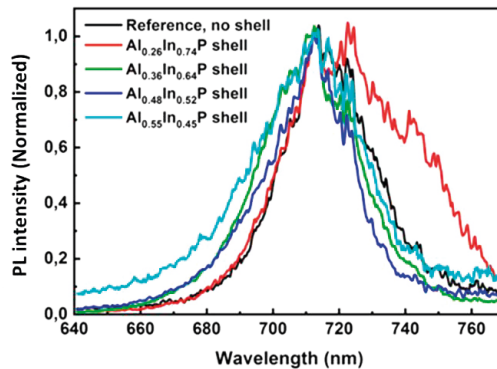


Figure 3.5.2. Time integrated PL spectrum of $\text{Ga}_x\text{In}_{(1-x)}\text{P}/\text{Al}_y\text{In}_{(1-y)}\text{P}$ core-shell NWs with different Al composition.

The NWs are uniform and straight when the Al composition of the shell is lower than 0.48. In contrast, when the Al composition of the shell is higher than 0.48, the NWs start to bend and kink due to the relatively high GaInP-AlInP lattice mismatch and facet selective nucleation and growth.^{164,165}

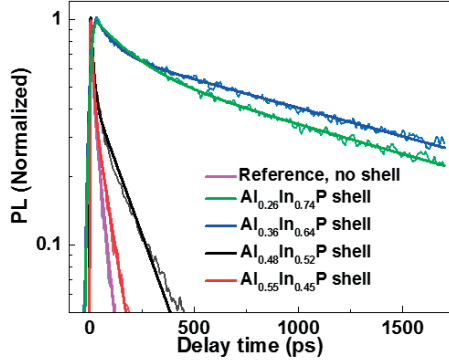


Figure 3.5.3. TRPL kinetics of $\text{Ga}_{0.41}\text{In}_{0.59}\text{P}/\text{Al}_x\text{In}_{(1-y)}\text{P}$ core/shell NWs after photoexcitation at 3.1 eV. The kinetics are fitted by two exponential decay functions, with details given in **Table 3.5.1**.

The PL at room temperature was depicted to character the optical properties of the $\text{Ga}_x\text{In}_{(1-x)}\text{P}/\text{Al}_y\text{In}_{(1-y)}\text{P}$ core-shell NWs with varied Al composition. The emission peak at ~ 1.74 eV indicates Ga composition x in $\text{Ga}_x\text{In}_{(1-x)}\text{P}$ is ~ 0.41 . The broad PL peaks could be the reason from the inhomogeneous distribution of Ga composition within an individual NW and among different NWs. Although substantial efforts have been dedicated to measuring PL from the shells, no sign of such emission was detected. A possible reason of this lack of emission could be that the photo-generated free charge carriers in the $\text{Al}_y\text{In}_{(1-y)}\text{P}$ shell are trapped by the surface states of the shell, which would quench the PL emission. The EDX measurement suggests that radial and axial variations of the Al composition and inhomogeneous shell thickness is commonly present over an individual NW.

Table 3.5.1. Fitting parameters of TRPL kinetics traces in **Figure 3.5.3** by two exponential decay functions considering IRF and $1/e$ lifetimes.

Sample	A_1	τ_1 [ps]	A_2	τ_2 [ps]	$1/e$ lifetime[ps]
Reference, no shell	0.79	8.50 ± 0.54	0.55	47.99 ± 2.20	26
$\text{Al}_{0.26}\text{In}_{0.74}\text{P}$ shell	0.44	186.94 ± 10.38	0.62	1678.53 ± 48.25	850
$\text{Al}_{0.36}\text{In}_{0.64}\text{P}$ shell	0.41	88.39 ± 5.95	0.72	1720.89 ± 27.22	1150
$\text{Al}_{0.48}\text{In}_{0.52}\text{P}$ shell	0.75	12.21 ± 0.37	0.47	171.17 ± 5.28	52
$\text{Al}_{0.55}\text{In}_{0.45}\text{P}$ shell	0.71	11.25 ± 0.31	0.47	76.52 ± 2.19	32

In **Figure 3.5.3**, we performed TRPL measurements to investigate the effect of $\text{Al}_y\text{In}_{(1-y)}\text{P}$ shells on carrier recombination dynamics in the $\text{Ga}_{0.41}\text{In}_{0.59}\text{P}$ NWs. As we discussed in **Section 1.7**, in semiconductor NWs, the free charge carrier depopulation processes mainly include bimolecular recombination, Auger recombination, trap-assisted recombination. In this study, however, we saw that the PL decay decelerate with increasing excitation fluence as shown in **Figure 3.5.4**, indicating that the PL decay is most probably dominated by the trap induced recombination rather than by the bimolecular and Auger recombination.¹⁶⁶⁻¹⁶⁸ It is worth to note that the non-monoexponential PL decay in **Figure 3.5.3** could result from an inhomogeneous distribution of traps in the NWs.^{102,169,170}

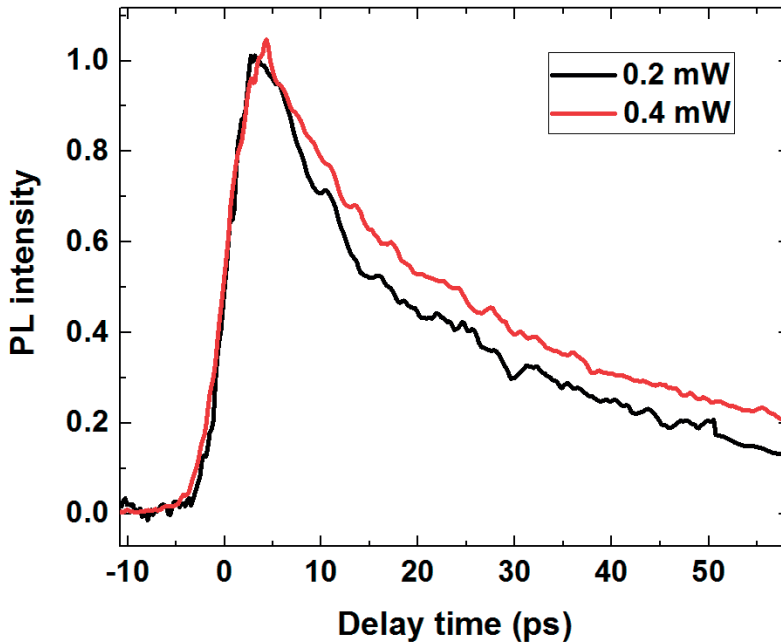


Figure 3.5.4. TRPL decays of $\text{Ga}_{0.41}\text{In}_{0.59}\text{P}$ NWs under indicated excitation powers.

To quantify the non-exponential PL decay like in the **Figure 3.5.3**, the lifetime is taken for the decay of the emission intensity to $1/e$ of its initial value, as shown in **Table 3.5.1**. We find that the TRPL lifetime is strongly dependent on the Al composition. The lifetime increases and then decreases with increase of the Al composition. When the composition is 0.36, the lifetime reaches the maximum (~ 1.1 ns) which is ~ 40 times longer than that of the bare $\text{Ga}_{0.41}\text{In}_{0.59}\text{P}$ NWs. We attribute this extended lifetime to the reduction of the trapping rate of electron, hole, or both. The further reduced lifetime we associate with introduction of more traps with higher Al composition.

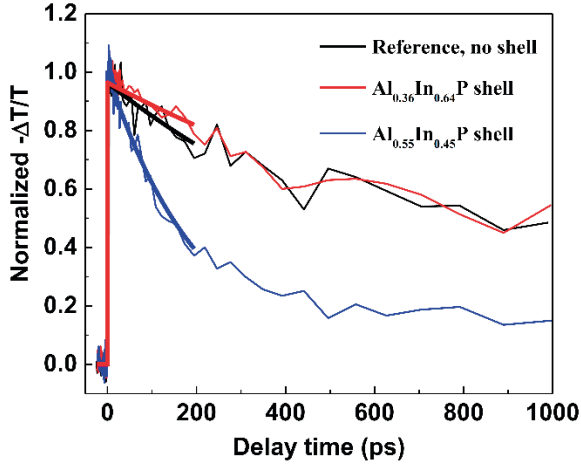


Figure 3.5.5. Normalized photoconductivity kinetics of Ga_{0.41}In_{0.59}P core without shell and with Al_{0.36}In_{0.64}P and Al_{0.55}In_{0.45}P shells.

Figure 3.5.5 shows the photoconductivity dynamics of bare Ga_{0.41}In_{0.59}P without shell and of Ga_{0.41}In_{0.59}P with Al_{0.36}In_{0.64}P and Al_{0.55}In_{0.45}P shells. We note that the photoconductivity lifetime of the bare Ga_{0.41}In_{0.59}P, Ga_{0.41}In_{0.59}P/Al_{0.36}In_{0.64}P, and Ga_{0.41}In_{0.59}P/Al_{0.55}In_{0.45}P NWs are about 0.8 ns, 1.2 ns, and 0.2 ns, respectively. To account for the photoconductivity decay processes, a series of excitation fluences were used in TRTS measurements, as shown in **Figure 3.5.6**. Similar to the trend in the excitation density dependent TRPL measurements, the slowing down of the TRTS decay with increasing excitation fluence is associated with the electron trap filling effect. Assuming that the electron mobility is a constant in the TRTS measured time range, the photoconductivity decay of Ga_{0.41}In_{0.59}P NWs can be attributed to charge recombination as well as to the electron trapping. Therefore, the longer lifetime of Ga_{0.41}In_{0.59}P/Al_{0.36}In_{0.64}P and Ga_{0.41}In_{0.59}P/Al_{0.55}In_{0.45}P NWs reflects slowing down of the electron recombination, trap passivation, or both.

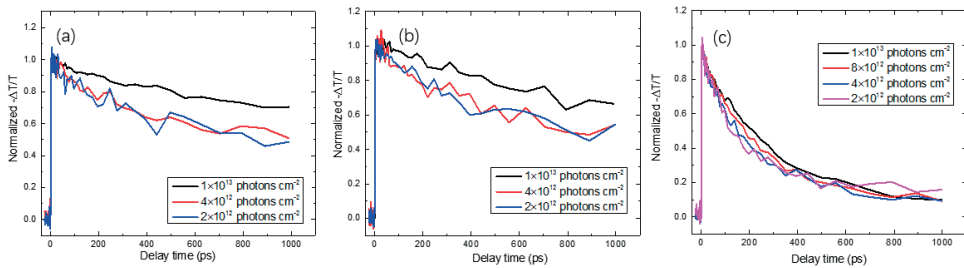


Figure 3.5.6. Normalized photoconductivity kinetics of Ga_{0.41}In_{0.59}P (a) without shell, with (b) Al_{0.36}In_{0.64}P, and (c) Al_{0.55}In_{0.45}P shells at indicated photoexcitation fluences after photoexcitation at 3.1 eV.

Additionally, to the bare $\text{Ga}_{0.41}\text{In}_{0.59}\text{P}$ NWs, $\text{Ga}_{0.41}\text{In}_{0.59}\text{P}/\text{Al}_{0.36}\text{In}_{0.64}\text{P}$, and $\text{Ga}_{0.41}\text{In}_{0.59}\text{P}/\text{Al}_{0.36}\text{In}_{0.64}\text{P}$ NWs, the TRTS lifetimes of these NW samples are longer than their TRPL lifetimes, suggesting that PL decay in the NWs is dominated by the hole trapping. Through comparing the TRPL and TRTS lifetime of bare $\text{Ga}_{0.41}\text{In}_{0.59}\text{P}$ NWs and $\text{Ga}_{0.41}\text{In}_{0.59}\text{P}/\text{Al}_{0.36}\text{In}_{0.64}\text{P}$ core-shell NWs, we find that the carrier lifetime in the core-shell NWs is longer than that in the bare core NWs. It is 40 times longer for holes, and 1.5 times longer for electrons. With increase of the Al fraction, we find that the lifetimes of hole and electron of $\text{Ga}_{0.41}\text{In}_{0.59}\text{P}/\text{Al}_{0.55}\text{In}_{0.45}\text{P}$ core-shell NWs reduce 35 and 5.5 times comparing to $\text{Ga}_{0.41}\text{In}_{0.59}\text{P}/\text{Al}_{0.36}\text{In}_{0.64}\text{P}$, as shown in **Figure 3.3.3** and **Figure 3.3.5**, respectively, which can be associated with new electron and hole traps created by too much Al in the shells.

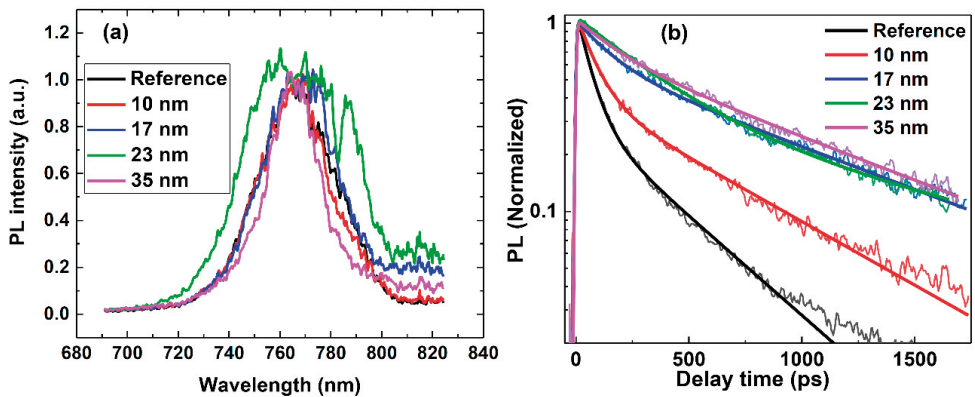


Figure 3.5.7.

Room temperature PL and TRPL decay of $\text{Ga}_{0.31}\text{In}_{0.69}\text{P}/\text{Al}_{0.22}\text{In}_{0.78}\text{P}$ core-shell NWs of the shell-thickness series. The kinetics are fitted by two exponential decay functions, with details given in Table 3.5.2.

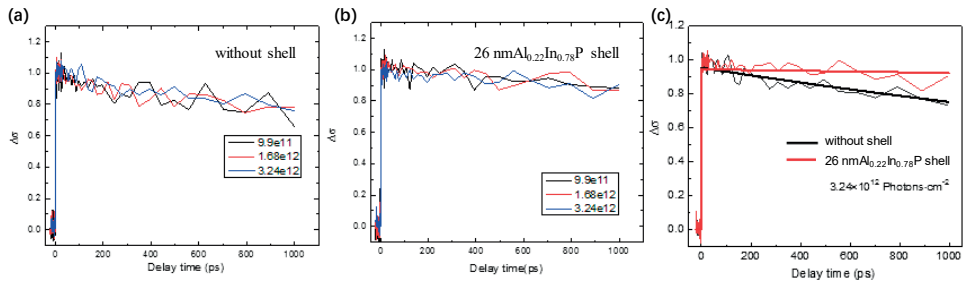
Furthermore, the influence of $\text{Al}_{0.21}\text{In}_{0.79}\text{P}$ shell thickness was examined by PL and TRPL studies as shown in **Figure 3.5.7**. The PL emission peak at ~ 1.61 eV (**Figure 3.5.7a**) suggests that the Ga composition is around 0.31. With various $\text{Al}_{0.21}\text{In}_{0.79}\text{P}$ shell thickness, we observe that the TRPL lifetime increases with increasing of the shell thickness. We also observe indications of saturation of this effect after the shell thickness of 17 nm. This suggests that a sufficient shell thickness is necessary for good passivation. Meanwhile, a thicker shell thickness in the range of thicknesses we applied does not contribute more to PL decay. Therefore, it is no need to increase the thickness of the shell.

Table 3.5.2.

Fitting parameters of TRPL kinetics traces in Fig. 3.5.7 (b) by two exponential decay functions considering IRF and 1/e lifetimes.

Shell thickness	A_1	τ_1 [ps]	A_2	τ_2 [ps]	1/e lifetime[ps]
Ref	0.86	62.19±1.19	0.32	412.37±14.74	124
10 nm	0.71	82.38±2.19	0.42	642.67±20.98	210
17 nm	0.42	149.36±7.68	0.63	956.94±29.16	515
23 nm	0.78	354.02±22.63	0.30	1630.83±346.26	570
35 nm	0.34	188.60±17.74	0.71	948.71±38.54	640

Besides, the photoconductivity of the sample with a shell thickness of 23 nm decays slower (see **Figure 3.5.8**) compared with that of the bare core NW. Combining the results of TRPL and TRTS, we conclude that both hole and electron trapping and the overall charge recombination in $\text{Ga}_x\text{In}_{(1-x)}\text{P}$ NWs can be substantially passivated by means of growing an $\text{Al}_y\text{In}_{(1-y)}\text{P}$ shell with an appropriate Al composition and with a proper thickness.

**Figure 3.5.8.**

Photoconductivity kinetics of $\text{Ga}_{0.31}\text{In}_{0.69}\text{P}$ (a) without shell and (b) with 26 nm and $\text{Al}_{0.22}\text{In}_{0.78}\text{P}$ shells at varies excitation fluences. (c) Comparison of TRTS kinetics of $\text{Ga}_{0.31}\text{In}_{0.69}\text{P}$ without shell and with 26 nm and $\text{Al}_{0.22}\text{In}_{0.78}\text{P}$ shells.

In conclusion, $\text{Al}_y\text{In}_{(1-y)}\text{P}$ shells were grown by MOVPE methods to passivate $\text{Ga}_x\text{In}_{(1-x)}\text{P}$ NWs. Based on the slowing down of the PL and photoconductivity decays, the hole and electron trap densities of the $\text{Ga}_x\text{In}_{(1-x)}\text{P}$ NWs with the $\text{Al}_{0.36}\text{In}_{0.64}\text{P}$ were found to be ~ 40 times and ~ 1.5 times smaller than that of the bare $\text{Ga}_x\text{In}_{(1-x)}\text{P}$ NWs, reflecting more effective surface passivation of the hole traps by the $\text{Al}_y\text{In}_{(1-y)}\text{P}$ shells. With higher Al composition shells, both hole and electron trap rates increase due to additional defect formation. Besides, a certain shell thickness of approximately ~ 20 nm is needed for sufficient passivation of $\text{Ga}_x\text{In}_{(1-x)}\text{P}$ NWs. In this study, an effective in situ passivation to $\text{Ga}_x\text{In}_{(1-x)}\text{P}$ NWs was achieved to improve their optical properties, and thus to potentially optimize the application of the $\text{Ga}_x\text{In}_{(1-x)}\text{P}$ NWs in high-performance optoelectronic devices.

3.6 The Influence of Oxides Passivation on Photovoltaic InP NWs

As a promising material for high-efficiency SCs, InP NW semiconductor with high SVR requires an appropriate passivation as well as an insulating layer. In this study, we used TRPL method to investigate the passivation effect of two kinds of oxide layers to InP NWs. We find that $\text{PO}_x/\text{Al}_2\text{O}_3$ layer has the potential to passivate the surface of InP NWs.

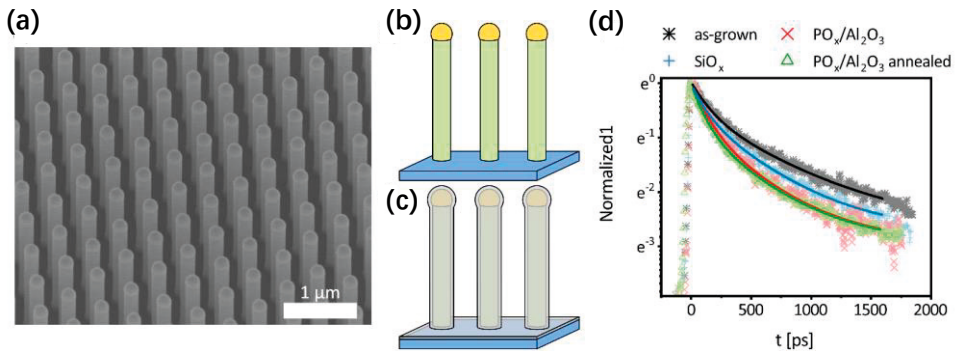


Figure 3.6.1.

(a) SEM image with 30° tilt of epitaxially VLS grown InP NWs with gold seeds. (b) schematics of as-grown and (c) oxide coated InP NW arrays. (d) TRPL decay of nominally intrinsic NWs coated by different insulating layers.

Figure 3.6.1a shows an SEM of the as grown NW arrays. **Figure 3.6.1b** and **Figure 3.6.1c** show the schematics of as-grown and coated NW arrays, respectively. To study the passivation effect and the underlying physical mechanisms of SiO_x and $\text{PO}_x/\text{Al}_2\text{O}_3$ on the surface of InP NWs, we have first measured the TRPL of intrinsic and intentionally doped as-grown NWs followed by measurements of the same NWs coated by the two oxides. Since the $\text{PO}_x/\text{Al}_2\text{O}_3$ layer is expected to provide better passivation effect,¹⁷¹ these NW samples were annealed after the first round of characterization and then re-measured. First, TRPL measurements were applied to the intrinsic NWs with various passivation layers as shown in **Figure 3.6.1d**. We observed that the PL decay becomes faster after coating with any oxide layer on the surface of intrinsic InP NWs. It should be noted that the measured lifetime appears to be shorter than the previously reported one, which was measured by TCSPC system.¹⁷¹ We attribute this to the fact that measurements by a streak camera with higher temporal resolution provide more details about the PL decay compared to TCSPC method.

As two-terminal multi-junction SCs consist of n-doped, p-doped, and intrinsic segments, we need to understand the carrier behavior in NWs with different doping.

Figure 3.6.2 shows the PL decay of doped NWs with different passivation layers. We also use compensation p -doping to minimize the effect of the unintentional n -doping which is typically presented during the growth procedure. Interestingly, compensation p -doping exhibits even faster decay than after heavy p -doping. This may come from the oxidation of the Zn from the dopant after exposure to air.¹⁷² From the TRPL result, it is clear that both n - and p -doped NWs covered with $\text{PO}_x/\text{Al}_2\text{O}_3$ have faster PL decays than as-grown NWs. However, after annealing at 250°C under N_2 atmosphere for 1 min, the PL decay of $\text{PO}_x/\text{Al}_2\text{O}_3$ -coated InP becomes slightly slower than that of the as-grown InP, indicating that the $\text{PO}_x/\text{Al}_2\text{O}_3$ passivation with an appropriate annealing has a potential for improving performance of InP NWs SCs.

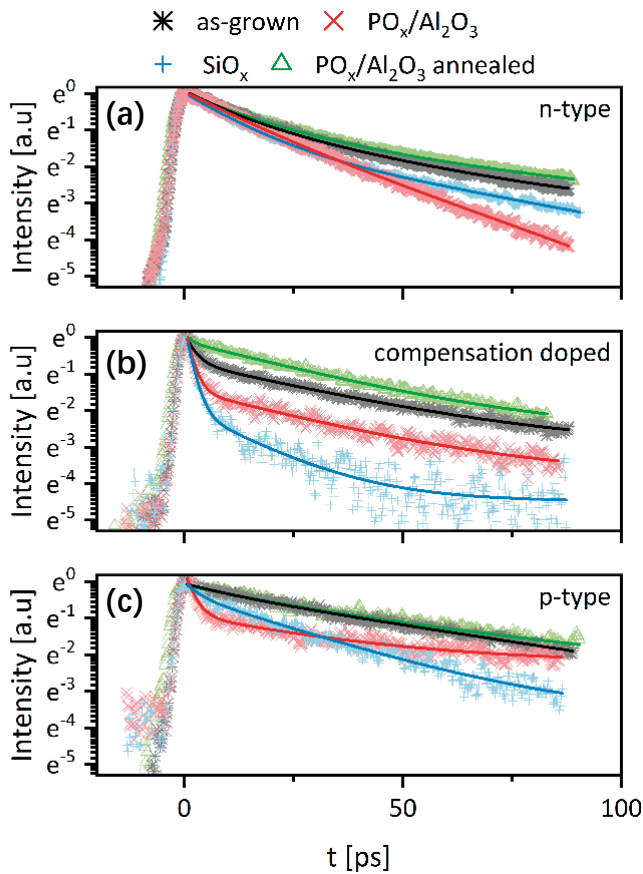


Figure 3.6.2.

TRPL decays of (a) n -doped, (b) compensation doped, and (c) p -doped InP NW arrays at an excitation flux of 3×10^{-12} photons cm^{-2} pulse $^{-1}$. The scatter plot shows the measured data points, while the solid line is a bi-exponential fit to the data. After deposition of oxides such as SiO_x (blue) and $\text{PO}_x/\text{Al}_2\text{O}_3$ (red) the optical properties of as-grown InP NWs (black) typically degrade. After an annealing step, the $\text{PO}_x/\text{Al}_2\text{O}_3$ is able to maintain and slightly improve the photoluminescence.

Chapter 4

Conclusion

We have studied semiconductor III-V NWs as promising material for optoelectronic applications. In this thesis, several surface passivation processes are applied during or after the materials growth processes to lower the density of trap states and consequently improve the lifetime of photogenerated charge carriers in group III-V bulk and NWs materials. These optimized materials are expected to obtain PV devices with high conversion efficiency and good stability. In order to characterize the above growth method and passivation effects, several non-contact, relatively less-damage, and material reusable steady-state and time-resolved spectroscopies were used to study the carrier dynamics in group III-V semiconductor bulk and NWs materials. These spectrum studies not only help us to select a candidate of well passivated group III-V bulk and NWs materials, but also present the carrier behaviors in these materials, which can help us understand how the photogenerated charge carriers works, provide a model to characterize the performance of optoelectronic materials, and guide further improvements of potential group III-V bulk- and NW-based optoelectronic devices.

With the investigations presented in the thesis, we revealed the photogenerated charge carrier recombination processes and achieved optimized passivated condition in the group III-V Semiconductors bulk and NWs materials. Here, the following conclusions are presented:

1. The growth method as the regulating HCl etching method in InP growth mentioned in this thesis is one of the potential research directions to improve the performance of group III-V NW materials. Optimal HCl etching providing less surface defect so that low trap density prolongs the lifetime of photogenerated charge carriers indicated through time-resolved photoluminescence method.
2. The composition of the group III-V atoms in ternary semiconductor materials plays a significant role in affecting the performance of NWs-based semiconductor materials. Like the Ga composition in $\text{Ga}_x\text{In}_{1-x}\text{P}$ NWs, with the increase of Ga fraction, the fast electron trapping, hole trapping, and non-radiative recombination become more efficient due to the unexpected formation of deep traps.

3. The recombination processes of photogenerated charge carriers are investigated in both unpassivated and passivated semiconductors. The TRPL and TRTS spectroscopy methods are utilized to get prospective long-lived carriers in optimized bulk and NWs materials. In the carrier recombination study, to the GaAs bulk and NWs materials, the trap-assisted non-radiative recombination dominates the overall recombination processes due to the extremely low quantum yield. Besides, the PL decay in GaAs bulk materials being dominated by the hole trapping process emerged through comparing the TRPL and TRTS decay.
4. In GaAs/AlGaAs core-shell NWs semiconductors, a geminate recombination process is first observed when there is around one electron and hole pair in one NWs, which also happens when this kind of NWs-based PVs is under one sun, indicating it could be a kind of one electron-hole pair devices. So the geminate radiative recombination dominates the radiative recombination in such NW PVs. Meanwhile, the steady-state PL QY at various excitation density being measured by an integrating sphere method indicates a trap filling effect. Through an attractive QY modelling and TRPL study, we proposed a new way to estimate the geminate, trap-assisted, bimolecular recombination coefficients, trap density, and trap lifetime.
 - Understanding the dynamics of photogenerated charge carriers in III-V semiconductors is a key for their optimization for opto-electronic applications.
 - We apply spectroscopy for contact-less characterization of the materials of interest prior to their further processing. A combination of spectroscopy methods allowed us to obtain a comprehensive description of charge carrier dynamics in several III-V semiconductors. In particular, we used time-resolved Transient Absorption, Photoluminescence, and Optical pump – THz probe and the steady-state absorption and photoluminescence as well as the photoluminescence quantum yield measurements.
 - In all studied semiconductors, charge trapping by several types of trap states dominates the primary steps of charge carrier dynamics and results in predominantly non-radiative recombination of photogenerated charges. Some trapping channels can be saturated via high charge generation rate under irradiation of the semiconductors by high intensity short optical pulses.
 - To scrutinize the role of the semiconductor surface, we conducted a comparative study of GaAs in bulk and in the form of NWs with different surface passivation treatments used. In both cases, we concluded that surface processes dominate the recombination of charge carriers.

Outlook

Understanding carrier recombination processes in opto-electronic semiconductors is a critical issue for their applications. Thus, the carrier recombination mechanism in group III-V bulk- and nano-materials have attracted people's attention and been studied extensively over the past decades. However, many issues, such as trap related charge trapping processes, are still not very clear.

In our work, we have focused on charge trapping dynamics in group III-V bulk- and nano-materials. Yet many processes, in particular the non-radiative recombination processes, need further studies. First, the non-radiative recombination mechanism in group III-V needs to be further clarified. The non-radiative recombination processes could have contributions of recombination of free electrons and trapped holes, of free holes and trapped electrons, or trapped holes and trapped electrons. What is the recombination mechanism for these types of recombination? Are they first or second-order type of recombination processes? Many non-radiative recombination details need to be studied. Second, it is still not clear what is the correlation between non-radiative recombination processes and device performances? From our study, radiative recombination is only a small part of the total recombination, suggesting that non-radiative recombination plays an important role in group III-V semiconductors. We note here that the devices based on the materials studied in our work typically exhibit very good performance, suggesting that the non-radiative recombination processes have little influence on the performance of devices. Why? Could it be that some shallow traps do not influence the extraction of the charges when the device is functioning? These questions need to be answered. Third, the influence of trap energy levels on the recombination as well as charge transport needs to be studied.

References

- 1 Goss, R. M. BP Statistical Review of World Energy. *BP World Energy* **2019**, *68*, 1–61.
- 2 Armaroli, N.; Balzani, V. The Future of Energy Supply: Challenges and Opportunities. *Angew. Chemie - Int. Ed.* **2007**, *46* (1–2), 52–66.
- 3 Goss, R. M. BP Statistical Review of World Energy_ Renewable energy Renewables. *BP World Energy* **2019**, *68*, A1–A5.
- 4 Iea. Snapshot of Global PV Markets 2020. *Technol. Collab. Program.* **2020**, 1–19.
- 5 Shan, H.; Yang, J. Sustainability of Photovoltaic Poverty Alleviation in China: An Evolutionary Game between Stakeholders. *Energy* **2019**, *181*, 264–280.
- 6 Becquerel, E. Recherches Sur Les Effets de La Radiation Chimique de La Lumiere Solaire Au Moyen Des Courants Electriques [Research on Sunlight Chemical Radiation Effects Using Electrical Currents.]. *C. R. Hebd. Seances Acad. Sci.* **1839**.
- 7 Fatet, J. Recreating Edmond Becquerel’s Electrochemical Actinometer. *Arch. des Sci.* **2005**, *58* (2), 149–158.
- 8 Fritts, C. E. On the Fritts Selenium Cells and Batteries. *J. Franklin Inst.* **1885**, *119* (3), 221–232.
- 9 Green, M. A. Third Generation Photovoltaics: Ultra-High Conversion Efficiency at Low Cost. *Prog. Photovoltaics Res. Appl.* **2001**, *9* (2), 123–135.
- 10 Conibeer, G. Third-Generation Photovoltaics. *Mater. Today* **2007**, *10* (11), 42–50.
- 11 NREL. Best Research-Cell Efficiencies: Rev. 04-06-2020. *Best Research-Cell Efficiency Chart | Photovoltaic Research | NREL.* 2020, <https://www.nrel.gov/pv/cell-efficiency.html>.
- 12 Geisz, J. F.; France, R. M.; Schulte, K. L.; Steiner, M. A.; Norman, A. G.; Guthrey, H. L.; Young, M. R.; Song, T.; Moriarty, T. Six-Junction III–V Solar Cells with 47.1% Conversion Efficiency under 143 Suns Concentration. *Nat. Energy* **2020**, *5* (4), 326–335.
- 13 Hfwxuh, R.; Hftxhuho, E. W. K. H.; Andreev, V. M.; Petersburg, S. III–V Heterostructure Photovoltaics in Russia. *Sol. Energy* **2001**, *7* (October).
- 14 Alferov, Z. I.; Andreev, V. M.; Rumyantsev, V. D. III-V Solar Cells and Concentrator Arrays. In *High-Efficient Low-Cost Photovoltaics*; Springer Berlin Heidelberg: Berlin, Heidelberg, **2009**; 101–141.
- 15 Wallentin, J.; Anttu, N.; Asoli, D.; Huffman, M.; Aberg, I.; Magnusson, M. H.; Siefert, G.; Fuss-Kailuweit, P.; Dimroth, F.; Witzigmann, B.; Xu, H. Q.; Samuelson, L.; Deppert, K.; Borgstrom, M. T. InP Nanowire Array Solar Cells Achieving 13.8% Efficiency by Exceeding the Ray Optics Limit. *Science (80-.)*. **2013**, *339* (6123), 1057–1060.
- 16 Aberg, I.; Vescovi, G.; Asoli, D.; Naseem, U.; Gilboy, J. P.; Sundvall, C.; Dahlgren, A.; Svensson, K. E.; Anttu, N.; Bjork, M. T.; Samuelson, L. A GaAs Nanowire

- Array Solar Cell with 15.3% Efficiency at 1 Sun. *IEEE J. Photovoltaics* **2016**, *6* (1), 185–190.
- 17 Gonzalez-Pedro, V.; Juarez-Perez, E. J.; Arsyad, W. S.; Barea, E. M.; Fabregat-Santiago, F.; Mora-Sero, I.; Bisquert, J. General Working Principles of $\text{CH}_3\text{NH}_3\text{PbX}_3$ Perovskite Solar Cells. *Nano Lett.* **2014**, *14* (2), 888–893.
- 18 Jung, H. S.; Park, N. G. Perovskite Solar Cells: From Materials to Devices. *Small* **2015**, *11* (1), 10–25.
- 19 Konstantakou, M.; Stergiopoulos, T. A Critical Review on Tin Halide Perovskite Solar Cells. *J. Mater. Chem. A* **2017**, *5* (23), 11518–11549.
- 20 Scharber, M. C.; Sariciftci, N. S. Efficiency of Bulk-Heterojunction Organic Solar Cells. *Prog. Polym. Sci.* **2013**, *38* (12), 1929–1940.
- 21 Nelson, J. Polymer: Fullerene Bulk Heterojunction Solar Cells. *Mater. Today* **2011**, *14* (10), 462–470.
- 22 Günes, S.; Neugebauer, H.; Sariciftci, N. S. Conjugated Polymer-Based Organic Solar Cells. *Chem. Rev.* **2007**, *107* (4), 1324–1338.
- 23 Bernède, J. C. Organic Photovoltaic Cells: History, Principle and Techniques. *J. Chil. Chem. Soc.* **2008**, *53* (3), 1549–1564.
- 24 Ebrahim, K. Dye Sensitized Solar Cells - Working Principles, Challenges and Opportunities. *Sol. Cells - Dye. Devices* **2011**.
- 25 Nazeeruddin, M. K.; Baranoff, E.; Grätzel, M. Dye-Sensitized Solar Cells: A Brief Overview. *Sol. Energy* **2011**, *85* (6), 1172–1178.
- 26 Gong, J.; Liang, J.; Sumathy, K. Review on Dye-Sensitized Solar Cells (DSSCs): Fundamental Concepts and Novel Materials. *Renew. Sustain. Energy Rev.* **2012**, *16* (8), 5848–5860.
- 27 Kong, F.-T.; Dai, S.-Y.; Wang, K.-J. Review of Recent Progress in Dye-Sensitized Solar Cells. *Adv. Optoelectron.* **2007**, *2007*, 1–13.
- 28 Gong, J.; Sumathy, K.; Qiao, Q.; Zhou, Z. Review on Dye-Sensitized Solar Cells (DSSCs): Advanced Techniques and Research Trends. *Renew. Sustain. Energy Rev.* **2017**, *68* (December 2015), 234–246.
- 29 Ramanujam, J.; Singh, U. P. Copper Indium Gallium Selenide Based Solar Cells - A Review. *Energy Environ. Sci.* **2017**, *10* (6), 1306–1319.
- 30 Lee, T. D.; Ebong, A. U. A Review of Thin Film Solar Cell Technologies and Challenges. *Renew. Sustain. Energy Rev.* **2017**, *70* (November), 1286–1297.
- 31 Reinhard, P.; Chirila, A.; Blosch, P.; Pianezzi, F.; Nishiwaki, S.; Buechelers, S.; Tiwari, A. N. Review of Progress toward 20% Efficiency Flexible CIGS Solar Cells and Manufacturing Issues of Solar Modules. In *2012 IEEE 38th Photovoltaic Specialists Conference (PVSC) PART 2*; IEEE, **2013**; 1–9.
- 32 Jang, Y. H.; Jang, Y. J.; Kim, S.; Quan, L. N.; Chung, K.; Kim, D. H. Plasmonic Solar Cells: From Rational Design to Mechanism Overview. *Chem. Rev.* **2016**, *116* (24), 14982–15034.
- 33 Ueno, K.; Oshikiri, T.; Sun, Q.; Shi, X.; Misawa, H. Solid-State Plasmonic Solar Cells. *Chem. Rev.* **2018**, *118* (6), 2955–2993.
- 34 Emin, S.; Singh, S. P.; Han, L.; Satoh, N.; Islam, A. Colloidal Quantum Dot Solar Cells. *Sol. Energy* **2011**, *85* (6), 1264–1282.
- 35 Beard, M. C.; Luther, J. M.; Nozik, A. J. Multiple Exciton Generation in Semiconductor Quantum Dots and Electronically Coupled Quantum Dot Arrays for

- Application to Third- Generation Photovoltaic Solar Cells. *Colloid. Quantum Dot Optoelectron. Photovoltaics* **2010**, 9780521198, 112–147.
- 36 Rühle, S.; Shalom, M.; Zaban, A. Quantum-Dot-Sensitized Solar Cells. *ChemPhysChem* **2010**, 11 (11), 2290–2304.
- 37 Tian, J.; Cao, G. Semiconductor Quantum Dot-Sensitized Solar Cells. *Nano Rev.* **2013**, 4 (1), 22578.
- 38 Liang, D.; Kang, Y.; Huo, Y.; Chen, Y.; Cui, Y.; Harris, J. S. High-Efficiency Nanostructured Window GaAs Solar Cells. *Nano Lett.* **2013**, 13 (10), 4850–4856.
- 39 Yao, M.; Huang, N.; Cong, S.; Chi, C. Y.; Seyedi, M. A.; Lin, Y. T.; Cao, Y.; Povinelli, M. L.; Dapkus, P. D.; Zhou, C. GaAs Nanowire Array Solar Cells with Axial P-i-n Junctions. *Nano Lett.* **2014**, 14 (6), 3293–3303.
- 40 Li, Y.; Yan, X.; Wu, Y.; Zhang, X.; Ren, X. Plasmon-Enhanced Light Absorption in GaAs Nanowire Array Solar Cells. *Nanoscale Res. Lett.* **2015**, 10 (1), 1–7.
- 41 Chao, J.-J.; Shiu, S.-C.; Hung, S.-C.; Lin, C.-F. GaAs Nanowire/Poly(3,4-Ethylenedioxythiophene):Poly(Styrenesulfonate) Hybrid Solar Cells. *Nanotechnology* **2010**, 21 (28), 285203.
- 42 Zhong, Z.; Li, Z.; Gao, Q.; Li, Z.; Peng, K.; Li, L.; Mokkaapati, S.; Vora, K.; Wu, J.; Zhang, G.; Wang, Z.; Fu, L.; Tan, H. H.; Jagadish, C. Efficiency Enhancement of Axial Junction InP Single Nanowire Solar Cells by Dielectric Coating. *Nano Energy* **2016**, 28, 106–114.
- 43 Svensson, C. P. T.; Mårtensson, T.; Trägårdh, J.; Larsson, C.; Rask, M.; Hessman, D.; Samuelson, L.; Ohlsson, J. Monolithic GaAs/InGaP Nanowire Light Emitting Diodes on Silicon. *Nanotechnology* **2008**, 19 (30), 305201.
- 44 Tomioka, K.; Motohisa, J.; Hara, S.; Hiruma, K.; Fukui, T. GaAs/AlGaAs Core Multishell Nanowire-Based Light-Emitting Diodes on Si. *Nano Lett.* **2010**, 10 (5), 1639–1644.
- 45 Wang, Z.; Tian, B.; Pantouvaki, M.; Guo, W.; Absil, P.; Van Campenhout, J.; Merckling, C.; Van Thourhout, D. Room-Temperature InP Distributed Feedback Laser Array Directly Grown on Silicon. *Nat. Photonics* **2015**, 9 (12), 837–842.
- 46 Saxena, D.; Mokkaapati, S.; Parkinson, P.; Jiang, N.; Gao, Q.; Tan, H. H.; Jagadish, C. Optically Pumped Room-Temperature GaAs Nanowire Lasers. *Nat. Photonics* **2013**, 7 (12), 963–968.
- 47 Kako, S.; Arakawa, Y.; Ho, J.; Iwamoto, S.; Tatebayashi, J.; Ota, Y. Growth of InGaAs/GaAs Nanowire-Quantum Dots on AlGaAs/GaAs Distributed Bragg Reflectors for Laser Applications. *J. Cryst. Growth* **2016**, 468, 144–148.
- 48 Hua, B.; Motohisa, J.; Kobayashi, Y.; Hara, S.; Fukui, T. Single GaAs/GaAsP Coaxial Core-Shell Nanowire Lasers. *Nano Lett.* **2009**, 9 (1), 112–116.
- 49 Jiang, H.; Liu, C. Y.; Qu, Y.; Yuan, S.; Liu, G.; Bo, B. High-Power InAlGaAs/GaAs and AlGaAs/GaAs Semiconductor Laser Arrays Emitting at 808 nm. *IEEE Photonics Technol. Lett.* **2004**, 16 (2), 389–391.
- 50 Zhou, Y.; Fu, L.; Li, F.; Jagadish, C.; Tan, L.; Li, Z.; Lysevych, M.; Tan, H. H.; Ma, J. Radiation Effects on GaAs/AlGaAs Core/Shell Ensemble Nanowires and Nanowire Infrared Photodetectors. *Nanotechnology* **2017**, 28 (12), 125702.
- 51 Dai, X.; Zhang, S.; Wang, Z.; Adamo, G.; Liu, H.; Huang, Y.; Couteau, C.; Soci, C. GaAs/AlGaAs Nanowire Photodetector. *Nano Lett.* **2014**, 14 (5), 2688–2693.

- 52 Buttar, C. M.; Berwick, K.; Brozel, M. R.; Sellin, P.; Cowperthwaite, M.; Hou, Y. Imaging of High Field Regions in Semi-Insulating GaAs under Bias. *Mater. Sci. Eng. B* **2003**, *28* (1–3), 485–487.
- 53 Sturge, M. D. Optical Absorption of Gallium Arsenide between 0.6 and 2.75 eV. *Phys. Rev.* **1962**, *127* (3), 768–773.
- 54 Piprek, J. Semiconductor Optoelectronic Devices; Elsevier, **2003**.
- 55 Tsai, C.-Y. Absorption Coefficients of Silicon: A Theoretical Treatment. *J. Appl. Phys.* **2018**, *123* (18), 183103.
- 56 Kitai, A. Principles of Solar Cells, LEDs and Related Devices. *John Wiley & Sons* **2018**.
- 57 Righini, G. C.; Enrichi, F. Solar Cells' Evolution and Perspectives: A Short Review. *Solar Cells and Light Management*, **2020**, 1-32.
- 58 Mokkaapati, S.; Saxena, D.; Tan, H. H.; Jagadish, C. Semiconductor Nanowire Optoelectronic Devices. *Semiconductors and Semimetals*; 2016; 1–15.
- 59 Brinker, D. J.; Weinberg, I. Recent Developments in Indium Phosphide Space Solar Cell Research. *NASA Tech. Memo.* **1987**.
- 60 Weinberg, I.; Swartz, C. K.; Hart, R. E. Potential for Use of Inp Solar Cells in the Space Radiation Environment. *Conf. Rec. IEEE Photovolt. Spec. Conf.* **1985**, 1722–1724.
- 61 King, R. R.; Law, D. C.; Edmondson, K. M.; Fetzer, C. M.; Kinsey, G. S.; Yoon, H.; Sherif, R. A.; Karam, N. H. 40% Efficient Metamorphic GaInPGaInAsGe Multijunction Solar Cells. *Appl. Phys. Lett.* **2007**, *90* (18), 90–93.
- 62 Geisz, J. F.; Kurtz, S.; Wanlass, M. W.; Ward, J. S.; Duda, A.; Friedman, D. J.; Olson, J. M.; McMahon, W. E.; Moriarty, T. E.; Kiehl, J. T. High-Efficiency GaInPGaAsInGaAs Triple-Junction Solar Cells Grown Inverted with a Metamorphic Bottom Junction. *Appl. Phys. Lett.* **2007**, *91* (2), 1–4.
- 63 Zhang, Y.; Liu, H. Nanowires for High-Efficiency, Low-Cost Solar Photovoltaics. *Crystals* **2019**, *9* (2).
- 64 Aspnes, D. E. Recombination at Semiconductor Surfaces and Interfaces. *Surf. Sci.* **1983**, *132* (1–3), 406–421.
- 65 Reitzenstein, S.; Münch, S.; Hofmann, C.; Forchel, A.; Crankshaw, S.; Chuang, L. C.; Moewe, M.; Chang-Hasnain, C. Time Resolved Microphotoluminescence Studies of Single InP Nanowires Grown by Low Pressure Metal Organic Chemical Vapor Deposition. *Appl. Phys. Lett.* **2007**.
- 66 Naz, M. Y.; Shukrullah, S.; Ghaffar, A.; Ali, K.; Sharma, S. K. Synthesis and Processing of Nanomaterials. *Solar Cells* **2020**; 1–23.
- 67 Kayes, B. M.; Atwater, H. A.; Lewis, N. S. Comparison of the Device Physics Principles of Planar and Radial p-n Junction Nanorod Solar Cells. *J. Appl. Phys.* **2005**, *97* (11), 1–11.
- 68 Zhang, Y.; Wang, L. W.; Mascarenhas, A. “Quantum Coaxial Cables” for Solar Energy Harvesting. *Nano Lett.* **2007**, *7* (5), 1264–1269.
- 69 Yu, R.; Lin, Q.; Leung, S. F.; Fan, Z. Nanomaterials and Nanostructures for Efficient Light Absorption and Photovoltaics. *Nano Energy* **2012**, *1* (1), 57–72.
- 70 Gudiksen, M. S.; Wang, J.; Lieber, C. M. Size-Dependent Photoluminescence from Single Indium Phosphide Nanowires. *J. Phys. Chem. B* **2002**, *106* (16), 4036–4039.
- 71 Alivisatos, A. P. Semiconductor Clusters, Nanocrystals, and Quantum Dots. *Science* (80-.). **1996**, *271* (5251), 933–937.

- 72 Thony, P. Semiconductor Nanowires for Solar Cells. *Semiconductor Nanowires*; Elsevier, **2015**; 411–439.
- 73 Anttu, N.; Xu, H. Q. Efficient Light Management in Vertical Nanowire Arrays for Photovoltaics. *Opt. Express* **2013**, *21* (S3), A558.
- 74 Daytè, V.; Anttu, N. Modal Analysis of Resonant and Non-Resonant Optical Response in Semiconductor Nanowire Arrays. *Nanotechnology* **2019**, *30* (2), 025710.
- 75 Chen, Y.; Pistol, M.-E.; Anttu, N. Design for Strong Absorption in a Nanowire Array Tandem Solar Cell. *Sci. Rep.* **2016**, *6* (1), 32349.
- 76 Espinet-Gonzalez, P.; Barrigón, E.; Otnes, G.; Vescovi, G.; Mann, C.; France, R. M.; Welch, A. J.; Hunt, M. S.; Walker, D.; Kelzenberg, M. D.; Åberg, I.; Borgström, M. T.; Samuelson, L.; Atwater, H. A. Radiation Tolerant Nanowire Array Solar Cells. *ACS Nano* **2019**, *13* (11), 12860–12869.
- 77 Cui, Y.; Wang, J.; Plissard, S. R.; Cavalli, A.; Vu, T. T. T.; Van Veldhoven, R. P. J.; Gao, L.; Trainor, M.; Verheijen, M. A.; Haverkort, J. E. M.; Bakkers, E. P. A. M. Efficiency Enhancement of InP Nanowire Solar Cells by Surface Cleaning. *Nano Lett.* **2013**, *13* (9), 4113–4117.
- 78 Aagesen, M.; Jørgensen, H. I.; Liu, H.; Holm, J. V.; Nygård, J.; Krogstrup, P. Surface-Passivated GaAsP Single-Nanowire Solar Cells Exceeding 10% Efficiency Grown on Silicon. *Nat. Commun.* **2013**, *4* (1), 1498.
- 79 Shockley, W.; Queisser, H. J. Detailed Balance Limit of Efficiency of p-n Junction Solar Cells. *J. Appl. Phys.* **1961**, *32* (3), 510–519.
- 80 Capper, P.; Irvine, S.; Joyce, T. Epitaxial Crystal Growth: Methods and Materials. In *Springer Handbook of Electronic and Photonic Materials*; Springer US: Boston, MA, 2006; pp 271–301.
- 81 Zhou, H. L.; Hoang, T. B.; Dheeraj, D. L.; Van Helvoort, A. T. J.; Liu, L.; Harmand, J. C.; Fimland, B. O.; Weman, H. Wurtzite GaAs/AlGaAs Core-Shell Nanowires Grown by Molecular Beam Epitaxy. *Nanotechnology* **2009**, *20* (41).
- 82 Dheeraj, D. L.; Zhou, H. L.; Moses, A. F.; Hoang, T. B.; Van, A. T. J.; Fimland, B. O.; Wem, H. Heterostructured III-V Nanowires with Mixed Crystal Phases Grown by Au-Assisted Molecular Beam Epitaxy. *Nanowires* **2010**.
- 83 Sköld, N.; Karlsson, L. S.; Larsson, M. W.; Pistol, M. E.; Seifert, W.; Trägårdh, J.; Samuelson, L. Growth and Optical Properties of Strained GaAs-GaxIn_{1-x}P Core-Shell Nanowires. *Nano Lett.* **2005**, *5* (10), 1943–1947.
- 84 Noborisaka, J.; Motohisa, J.; Hara, S.; Fukui, T. Fabrication and Characterization of Freestanding GaAs/AlGaAs Core-Shell Nanowires and AlGaAs Nanotubes by Using Selective-Area Metalorganic Vapor Phase Epitaxy. *Appl. Phys. Lett.* **2005**, *87* (9).
- 85 Ren, S.; Zhao, N.; Crawford, S. C.; Tambe, M.; Bulović, V.; Gradečak, S. Heterojunction Photovoltaics Using GaAs Nanowires and Conjugated Polymers. *Nano Lett.* **2011**, *11* (2), 408–413.
- 86 Brossset, D.; Ai, B.; Segui, Y. New Method of GaAs Passivation with Thin Polymer Films. *Appl. Phys. Lett.* **1978**, *33* (1), 87–89.
- 87 Herz, L. M.; Johnston, M. B.; Noori, K.; Yong, C. K.; Tan, H. H.; Giustino, F.; Gao, Q.; Joyce, H. J.; Jagadish, C. Strong Carrier Lifetime Enhancement in GaAs Nanowires Coated with Semiconducting Polymer. *Nano Lett.* **2012**, *12* (12), 6293–6301.

- 88 Lai, L.-W.; Chen, J.-T.; Lou, L.-R.; Wu, C.-H.; Lee, C.-T. Performance Improvement of $(\text{NH}_4)_2\text{S}_x$ -Treated III-V Compounds Multijunction Solar Cell Using Surface Treatment. *J. Electrochem. Soc.* **2008**, *155* (12), B1270.
- 89 Zou, X.; Li, C.; Su, X.; Liu, Y.; Finkelstein-Shapiro, D.; Zhang, W.; Yartsev, A. Carrier Recombination Processes in GaAs Wafers Passivated by Wet Nitridation. *ACS Appl. Mater. & Interfaces* **2020**, *12* (25), 28360–28367.
- 90 Berkovits, V. L.; Paget, D.; Karpenko, A. N.; Ulin, V. P.; Tereshchenko, O. E. Soft Nitridation of GaAs(100) by Hydrazine Sulfide Solutions: Effect on Surface Recombination and Surface Barrier. *Appl. Phys. Lett.* **2007**, *90* (2), 2–5.
- 91 Berkovits, V. L.; Ulin, V. P.; Losurdo, M.; Capezzuto, P.; Bruno, G.; Perna, G.; Capozzi, V. Wet Chemical Nitridation of GaAs (100) by Hydrazine Solution for Surface Passivation. *Appl. Phys. Lett.* **2002**, *80* (20), 3739–3741.
- 92 Alekseev, P. A.; Dunaevskiy, M. S.; Ulin, V. P.; Lvova, T. V.; Filatov, D. O.; Nezhdanov, A. V.; Mashin, A. I.; Berkovits, V. L. Nitride Surface Passivation of GaAs Nanowires: Impact on Surface State Density. *Nano Lett.* **2015**, *15* (1), 63–68.
- 93 Lu, H. L.; Terada, Y.; Shimogaki, Y.; Nakano, Y.; Sugiyama, M. *In Situ* Passivation of InP Surface Using H_2S during Metal Organic Vapor Phase Epitaxy. *Appl. Phys. Lett.* **2009**, *95* (15), 1–4.
- 94 Zhang, W.; Borgström, M. T.; Lehmann, S.; Yartsev, A.; Pistol, M.-E.; Wallentin, J.; Mergenthaler, K. Carrier Recombination Dynamics in Sulfur-Doped InP Nanowires. *Nano Lett.* **2015**, *15* (11), 7238–7244.
- 95 Hu, J.; Odom, T. W.; Lieber, C. M. Chemistry and Physics in One Dimension: Synthesis and Properties of Nanowires and Nanotubes. *Acc. Chem. Res.* **1999**, *32* (5), 435–445.
- 96 Li, Y.; Qian, F.; Xiang, J.; Lieber, C. M. Nanowire Electronic and Optoelectronic Devices. *Mater. Today* **2006**, *9* (10), 18–27.
- 97 Howard, I. A.; Laquai, F. Optical Probes of Charge Generation and Recombination in Bulk Heterojunction Organic Solar Cells. *Macromol. Chem. Phys.* **2010**, *211* (19), 2063–2070.
- 98 Wolford, D. J.; Gilliland, G. D.; Kuech, T. F.; Smith, L. M.; Martinsen, J.; Bradley, J. A.; Tsang, C. F.; Venkatasubramanian, R.; Ghandi, S. K.; Hjalmarsen, H. P. Intrinsic Recombination and Interface Characterization in “Surface-Free” GaAs Structures. *J. Vac. Sci. Technol. B Microelectron. Nanom. Struct.* **1991**, *9* (4), 2369–2376.
- 99 Titova, L. V.; Hoang, T. B.; Jackson, H. E.; Smith, L. M.; Yarrison-Rice, J. M.; Kim, Y.; Joyce, H. J.; Tan, H. H.; Jagadish, C. Temperature Dependence of Photoluminescence from Single Core-Shell GaAs-AlGaAs Nanowires. *Appl. Phys. Lett.* **2006**, *89* (17), 14–17.
- 100 Joyce, H. J.; Docherty, C. J.; Gao, Q.; Tan, H. H.; Jagadish, C.; Lloyd-Hughes, J.; Herz, L. M.; Johnston, M. B. Electronic Properties of GaAs, InAs and InP Nanowires Studied by Terahertz Spectroscopy. *Nanotechnology* **2013**, *24* (21).
- 101 Zhang, W.; Borgström, M. T.; Lehmann, S.; Yartsev, A.; Pistol, M.-E.; Wallentin, J.; Mergenthaler, K. Carrier Recombination Dynamics in Sulfur-Doped InP Nanowires. *Nano Lett.* **2015**, *15* (11), 7238–7244.
- 102 Zhang, W.; Yang, F.; Messing, M. E.; Mergenthaler, K.; Pistol, M. E.; Deppert, K.; Samuelson, L.; Magnusson, M. H.; Yartsev, A. Recombination Dynamics in

- Aerotaxy-Grown Zn-Doped GaAs Nanowires. *Nanotechnology* **2016**, *27* (45), 455704.
- 103 Joyce, H. J.; Wong-Leung, J.; Yong, C. K.; Docherty, C. J.; Paiman, S.; Gao, Q.; Tan, H. H.; Jagadish, C.; Lloyd-Hughes, J.; Herz, L. M.; Johnston, M. B. Ultralow Surface Recombination Velocity in InP Nanowires Probed by Terahertz Spectroscopy. *Nano Lett.* **2012**, *12* (10), 5325–5330.
- 104 Titova, L. V.; Hoang, T. B.; Jackson, H. E.; Smith, L. M.; Yarrison-Rice, J. M.; Kim, Y.; Joyce, H. J.; Tan, H. H.; Jagadish, C. Temperature Dependence of Photoluminescence from Single Core-Shell GaAs-AlGaAs Nanowires. *Appl. Phys. Lett.* **2006**, *89* (17), 56–59.
- 105 Noborisaka, J.; Motohisa, J.; Hara, S.; Fukui, T. Fabrication and Characterization of Freestanding GaAs/AlGaAs Core-Shell Nanowires and AlGaAs Nanotubes by Using Selective-Area Metalorganic Vapor Phase Epitaxy. *Appl. Phys. Lett.* **2005**, *87* (9), 28–31.
- 106 Zhang, W.; Yang, F.; Messing, M. E.; Mergenthaler, K.; Pistol, M. E.; Deppert, K.; Samuelson, L.; Magnusson, M. H.; Yartsev, A. Recombination Dynamics in Aerotaxy-Grown Zn-Doped GaAs Nanowires. *Nanotechnology* **2016**, *27* (45), 455704.
- 107 Chen, S. L.; Chen, W. M.; Ishikawa, F.; Buyanova, I. A. Suppression of Non-Radiative Surface Recombination by N Incorporation in GaAs/GaNAs Core/Shell Nanowires. *Sci. Rep.* **2015**, *5* (1), 11653.
- 108 Lunt, S. R.; Ryba, G. N.; Santangelo, P. G.; Lewis, N. S. Chemical Studies of the Passivation of GaAs Surface Recombination Using Sulfides and Thiols. *J. Appl. Phys.* **1991**, *70* (12), 7449–7467.
- 109 Zanatta, A. R. Revisiting the Optical Bandgap of Semiconductors and the Proposal of a Unified Methodology to Its Determination. *Sci. Rep.* **2019**, *9* (1), 11225.
- 110 Guo, H.; Wen, L.; Li, X.; Zhao, Z.; Wang, Y. Analysis of Optical Absorption in GaAs Nanowire Arrays. *Nanoscale Res. Lett.* **2011**, *6*, 1–6.
- 111 Mott, N. F. Recombination; a Survey. *Solid State Electron.* **1978**, *21* (11–12), 1275–1280.
- 112 Hopkins, M. A.; Allsopp, D. W. E.; Kappers, M. J.; Oliver, R. A.; Humphreys, C. J. The ABC Model of Recombination Reinterpreted: Impact on Understanding Carrier Transport and Efficiency Droop in InGaN/GaN Light Emitting Diodes. *J. Appl. Phys.* **2017**, *122* (23).
- 113 Mander, H. F. Physics of Semiconductor Devices. *Microelectronics J.* **1982**, *13* (4), 44.
- 114 Blakemore, J. S. Semiconducting and Other Major Properties of Gallium Arsenide. *J. Appl. Phys.* **1982**, *53* (10).
- 115 Chåbera, P.; Fredin, L. A.; Kjær, K. S.; Rosemann, N. W.; Lindh, L.; Prakash, O.; Liu, Y.; Wärmarm, K.; Uhlig, J.; Sundström, V.; Yartsev, A.; Persson, P. Band-Selective Dynamics in Charge-Transfer Excited Iron Carbene Complexes. *Faraday Discuss.* **2019**, *216*, 191–210.
- 116 Joyce, H. J.; Baig, S. A.; Parkinson, P.; Davies, C. L.; Boland, J. L.; Tan, H. H.; Jagadish, C.; Herz, L. M.; Johnston, M. B. The Influence of Surfaces on the Transient Terahertz Conductivity and Electron Mobility of GaAs Nanowires. *J. Phys. D: Appl. Phys.* **2017**, *50* (22), 224001.

- 117 Zhang, W.; Zeng, X.; Su, X.; Zou, X.; Mante, P. A.; Borgström, M. T.; Yartsev, A. Carrier Recombination Processes in Gallium Indium Phosphide Nanowires. *Nano Lett.* **2017**, *17* (7), 4248–4254.
- 118 Parkinson, P.; Lloyd-Hughes, J.; Gao, Q.; Tan, H. H.; Jagadish, C.; Johnston, M. B.; Herz, L. M. Transient Terahertz Conductivity of GaAs Nanowires. *Nano Lett.* **2007**, *7* (7), 2162–2165.
- 119 Schmuttenmaer, C. A. Using Time-Resolved THz Spectroscopy to Study Carrier Dynamics and Solar Energy Conversion in Nanostructured Materials. *2015 40th International Conference on Infrared, Millimeter, and Terahertz waves (IRMMW-THz)*; IEEE, **2015**; 1–2.
- 120 Rode, D. L. Chapter 1 Low-Field Electron Transport. *Semicond. Semimetals* **1975**, *10*, 1–89.
- 121 Wiley, J. D. Chapter 2 Mobility of Holes in III-V Compounds. *Semiconductors and Semimetals*; **1975**; *10*, 91–174.
- 122 Chuang, S. L.; Schmitt-Rink, S.; Greene, B. I.; Saeta, P. N.; Levi, A. F. J. Optical Rectification at Semiconductor Surfaces. *Phys. Rev. Lett.* **1992**, *68* (1), 102–105.
- 123 Lu, Z. G.; Campbell, P.; Zhang, X. C. Free-Space Electro-Optic Sampling with a High-Repetition-Rate Regenerative Amplified Laser. *Appl. Phys. Lett.* **1997**, *71* (5), 593–595.
- 124 Wu, Q.; Zhang, X. - C. Free-Space Electro-Optic Sampling of Terahertz Beams. *Appl. Phys. Lett.* **1995**, *67* (24), 3523–3525.
- 125 Spirkoska, D.; Arbiol, J.; Gustafsson, A.; Conesa-Boj, S.; Glas, F.; Zardo, I.; Heigoldt, M.; Gass, M. H.; Bleloch, A. L.; Estrade, S.; Kaniber, M.; Rossler, J.; Peiro, F.; Morante, J. R.; Abstreiter, G.; Samuelson, L.; Fontcuberta I Morral, A. Structural and Optical Properties of High Quality Zinc-Blende/Wurtzite GaAs Nanowire Heterostructures. *Phys. Rev. B - Condens. Matter Mater. Phys.* **2009**, *80* (24), 1–9.
- 126 Smith, L. M.; Jackson, H. E.; Yarrison-Rice, J. M.; Jagadish, C. Insights into Single Semiconductor Nanowire Heterostructures Using Time-Resolved Photoluminescence. *Semicond. Sci. Technol.* **2010**, *25* (2), 024010.
- 127 Rong, Z.; Azizur-Rahman, K. M.; Huffaker, D. L.; Ren, D.; Somasundaram, S.; Liang, B. A Three-Dimensional Insight into Correlation between Carrier Lifetime and Surface Recombination Velocity for Nanowires. *Nanotechnology* **2018**, *29* (50), 504003.
- 128 Ren, D.; Liang, B. L.; Huffaker, D.; Laghumavarapu, R. B.; Rong, Z.; Scofield, A. C.; Farrell, A. C.; Haddad, M. A. Exploring Time-Resolved Photoluminescence for Nanowires Using a Three-Dimensional Computational Transient Model. *Nanoscale* **2018**, *10* (16), 7792–7802.
- 129 Heurlin, M.; Borgström, M. T.; Zeng, X.; Otnes, G.; Barrigón, E.; Anttu, N.; Zhang, W.; Dagytė, V. Time-Resolved Photoluminescence Characterization of GaAs Nanowire Arrays on Native Substrate. *Nanotechnology* **2017**, *28* (50), 505706.
- 130 Park, K.; Ravindran, S.; Ju, G. W.; Min, J. W.; Kang, S.; Myoung, N. S.; Yim, S. Y.; Jo, Y. R.; Kim, B. J.; Lee, Y. T. Optical Properties and Carrier Dynamics of GaAs/GaInAs Multiple-Quantum-Well Shell Grown on GaAs Nanowire by Molecular Beam Epitaxy. *Curr. Appl. Phys.* **2016**, *16* (12), 1622–1626.
- 131 Herz, L. M.; Johnston, M. B.; Noori, K.; Yong, C. K.; Tan, H. H.; Giustino, F.; Gao, Q.; Joyce, H. J.; Jagadish, C. Strong Carrier Lifetime Enhancement in GaAs

- Nanowires Coated with Semiconducting Polymer. *Nano Lett.* **2012**, *12* (12), 6293–6301.
- 132 Spears, K. G.; Cramer, L. E.; Hoffland, L. D. Subnanosecond Time - correlated Photon Counting with Tunable Lasers. *Rev. Sci. Instrum.* **1978**, *49* (2), 255–262.
- 133 O'Connor, A. V.; Philips, D. Time-Correlated Single Photon Counting. Elsevier, **1984**.
- 134 Szuber, J.; Hollinger, G.; Bergignat, E. Sulfide Passivation of GaAs Surface. *Electron Technol.* **1998**, *31* (3–4), 328–337.
- 135 Bessolov, V. N. Passivation of GaAs in Alcohol Solutions of Ammonium Sulfide. *Semiconductors* **1997**, *31* (11), 1164.
- 136 Berkovits, V. L.; Ulin, V. P.; Losurdo, M.; Capezzuto, P.; Bruno, G. Wet Chemical Treatment in Hydrazine-Sulfide Solutions for Sulfide and Nitride Monomolecular Surface Films on GaAs(100). *J. Electrochem. Soc.* **2005**, *152* (5), 349–353.
- 137 Dmitruk, N. L.; Borkovskaya, O. Y.; Mamontova, I. B. Sulfide Passivation of a Textured Interface of a Gallium Arsenide Surface-Barrier Photovoltaic Cell. *Tech. Phys.* **2002**, *44* (6), 726–728.
- 138 Yong, C. K.; Wong-Leung, J.; Joyce, H. J.; Lloyd-Hughes, J.; Gao, Q.; Tan, H. H.; Jagadish, C.; Johnston, M. B.; Herz, L. M. Direct Observation of Charge-Carrier Heating at WZ–ZB InP Nanowire Heterojunctions. *Nano Lett.* **2013**, *13* (9), 4280–4287.
- 139 Yablonovitch, E.; Skromme, B. J.; Bhat, R.; Harbison, J. P.; Gmitter, T. J. Band Bending, Fermi Level Pinning, and Surface Fixed Charge on Chemically Prepared GaAs Surfaces. *Appl. Phys. Lett.* **1989**, *54* (6), 555–557.
- 140 Reddy, P.; Bryan, I.; Bryan, Z.; Guo, W.; Hussey, L.; Collazo, R.; Sitar, Z. The Effect of Polarity and Surface States on the Fermi Level at III-Nitride Surfaces. *J. Appl. Phys.* **2014**, *116* (12), 123701.
- 141 Berkovits, V. L.; L'Vova, T. V.; Ulin, V. P. Chemical Nitridation of GaAs(100) by Hydrazine-Sulfide Water Solutions. *Vacuum* **2000**, *57* (2), 201–207.
- 142 DeSalvo, G. C. Wet Chemical Digital Etching of GaAs at Room Temperature. *J. Electrochem. Soc.* **1996**, *143* (11), 3652–3656.
- 143 Lukes, F. Oxidation of Si and GaAs in Air at Room Temperature. *Surf. Sci.* **1972**, *30* (1), 91–100.
- 144 Pavesi, L.; Guzzi, M. Photoluminescence of $Al_xGa_{1-x}As$ Alloys. *J. Appl. Phys.* **1994**, *75* (10), 4779–4842.
- 145 Adachi, S. GaAs and Related Materials. *WORLD SCIENTIFIC*, **1994**.
- 146 Baldereschi, A.; Maschke, K.; Hess, E.; Neumann, H.; Schulze, K. R.; Unger, K. Energy Band Structure of $Al_xGa_{1-x}As$. *J. Phys. C Solid State Phys.* **1977**, *10* (23), 4709–4717.
- 147 Parkinson, P.; Joyce, H. J.; Gao, Q.; Tan, H. H.; Zhang, X.; Zou, J.; Jagadish, C.; Herz, L. M.; Johnston, M. B. Carrier Lifetime and Mobility Enhancement in Nearly Defect-Free Core-Shell Nanowires Measured Using Time-Resolved Terahertz Spectroscopy. *Nano Lett.* **2009**, *9* (9), 3349–3353.
- 148 Wells, N. P.; Driskell, T. U.; Hudson, A. I.; LaLumondiere, S. D.; Lotshaw, W. T.; Forbes, D. V.; Hubbard, S. M. Carrier Quenching in InGaP/GaAs Double Heterostructures. *J. Appl. Phys.* **2015**, *118* (6), 065703.

- 149 Jin, H.; Debroye, E.; Keshavarz, M.; Scheblykin, I. G.; Roeffaers, M. B. J.; Hofkens, J.; Steele, J. A. It's a Trap! On the Nature of Localised States and Charge Trapping in Lead Halide Perovskites. *Mater. Horizons* **2020**, *7* (2), 397–410.
- 150 Schricker, A. D.; Davidon, F. M.; Wiacek, R. J.; Korgel, B. A. Space Charge Limited Currents and Trap Concentrations in GaAs Nanowires. *Nanotechnology* **2006**, *17* (10), 2681–2688.
- 151 Songmuang, R.; Giang, L. T. T.; Bleuse, J.; Den Hertog, M.; Niquet, Y. M.; Dang, L. S.; Mariette, H. Determination of the Optimal Shell Thickness for Self-Catalyzed GaAs/AlGaAs Core-Shell Nanowires on Silicon. *Nano Lett.* **2016**, *16* (6), 3426–3433.
- 152 Onton, A.; Lorenz, M. R.; Reuter, W. Electronic Structure and Luminescence Processes in $\text{In}_{1-x}\text{Ga}_x\text{P}$ Alloys. *J. Appl. Phys.* **1971**, *42* (9), 3420–3432.
- 153 Ferry, D. K. Alloy Scattering in Ternary III-V Compounds. *Phys. Rev. B* **1978**, *17* (2), 912–913.
- 154 Macksey, H. M.; Holonyak, N.; Dupuis, R. D.; Campbell, J. C.; Zack, G. W. Crystal Synthesis, Electrical Properties, and Spontaneous and Stimulated Photoluminescence of $\text{In}_{1-x}\text{Ga}_x\text{P}:\text{N}$ Grown from Solution. *J. Appl. Phys.* **1973**, *44* (3), 1333–1341.
- 155 Chang, C. C.; Chi, C. Y.; Yao, M.; Huang, N.; Chen, C. C.; Theiss, J.; Bushmaker, A. W.; Lalumondiere, S.; Yeh, T. W.; Povinelli, M. L.; Zhou, C.; Dapkus, P. D.; Cronin, S. B. Electrical and Optical Characterization of Surface Passivation in GaAs Nanowires. *Nano Lett.* **2012**, *12* (9), 4484–4489.
- 156 Jiang, N.; Gao, Q.; Parkinson, P.; Wong-Leung, J.; Mokkapati, S.; Breuer, S.; Tan, H. H.; Zheng, C. L.; Etheridge, J.; Jagadish, C. Enhanced Minority Carrier Lifetimes in GaAs/AlGaAs Core-Shell Nanowires through Shell Growth Optimization. *Nano Lett.* **2013**, *13* (11), 5135–5140.
- 157 Dagtý, V.; Barrigón, E.; Zhang, W.; Zeng, X.; Heurlin, M.; Otnes, G.; Anttu, N.; Borgström, M. T. Time-Resolved Photoluminescence Characterization of GaAs Nanowire Arrays on Native Substrate. *Nanotechnology* **2017**, *28* (50), 505706.
- 158 Nakai, E.; Chen, M.; Yoshimura, M.; Tomioka, K.; Fukui, T. InGaAs Axial-Junction Nanowire-Array Solar Cells. *Jpn. J. Appl. Phys.* **2015**, *54* (1), 015201.
- 159 Alekseev, P. A.; Dunaevskiy, M. S.; Ulin, V. P.; Lvova, T. V.; Filatov, D. O.; Nezhdanov, A. V.; Mashin, A. I.; Berkovits, V. L. Nitride Surface Passivation of GaAs Nanowires: Impact on Surface State Density. *Nano Lett.* **2015**, *15* (1), 63–68.
- 160 Skromme, B. J.; Sandroff, C. J.; Yablonovitch, E.; Gmitter, T. Effects of Passivating Ionic Films on the Photoluminescence Properties of GaAs. *Appl. Phys. Lett.* **1987**, *51* (24), 2022–2024.
- 161 Dhaka, V.; Perros, A.; Naureen, S.; Shahid, N.; Jiang, H.; Kakko, J.-P.; Haggren, T.; Kauppinen, E.; Srinivasan, A.; Lipsanen, H. Protective Capping and Surface Passivation of III-V Nanowires by Atomic Layer Deposition. *AIP Adv.* **2016**, *6*, 015016.
- 162 Haggren, T.; Jiang, H.; Kakko, J. P.; Huhtio, T.; Dhaka, V.; Kauppinen, E.; Lipsanen, H. Strong Surface Passivation of GaAs Nanowires with Ultrathin InP and GaP Capping Layers. *Appl. Phys. Lett.* **2014**, *105* (3), 1–6.
- 163 Black, L. E.; Cavalli, A.; Verheijen, M. A.; Haverkort, J. E. M.; Bakkers, E. P. A. M.; Kessels, W. M. M. Effective Surface Passivation of InP Nanowires by Atomic-Layer-Deposited Al_2O_3 with PO_x Interlayer. *Nano Lett.* **2017**, *17* (10), 6287–6294.

- 164 Wallentin, J.; Jacobsson, D.; Osterhoff, M.; Borgström, M. T.; Salditt, T. Bending and Twisting Lattice Tilt in Strained Core-Shell Nanowires Revealed by Nanofocused X-Ray Diffraction. *Nano Lett.* **2017**, *17* (7), 4143–4150.
- 165 Gagliano, L.; Albani, M.; Verheijen, M. A.; Bakkers, E. P. A. M.; Miglio, L. Twofold Origin of Strain-Induced Bending in Core-Shell Nanowires: The GaP/InGaP Case. *Nanotechnology* **2018**, *29* (31), 315703.
- 166 Zhang, W.; Zeng, X.; Su, X.; Zou, X.; Mante, P. A.; Borgström, M. T.; Yartsev, A. Carrier Recombination Processes in Gallium Indium Phosphide Nanowires. *Nano Lett.* **2017**, *17* (7), 4248–4254.
- 167 Su, X.; Zeng, X.; Němec, H.; Zou, X.; Zhang, W.; Borgström, M. T.; Yartsev, A. Effect of Hydrogen Chloride Etching on Carrier Recombination Processes of Indium Phosphide Nanowires. *Nanoscale* **2019**, *11* (40), 18550–18558.
- 168 Zou, X.; Li, C.; Su, X.; Liu, Y.; Finkelstein-Shapiro, D.; Zhang, W.; Yartsev, A. Carrier Recombination Processes in GaAs Wafers Passivated by Wet Nitridation. *ACS Appl. Mater. Interfaces* **2020**, *12* (25), 28360–28367.
- 169 Jacobsson, D.; Persson, J. M.; Kriegner, D.; Etzelstorfer, T.; Wallentin, J.; Wagner, J. B.; Stangl, J.; Samuelson, L.; Deppert, K.; Borgström, M. T. Particle-Assisted $\text{Ga}_x\text{In}_{1-x}\text{P}$ Nanowire Growth for Designed Bandgap Structures. *Nanotechnology* **2012**, *23* (24), 245601.
- 170 Yong, C. K.; Wong-Leung, J.; Joyce, H. J.; Lloyd-Hughes, J.; Gao, Q.; Hoe Tan, H.; Jagadish, C.; Johnston, M. B.; Herz, L. M. Direct Observation of Charge-Carrier Heating at WZ–ZB InP Nanowire Heterojunctions. *Nano Lett.* **2013**, *13*, 4287.
- 171 Haverkort, J. E. M.; Cavalli, A.; Bakkers, E. P. A. M.; Kessels, W. M. M.; Black, L. E.; Verheijen, M. A. Effective Surface Passivation of InP Nanowires by Atomic-Layer-Deposited Al_2O_3 with PO_x Interlayer. *Nano Lett.* **2017**, *17* (10), 6287–6294.
- 172 Kim, S. H.; Joo, S. Y.; Jin, H. S.; Kim, W.-B.; Park, T. J. Ultrathin ZnS and ZnO Interfacial Passivation Layers for Atomic-Layer-Deposited HfO_2 Films on InP Substrates. *ACS Appl. Mater. Interfaces* **2016**, *8* (32), 20880–20884.

I would like to finish this thesis with another quotation from mottoes that my grandfather wrote to me when I just started my undergraduate study for further exhorting and encouraging in the future.

学以求真，行以为善。

Seeking truth, being kind.



In 2018, the author was with the statue of Erwin Schrödinger in Wien.

Advanced spectroscopic technologies assist in developing new generation optoelectronic devices

The new generation of stable, lightweight, and high-efficient solar cells based on group III-V nanowires will be optimal to power portable charging devices, especially for satellites, space stations, and extraterrestrial landing vehicles. Understanding the photo-generated carrier recombination processes in group III-V semiconductors is essential for the optimization of their applications as a new generation of solar cells. In this thesis, the carrier recombination processes of photo-generated charge carriers in these nanostructured semiconductors have been investigated by various steady-state and time-resolved spectroscopy methods. These research results will be helpful to guide improvements of material fabrication and design of optoelectronic devices based on the group III-V semiconductors. The author looks forward to seeing the widespread use of nanowire-based solar cells in civil and scientific exploratory.